REGULATION AND EXPRESSION OF GENES ASSOCIATED WITH NEURODEGENERATION WITH BRAIN IRON ACCUMULATION

By

Brenda Jo Polster

A DISSERTATION

Presented to the Department of Molecular and Medical Genetics

and the Oregon Health & Science University School of Medicine

in partial fulfillment of the requirements for the degree of

Doctor of Philosophy

July 2010

School of Medicine

Oregon Health & Science University

CERTIFICATE OF APPROVAL

This is to certify that the Ph.D. dissertation of

Brenda Jo Polster

has been approved

_____

Mentor/Advisor

_____

Member

_____

Member

_____

Member

TABLE OF CONTENTS

LIST OF FIGURES

LIST OF TABLES

LIST OF ABBREVIATIONS

AD	Alzheimer's disease
BACE1	β-site precursor protein cleaving enzyme
BEL	bromoenol lactone
BF	bezafibrate
coA	coenzyme A
CP	ceruloplasmin
cPANK2	cytosolic PANK2
DCT1	divalent catiaon transporter
DIG	digoxygenin
DMSO	dimethyl sulfoxide
DTT	dithiothreitol
EC	entorhinal cortex
EMSA	electophoresis mobility shift assay
EST	expressed sequence tag
FA2H	fatty acid 2-hydroxylase gene
FAHN	fatty acid hydroxylase-associated neurodegeneration
FF	fenofibrate
FTL	ferritin light chain
GRN	granulin
HDBR	Human Developmental Biology Resource
HIF-1β	hypoxia inducible factor-1β
hnRNPA/B	heterogeneous nuclear ribonucleprotein A/B
INAD	infantile neuroaxonal dystrophy
iPANK2	intermediate PANK2
$iPLA_2$	calcium-independent PLA2
IRE	iron responsive element
IRP	iron-regulatory protein
LfR	lactotransferrin receptor
MIN	mitochondrial-missing in NBIA
miRNA	microRNA
MPAN	mitochondrial protein-associated neurodegeneration
mPANK2	mature PANK2
MPP	mitochondrial processing protein
MRE	microRNA recognition elements
mRNA	messenger RNA
mRNP	microribonuclear particles
MTf	melanotransferrin
NAD	neuroaxonal dystrophy
NBIA	neurodegeneration with brain iron accumulation
NC	negative control
NEP	neuroepithelium

NTE	neuropathy target esterase
PCR	polymerase chain reaction
PCW	post conception weeks
PKAN	pantothenate kinase-associated neurodegeneration
PLAN	PLA2G6-associated neurodegeneration
PMSF	phenyl methylsulfonyl fluoride
pPANK2	precursor PANK2
PPAR	peroxisome proliferator-activated receptor
pre-miRNA	precursor miRNA
pri-miRNA	primary miRNA
RACE	rapid amplification of cDNA ends
RISC	RNA-induced silencing complex
RLU	relative luciferase activity
RPE	retinal pigment epithelium
RT	room temperature
RXR	retinoid X receptor
shRNA	short hairpin RNA
sPANK2	short PANK2
SREPB	sterol regulatory element binding protein
SVZ	subventricular zone
TEC	transentorhinal cortex
Tfr	transferrin receptor
TG	troglitazone
TSS	transcriptional start site
VZ	ventricular zone

ACKNOWLEGEMENTS

First and foremost, I would like to acknowledge my mentor, Dr. Susan Hayflick. She is an outstanding physician and determined scientist, as well as a kind and compassionate person. I am continually inspired by her committment to the families affected by NBIA. In addition, she has been a steadfast source of support and encouragement through the highs and lows of graduate school. I will carry the lessons she has taught me throughout my professional career. Thank you, Susan.

I also extend sincere thanks to my committee members; Drs. Soren Impey, David Farrell, and Philip Copenhaver. I appreciate the time they dedicated to individual and formal Thesis Advisory Committee meetings, which were all essential to the completion of my dissertation.

In these years at OHSU, I am honored to have worked and studied alongside of many wonderful people. Many thanks to the past and present members of the Hayflick laboratory: Dr. Micheal Kruer, Wendy Wagoner, Lynn Sanford, Dr. Wei-Hong Xiong, Allison Gregory, Moon Yoon, Dr. Shawn Westaway, Thuy Nguyen, Scott Sonek, and Kathy Lew-Eells. In no particular order but with heartfelt gratitude, I'd like to also thank Deanne Tibbitts and Drs. Ashleigh Miller, Chantelle Rein, Jennifer Johnson, Beth Wilmot, Julie Powers, Brenda Marsh, and Jodi Johnson for their support and sharing in life's trials and triumphs.

Along my academic journey there have been many key mentors and professors who I feel have shaped and guided my journey to this point. I would like to thank Henri Weeks, my high school science teacher, for introducing me to the research side of science and starting this journey. Thanks to Dr. Sigfred Lodwig, my Centralia College organic

chemistry professor, for suggesting I pursue science to the level of philosophy, instead of being a philosophy major. Thanks to Dr. Craig Vierra for challenging me in class and in his research laboratory at University of the Pacific. Finally, thanks to Dr. Kathryn Stowell for providing my first exposure to research in medical genetics at Massey University in New Zealand.

I could not have achieved so much in my academic pursuits without the love and support of my family. My parents, Jack and Mary Jo Belmont, let me bring home a cow's eye to dissect in second grade. They have encouraged my scientific interests, provided financial assistance for college and attended many oral presentations that only a parent could love. Thanks, Mom and Dad. In addition, my loving sisters, Melinda and Donna, are eternal sources of comradery. Thanks for everything. I would also like to thank to my wonderful in-laws; Patty, Phil, Sarah and Steve for their support, encouragement and help with childcare. Sadly, Steve died during the preparation of this final written dissertation. I miss you, Steve.

My final thanks belong to my best friend and dear husband, Matt Polster. Since being my calculus tutor in 1999, he has always been there to motivate, encourage, and give me strength to pursue my dreams. Thank you for years of steadfast support during graduate school, including housework, making meals, providing rides to work, taking more than your fair share on the baby night-shift and editing even these very words.

Lastly, I would like to dedicate this dissertation to my beautiful daughter, Sierra Jacquelyn Polster. May you, too, have so many to support you in your endeavors.

ABSTRACT

Neurodegeneration with brain iron accumulation (NBIA) is a heterogeneous class of disorders with the distinctive feature of axonal swellings throughout the central nervous system. Two causative NBIA genes have been identified by linkage analysis: *PANK2*, encoding a pantothenate kinase, and *PLA2G6*, encoding a group VI calcium-independent phospholipase A_2 (iPLA$_2$-VIA). Mutations in these genes are hypothesized to cause lipid dyshomeostasis and oxidative stress, leading to pantothenate kinase-associated neurodegeneration (PKAN) and infantile and atypical neuroaxonal dystrophy. However, in order to investigate specific mechanisms of disease and develop therapies for NBIA, it is necessary to fully characterize each gene and its function. Toward that goal, my thesis research includes three projects focused on investigating the transcriptional regulation and expression of NBIA genes.

First, I identified a *PANK2* promoter. Historically, two nearly identical PANK2 isoforms have been described: short PANK2 and mature PANK2. However, the biological relevance of these isoforms remains unclear. I have shown that their regulation is distinct and describe a promoter for the short isoform of PANK2. In addition, I identified potential regulators of *PANK2* expression, including NF-Y, FOXN4 and the human heterogeneous nuclear ribonucleoprotein A/B family. These findings validate expression of the short PANK2 isoform and enable predictions about potentially deleterious sequence variants in the PANK2 promoter region. Furthermore, I provided preliminary evidence that *PANK2* transcription is not effected by iron overload and depletion, oxidative stress induced by low dosage of hydrogen peroxide or peroxisome proliferator-activated receptor (PPAR) agonists.

Second, I investigated the expression and function of a family of microRNAs (miR-103/7) conserved in pantothenate kinase genes. In recent years, miR-103 and miR-107 have been proposed to play a role in multiple cellular processes, including metabolism and neurodegeneration, suggesting that their cellular role may complement pantothenate kinase activity. Interestingly, I demonstrated by qRT-PCR that mir-103 and miR-107 expression does not correlate with expression of pantothenate kinase genes in mouse tissues. In addition, the expression profile of miR-103 and its *PANK2* encoded precursor, pre-miR-103, also did not correlate in mouse tissues. Therefore, miR-103-2 expression may be regulated at the level of post-transcriptional processing. Finally, in attempt to dissect miR-103/7 cellular function, I tested several predicted miR-103 targets by luciferase reporter assays and miR-103 over expression experiments; however, I was unable to confirm regulation of candidate targets.

Third, I analyzed the expression of *PLA2G6* and *PANK2* in human fetal development. As shown by *in situ* hybridization histochemistry, *PLA2G6* is expressed throughout the developing brain in proliferative zones, as well as in the differentiated neurons in the developing cerebral neocortex and hindbrain. Likewise, *PANK2* expression is found in brain and eye, although technical difficulties prevented a more detailed study of its temporal and spatial patterning. Also, *PANK2* and *PLA2G6* expression were observed in basal ganglia, lateral ventricle, midbrain and thalamus of the fetal brain, as well as in spinal cord, kidney, liver, eye and lung. These results suggest that *PLA2G6* and *PANK2* are positioned to play a role in early neuronal development. Disruption of this process may contribute to the widespread neurological problems observed in NBIA.

Chapter 1:

Introduction

1.1 Neurodegeneration with Brain Iron Accumulation

Neurodegeneration with brain iron accumulation (NBIA) describes a spectrum of neurological disease in children and adults with high amounts of iron in the basal ganglia (Gregory et al., 2009).

1.1.1 History and nomenclature

NBIA was first described by Drs. Hallervorden and Spatz in 1922 as a familial progressive extrapyramidal disorder with accumulation of iron in the globus palidus and neuroaxonal spheroids throughout the central nervous system (Hallervorden and Spatz, 1922). Subsequently, Hallervorden-Spatz syndrome was used to describe a broad spectrum of disease involving these features (Halliday, 1995). In the 1950s, Seitelberger and Gross described an infantile form of the syndrome, which often lacked brain iron accumulation (Seitelberger and Gross, 1957). This disorder became known as infantile neuroaxonal dystrophy (INAD).

In 2003, Hallervorden-Spatz syndrome was renamed NBIA (Hayflick et al., 2003). Under this descriptive title, the disorders are stratified by age at onset, rate of disease progression, and genetic basis of disease. Currently, NBIA is described as two clinical subtypes: early onset with rapid progression of disease and later onset with slower progression of disease (Figure 1.1) (Gregory et al., 2009). Notably, renaming the syndrome also removes honor from Julius Hallervorden and Hugo Spatz, who committed unethical medical practices in Nazi Germany (Shevell, 2003).

Early onset disorders can be stratified by their causative genes. Pantothenate kinase 2 (*PANK2*) mutations give rise to classic pantothenate kinase-associated

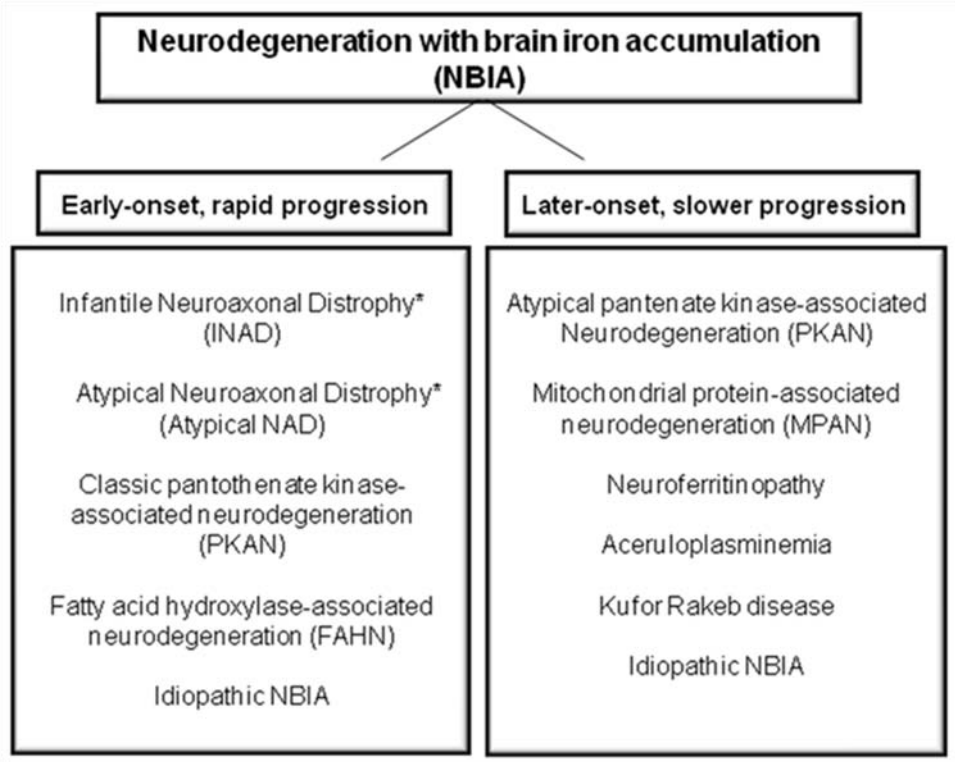

Figure 1.1: Sub-classification of neurodegeneration with brain iron accumulation (NBIA)

* Infantile neuroaxonal dystrophy (INAD) and atypical neuroaxonal dystrophy (NAD) are also known as *PLA2G6*-associated neurodegeneration (PLAN).

neurodegeneration (PKAN) (Zhou et al., 2001). Infantile neuroaxonal dystrophy and atypical neuroaxonal dystrophy are caused by mutations in the phospholipase gene *PLA2G6* (Morgan et al., 2006). Notably, it has also been suggested to classify INAD and atypical NAD cases as *PLA2G6*-associated neurodegeneration (PLAN) (Kurian et al., 2008). Finally, mutations in a fatty acid 2-hydroxylase gene (*FA2H*) were recently identified in early onset NBIA patients, and this subgroup has been named fatty acid hydroxylase-associated neurodegeneration (FAHN) (Kruer et al., 2010). Idiopathic NBIA is used to describe cases with unknown genetic basis.

Later onset NBIA includes atypical PKAN, neuroferritinopathy, aceruloplasminemia, Kufor Rakeb disease and mitochondrial protein-associated neurodegeneration (MPAN). Neuroferritinopathy and aceruloplasminemia are caused by mutations in ferritin light chain (*FTL*) and ceruloplasmin (*CP*) genes, respectively (Curtis et al., 2001; Yoshida et al., 1995). Kufor Rakeb disease results from mutations in a lysosomal ATPase (*ATP13A2*) (Schneider et al., 2010). Lastly, MPAN is defined by mutations in a novel gene, termed mitochondrial-missing in NBIA (*MIN*). Idiopathic late-onset NBIA is also common.

1.1.2 Pantothenate kinase-associated neurodegeneration

The majority of NBIA cases are caused by *PANK2* mutations, resulting in pantothenate kinase-associated neurodegeneration (PKAN) (Zhou et al., 2001). This autosomal recessive disorder has the pathological features of neuroaxonal spheroids in the central nervous system and brain iron accumulation (Hayflick et al., 2003). On T2 weighted MRI, PKAN patients have a distinctive pattern of tissue damage and iron

accumulation in the globus pallidus, which is coined an eye-of-the-tiger sign (Figure 1.2) (Hayflick et al., 2003).

PKAN is segmented into classic and atypical forms. Classic PKAN typically presents with dystonia within the first decade of life and rapidly progresses (Hayflick et al., 2003). Dystonia confines patients to a wheelchair within 10-15 years of symptom onset and eventually dysphagia causes patients to require a feeding tube (Gregory et al., 2009). In addition, pigmentary retinopathy develops in most children, and acanthocytes have been reported in some cases (Ching et al., 2002; Egan et al., 2005). In contrast, the average onset of atypical PKAN is 13-14 years old and patients typically present with speech difficulties, mild gait abnormalities or prominent neuropsychiatric symptoms (Gregory et al., 2009; Hayflick et al., 2003). Atypical PKAN has slower progression of disease and patients do not become confined to a wheelchair until 15-40 years after onset (Gregory et al., 2009). Interestingly, classic and atypical PKAN patients tend to have periods of rapid physical decline interspersed with longer periods of relative stability. Ultimately, death occurs from secondary complications, including aspiration pneumonia and malnutrition.

1.1.3 Infantile and atypical neuroaxonal dystrophy

Infantile and atypical neuroaxonal dystrophies are autosomal recessive disorders resulting from *PLA2G6* mutations (Morgan et al., 2006). On MRI, nearly all infantile and atypical NAD patients have cerebellar atrophy, and a subset have brain iron accumulation (Figure 1.2) (Gregory et al., 2008). In addition, neuroaxonal spheroids are typically present throughout both the central and peripheral nervous systems, and the majority of

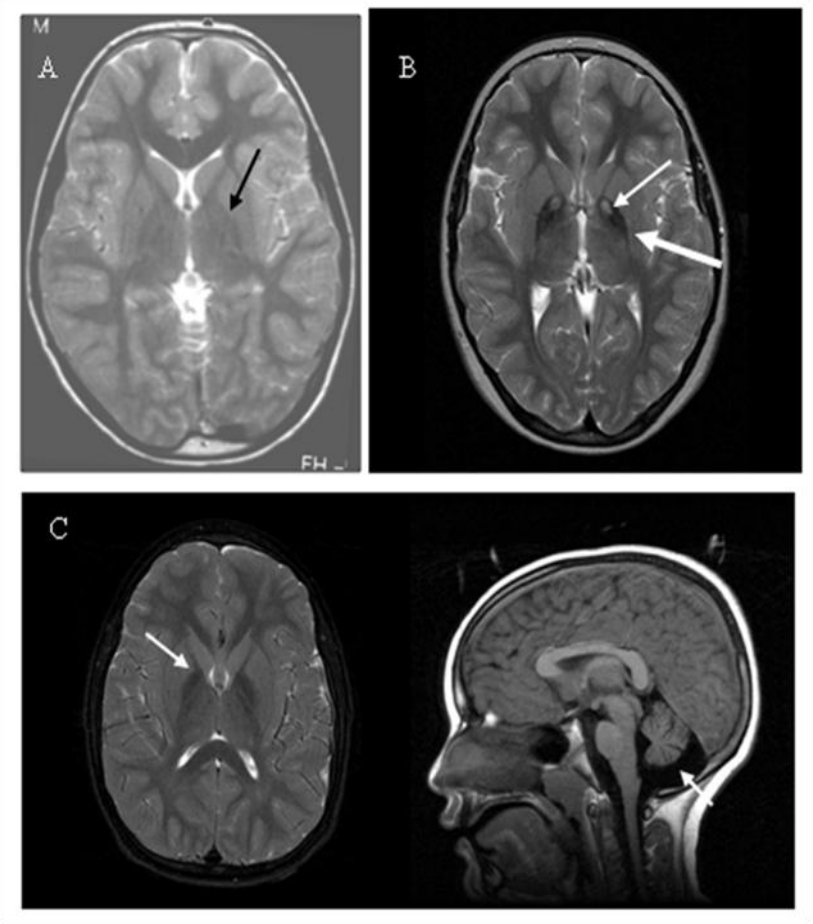

Figure 1.2: Radiographic features of PKAN and INAD

A) T2-weighted MRI of a normal patient. B) T2-weighted MRI of a PKAN patient showing the eye-of-the-tiger sign: a region of hypointensity (thick arrow) with a central region of hyperintensity (thin arrow) in the medial globus pallidus. C) MRI images of an INAD patient with brain iron accumulation and cerebellar atrophy. The image on the left shows a region of hypointensity (arrow) in the medial globus pallidus. The image on the right shows cerebellar atrophy (arrow). These findings appear similarly in patients with the infantile and atypical forms of neuroaxonal dystrophy. Figure adapted and used with permission from (Gregory et al., 2009).

patients have optic atrophy.

Infantile and atypical neuroaxonal dystrophies differ in the age of onset and disease course (Gregory et al., 2008). Infantile neuroaxonal dystrophy typically begins before the second year of life with psychomotor regression and truncal hypotonia, followed by later development of tetraparesis (Nardocci et al., 1999). Optic atrophy, nystagmus, strabismus and seizures also occur. INAD patients often die in their first decade, although some individuals survive into their early twenties (Gregory et al., 2009). In atypical NAD, the average age of symptom onset is 4.4 years old (Gregory et al., 2009). Similar to INAD, optic atrophy, nystagmus, strabismus, muscular weakness, and seizures are common. However, speech delay, dystonia, dysarthia and autism-like behaviors have also been observed.

1.2 Pantothenate kinase 2

In 2001, *PANK2* was identified by linkage analysis as a causative gene for NBIA (Zhou et al., 2001).

1.2.1 Gene and protein structure

In humans, pantothenate kinases are encoded by four genes. *PANK1*, *PANK2* and *PANK3* have nearly identical gene structure: unique initiating exons followed by six highly conserved exons encoding a ~355 residue catalytic domain (Zhou et al., 2001). In addition, *PANK1*, *PANK2* and *PANK3* each host a member of the miR-103/7 family of microRNAs in the 5' region of their introns 5 (Rodriguez et al., 2004). *PANK1* gives rise to cytosolic PANK1α and PANK1β (Rock et al., 2002), *PANK2* gives rise to

mitochondrial isoforms (Hortnagel et al., 2003; Johnson et al., 2004; Kotzbauer et al., 2005) and *PANK3* encodes an additional cytosolic isoform (Zhang et al., 2005). In contrast, *PANK4* is composed of 19 exons that are homologous to pantothenate kinase genes in prokaryotes and *Caenorhabditis elegans* (Zhou et al., 2001). Based on structural and biochemical analysis of *Staphylococcus aureus* PanK (CoaA), PANK4 lacks an essential catalytic glutamate residue for kinase activity (Hong et al., 2006). In addition, PANK4 is not catalytically active *in vitro* (Zhang et al., 2007). Interestingly, however, PANK4 is capable of rescuing pantothenate kinase deficiency in *E.coli* and *Drosophila*, suggesting that it may be functional *in vivo* (Hortnagel et al., 2003; Wu et al., 2009). Northern blot analysis of the PANK family members indicates that they have overlapping expression across human tissues (Zhou et al., 2001).

PANK2 spans over 35 kb on human chromosome 20. In 2001, Zhou et al predicted five *PANK2* transcript variants based on expressed sequence tag (EST) and 5'RACE analysis (Zhou et al., 2001). However, only three *PANK2* transcript variants are currently recognized in NCBI databases (Figure 1.3). *PANK2* transcript variant 1 (NM_153638) has three potential translation initiation codons, which give rise to short (sPANK2), cytosolic (cPANK2) and precursor (pPANK2) isoforms. sPANK2 is 48 kDa and initiates translation at a CUG leucine codon (chr20:3869748 on Human GRCh37 Assembly (hg19)) (Zhou et al., 2001). cPANK2 initiates translation at an AUG codon located 42 nucleotides downstream of the CUG codon (Johnson et al., 2004). Finally, pPANK2 initiates with an AUG leucine codon located 330 nucleotides upstream of the sPANK2 initiating codon (Hortnagel et al., 2003; Kotzbauer et al., 2005). *PANK2*

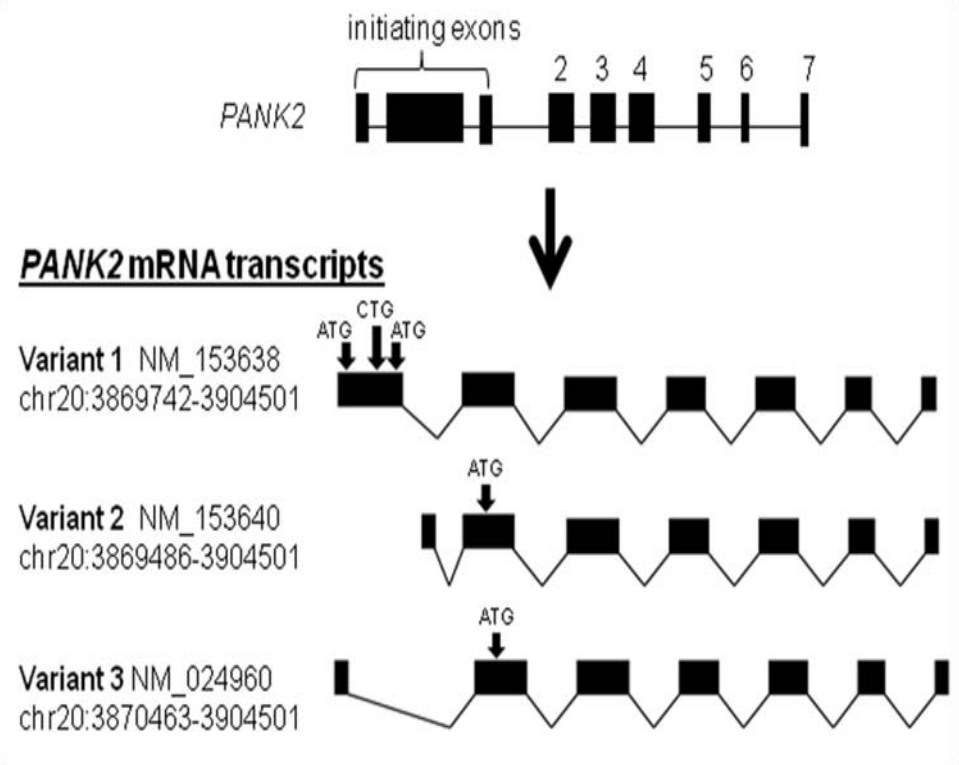

Figure 1.3: *PANK2* geonomic structure and mRNA transcripts

Transcript variants 1-3 are listed in the RefSeq database and the genomic sequence location is based on Human GRCh37 Assembly (hg19) (Kent et al., 2002). The relative location of proposed translational start sites are indicated by arrows.

transcript variants 2 (NM_153640) and 3 (NM_024960) utilize the same translation initiation site within exon 2, which produces an inactive cytosolic PANK2 isoform (isoform 2) (Zhang et al., 2006). PANK2 isoforms are summarized in Figure 1.4.

sPANK2 was originally described as the primary *PANK2* product (Zhou et al., 2001). Prediction of the uncommon leucine start codon (CUG) for this isoform was based on two findings. First, the leucine start codon is flanked by an initiation consensus sequence and followed by a stem-loop structure, which enhances translation initiation at non-AUG initiation codons (Kozak, 1989; Kozak, 1990). Second, *PANK2*'s evolutionarily conserved nucleotide sequence diverges from mouse sequence 5' of the leucine codon. In 2004, Johnson et al. confirmed that the leucine codon initiates sPANK2 expression by a series of transfection experiments, and also found that sPANK2 amino acids 1-29 contain a mitochondrial localization signal that is necessary and sufficient for targeting to the mitochondria (Johnson et al., 2004).

While studying sPANK2 localization, Johnson et al. discovered that an AUG codon located 42 nucleotides downstream of the CUG start site is sufficient to drive cytosolic PANK2 expression (Johnson et al., 2004). Here I identify the proposed cytosolic PANK2 isoform as cPANK2; however, it has not been further studied and its biological relevance is unknown.

In 2003, pPANK2 was identified as a long isoform of PANK2 (Hortnagel et al., 2003). pPANK2 initiates translation at an AUG codon located 330 nucleotides upstream of the CUG codon. Similar to sPANK2, amino acids 1-46 of pPANK2 are sufficient for mitochondrial targeting (Hortnagel et al., 2003). In addition, pPANK2 contains two mitochondrial processing protein (MPP) cleavage sites at amino acids 32 and 141, which

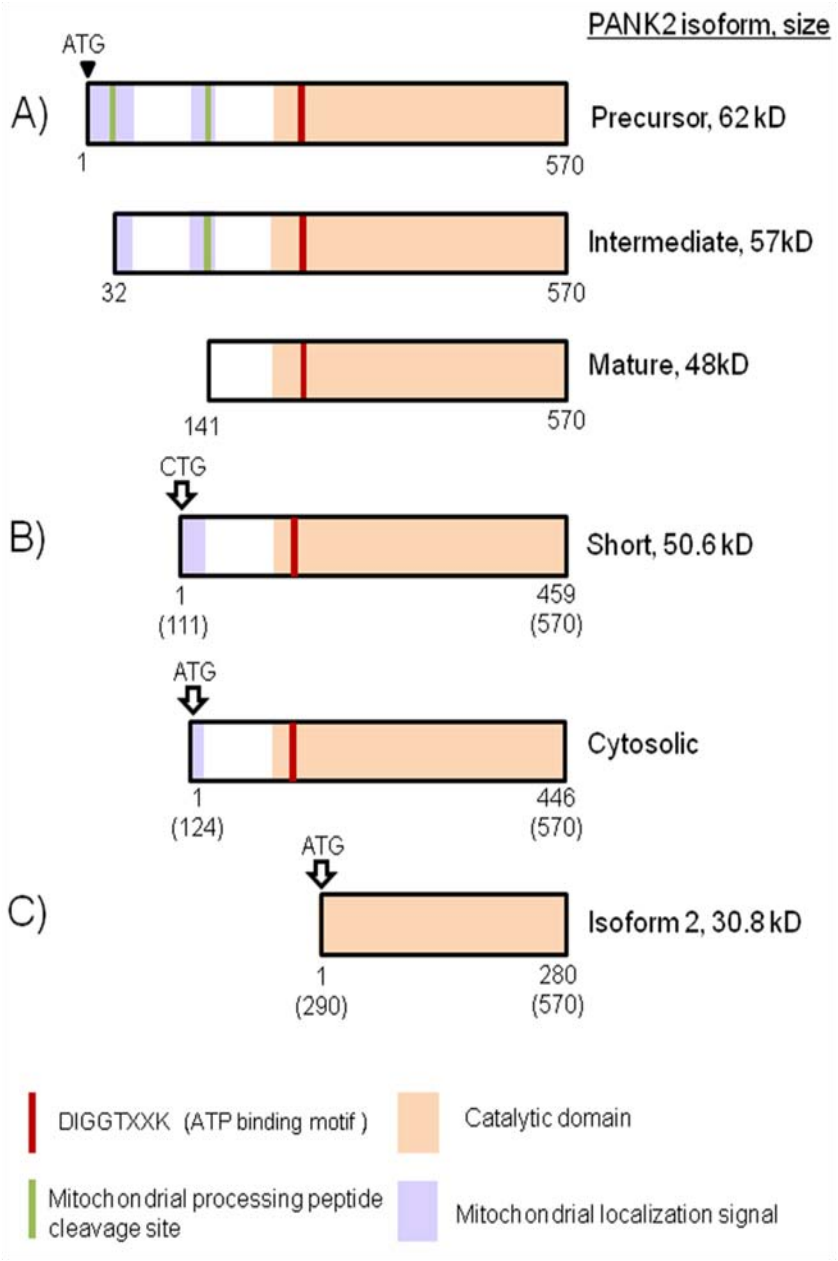

Figure 1.4: PANK2 isoforms

A) PANK2 isoforms arising from the methionine (ATG) start codon in *PANK2* transcript variant 1
B) Proposed PANK2 short isoforms arising from downstream leucine (CTG) and methionine (ATG) start codons on transcript variant 1.
C) PANK2 isoform 2, lacking the ATP binding motif, is predicted to arise from *PANK2* transcript variants 2 and 3.

create iPANK2 and mPANK2 isoforms (Kotzbauer et al., 2005). Kotzbauer et al. observed these isoforms following transfection of a pPANK2 construct in 293 cells and subsequently demonstrated the processing of pPANK2 by pulse-chase ^{35}S labeling of cells (Kotzbauer et al., 2005). The precursor and intermediate isoforms are short lived, although the 48kDa mPANK2 isoform has a half-life of ~30 hours (Kotzbauer et al., 2005). Additionally, the 48kDa mPANK2 isoform was detected in human brain extracts (Kotzbauer et al., 2005).

Some controversy surrounds the proposed PANK2 isoforms. The lack of sequence conservation between mouse, rat and human upstream of the sPANK2 leucine codon has cast doubt on pPANK2's biological relevance (Johnson et al., 2004). In addition, no spliced ESTs document the presence of a stable mRNA transcript that includes the 330 nucleotides upstream of the leucine codon (Rhead et al., 2010). However, western blot and *in vitro* protein analysis provide strong evidence for the expression, processing and stability of isoforms arising from the pPANK2 initiation codon (Kotzbauer et al., 2005; Zhang et al., 2006). Also, it is notable that sPANK2 expression was not detected by Kotzbauer et al. in their pulse-chase analysis (Kotzbauer et al., 2005). Clarification of these discrepancies and the significance of multiple translation initiation codons require further study.

1.2.2 Function and regulation

Pantothenate kinase is an essential regulatory enzyme in the biosynthesis of coenzyme A (coA) (Rock et al., 2000). CoA is an acyl carrier employed in protein, carbohydrate, fat and lipid metabolism (Leonardi et al., 2005). It is essential to glycolysis,

the tricarboxylic acid cycle, fatty acid synthesis, beta oxidation, and steroidogenesis. Within the CoA biosynthesis pathway, pantothenate kinase catalyzes the phosphorylation of pantothenate (vitamin B5), N-pantothenoylcysteine, and pantetheine (Figures 1.5 and 1.6).

The pantothenate kinases are differentially inhibited by CoA and CoA thioesters (Vallari et al., 1987). PANK1α contains a unique N-terminal regulatory domain that increases its sensitivity to feedback inhibition in comparison with PANK1β (Rock et al., 2002), while PANK3 is more sensitive than either PANK1 isoform due to its high affinity for CoA thioester binding (Zhang et al., 2005). However, PANK2 is significantly more sensitive to inhibition than PANK1α, PANK1β and PANK3. For comparison, the half maximal inhibitory concentration (IC_{50}) values for CoA and CoA thioesters in PANK1α, PANK1β and PANK3 are in the range of 1-125μM (Rock et al., 2002; Zhang et al., 2005), while the mPANK2 isoform has CoA and CoA thioester IC_{50} values between 250 and 500nM (Zhang et al., 2006). According to this sensitivity, intracellular and intramitochondrial CoA concentrations are sufficient to inhibit PANK2 activity *in vivo* (Zhang et al., 2006).

Interestingly, however, PANK2 inhibition by CoA thioesters can be reversed by palmitoylcarnitine (Leonardi et al., 2007a). Palmitoylcarnitine is a long-chain fatty acid ester of carnitine that facilitates the transfer of long-chain fatty acids from cytoplasm into mitochondria during the oxidation of fatty acids. Leonardi et al. found that palmitoylcarnitine, as well as other long-chain species of acylcarnitine, are competitive antagonists of acetyl-CoA (Leonardi et al., 2007a). Therefore, they hypothesize that PANK2 is typically inactive within the mitochondria, but an increase in long-chain

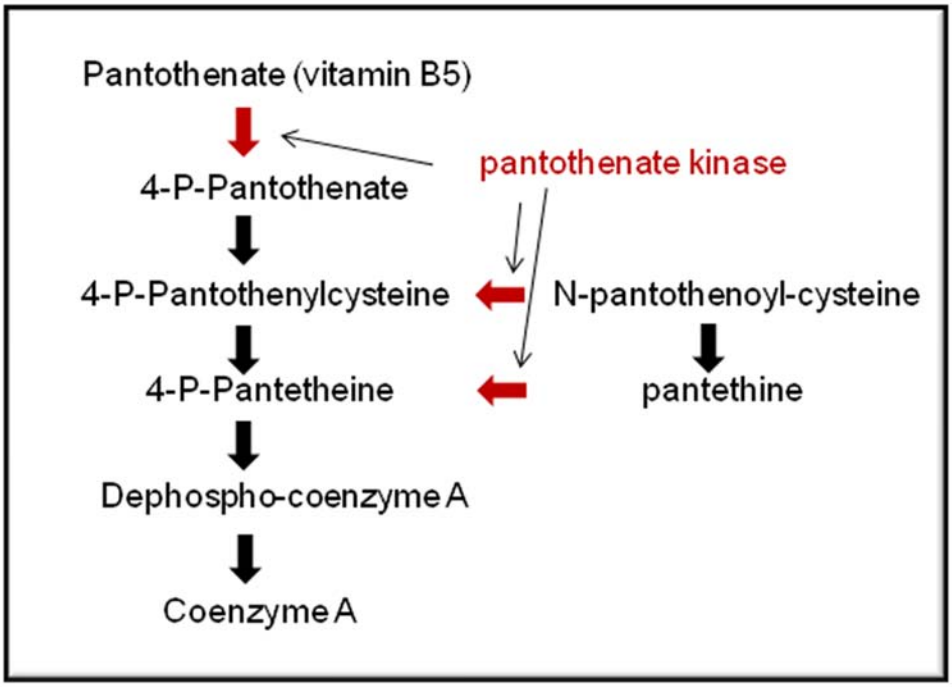

Figure 1.5: Coenzyme A biosynthesis pathway

Red arrows indicate regulatory steps catalyzed by pantothenate kinase.

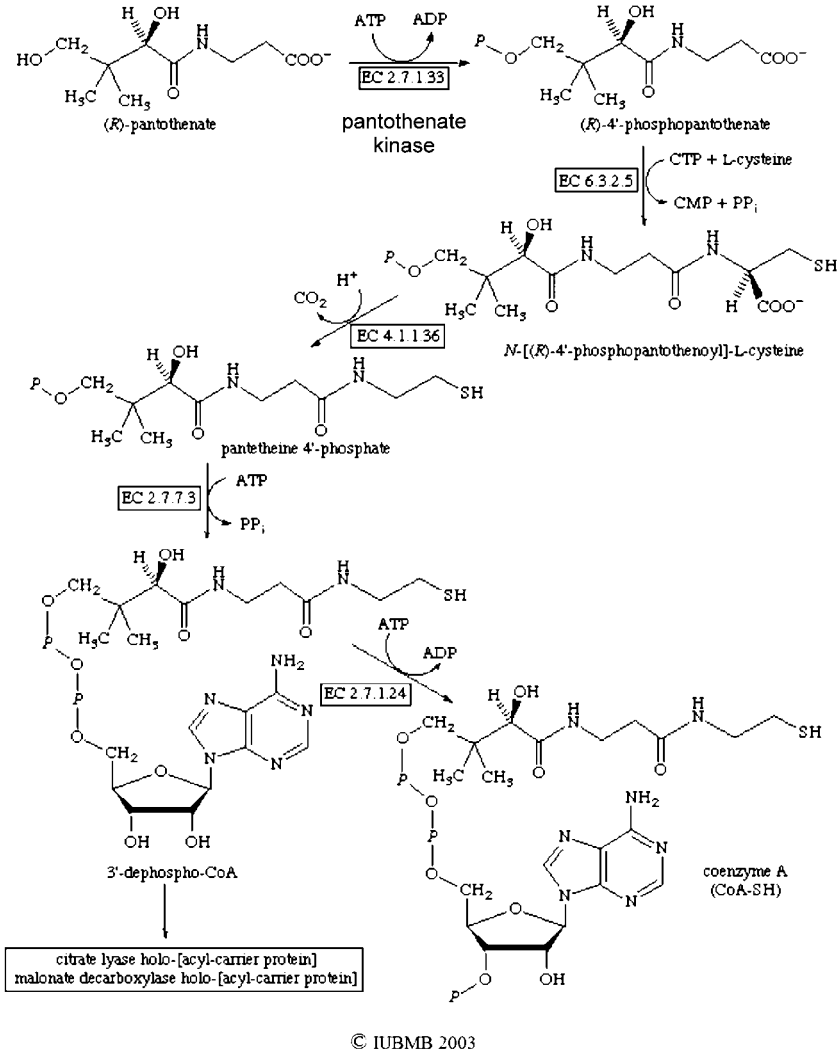

Figure 1.6: Coenzyme A biosynthesis pathway with chemical structures

Adapted from (http://www.chem.qmul.ac.uk/iubmb/enzyme/reaction/misc/CoA2.html)

acylcarnitine activates the kinase for CoA biosynthesis. By this mechanism, PANK2 may function as a molecular sensor to detect the need to increase mitochondrial β-oxidation.

1.2.3 Mutations and hypotheses of disease

A variety of *PANK2* mutations lead to PKAN. Null mutations correlate with classic PKAN, while missense mutations are seen in both classic and atypical disease (Hayflick et al., 2003).

In 2007, Hong et al. superimposed *PANK2* mutations onto the crystal structure of PANK3 (Hong et al., 2007). They found that mutations disrupting the pantothenate kinase active site result in an improperly folded and catalytically inactive kinase. Additionally, mutations found in the homodimer interface and protein interior affect protein stability. Most early-onset PKAN cases are due to missense mutations in these regions, suggesting that disrupting PANK2 kinase activity correlates with severe disease. In contrast, protein surface mutations correlate with both early and late-onset disease. These mutations may disrupt binding of undefined regulatory ligands or association with partner proteins.

In PKAN, *PANK2* mutations are predicted to lead to mitochondrial CoA deficiency and thereby hinder β-oxidation of fatty acids (Zhou et al., 2001). The resulting oxidative stress may be compounded by accumulation of cysteine, a substrate in CoA biosynthesis (Johnson et al., 2004). This hypothesis is supported by the observation of excess cysteine in the globus pallidus of NBIA patients (Perry et al., 1985). Cysteine accumulation is hazardous to cells because cysteine undergoes rapid auto-oxidation in the presence of free iron, generating free radicals and causing oxidative stress.

Notably, the tissue-specific clinical features of PKAN are unexpected in light of the broad cellular processes that are predicted to be impaired by disruption of CoA biosynthesis. Perhaps the vulnerability of the basal ganglia and other tissues is from their high metabolic demands and exposure to oxidative stressors, including normally high iron in basal ganglia, and light in retina.

1.3 Pantothenate kinase intronic microRNAs: miR-103/7 family

1.3.1 microRNA biogenesis and function

MicroRNAs (miRNAs) are ~22 nucleotide non-coding RNAs that negatively regulate gene expression (Bartel, 2004). These small RNAs are found in the human genome as independent genes (Cai et al., 2004; Lee et al., 2004) or embedded in the introns of protein-coding genes (Rodriguez et al., 2004). Intronic miRNAs can be co-transcribed with the host gene (Morlando et al., 2008) or transcribed independently (Monteys et al., 2010). Following transcription by RNA polymerase II (Lee et al., 2004) or RNA polymerase III (Borchert et al., 2006), miRNA biogenesis is a multistep process (Figure 1.7). The primary miRNA transcript (pri-miRNA) folds into a hair pin structure and is cleaved by the Drosha-DGCR8 microprocessor complex to release a ~70 nucleotide hairpin structure, termed the precursor miRNA (pre-miRNA) (Denli et al., 2004). Interestingly, some small spliced introns containing microRNAs readily form ~70 nucleotide hairpins (mirtrons) and bypass Drosha-DGCR8 cleavage (Ruby et al., 2007). pre-miRNAs are exported from the nucleus by Exportin5 (Bohnsack et al., 2004) and cleaved by Dicer to create ~20 nucleotide miRNA duplexes (Chendrimada et al., 2005). One strand functions as the mature miRNA and is incorporated into a RNA-induced

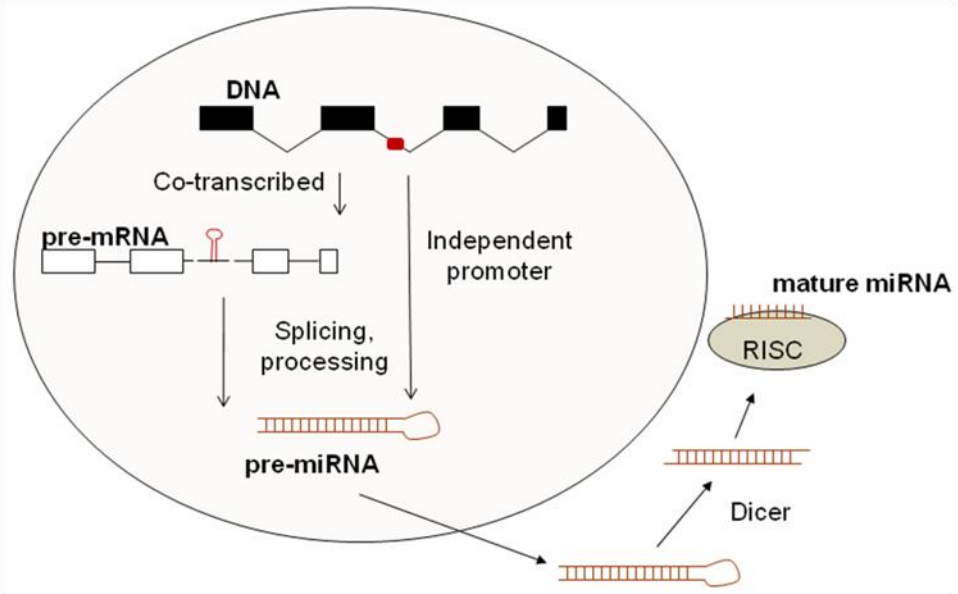

Figure 1.7: Intronic microRNA biogenesis

Intronic miRNA can be co-transcribed with its host gene or transcribed from an independent promoter. The intron or primary transcript is cleaved by the Drosha-DGCR8 microprocessor complex to yield a ~70 nucleotide pre-miRNA. The pre-miRNA is transported to cytoplasm by Exportin 5 where the stem loop is cleaved by Dicer and one strand is preferentially selected for incorporation into the RNA-induced silencing complex (RISC).

silencing complex (RISC), while the other strand is degraded (Schwarz et al., 2003). Typically, the mature miRNA functions by inhibiting translation or stability of mRNA transcripts within the cytoplasm (Filipowicz et al., 2008).

1.3.2 miR-103/7 structure and conservation

Pantothenate kinase genes *PANK1, PANK2* and *PANK3* host the highly conserved miR-103/7 microRNA family (Figure 1.8). miR-103 arises from miR-103-1 and miR-103-2 pre-miRNA sequences located within intron 5 of *PANK3* and *PANK2*, respectively. miR-107 differs from miR-103 by a single nucleotide and is located within *PANK1* intron 5. These microRNAs are conserved in all known vertebrates but not found in invertebrates (Wilfred et al., 2007). The conservation of miR-103-2, located within *PANK2*, is shown in Figure 1.9.

1.3.3 miR-103/7 expression

miR-103 and miR-107, first cloned from HeLa cells in 2002 (Mourelatos et al., 2002), have been detected in a multitude of tissues and cell lines. (Notably, high homology between miR-103 and miR-107 make it likely that they cross-hybridize in microarray, Northern and *in situ* hybridization histochemistry experiments; therefore, I will generalize the results from these experiments as representing miR-103/7 expression.) miR-103/7 are ubiquitously expressed (Babak et al., 2004; Baskerville and Bartel, 2005; Peltier and Latham, 2008), although miR-103/7 expression is enriched in the brain in humans (Babak et al., 2004; Baskerville and Bartel, 2005; Mellios et al., 2008; Wang, 2006) and mouse (Krichevsky et al., 2003; Miska et al., 2004). Recently, Peltier et al.

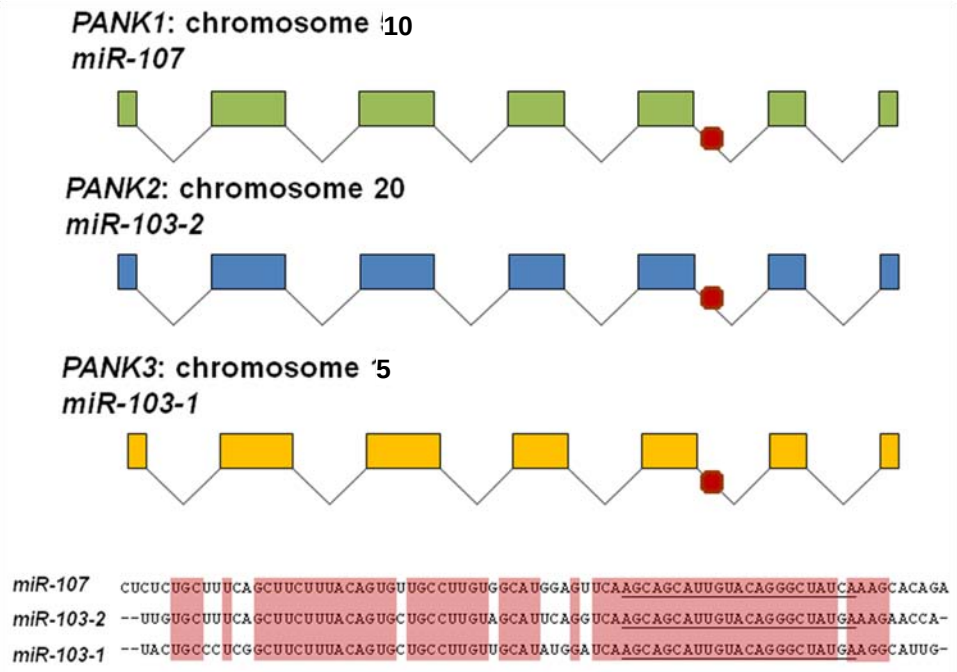

Figure 1.8: miR-103/7 family

The location of miR-107, miR-103-2 and miR-103-1 within exon 5 of *PANK1*, *PANK2* and *PANK3* are indicated by red octagons. The pre-miRNA sequences for these microRNAs are listed and nucleotides conserved in all miR-103/7 family members are highlighted. The mature microRNA sequences are underlined.

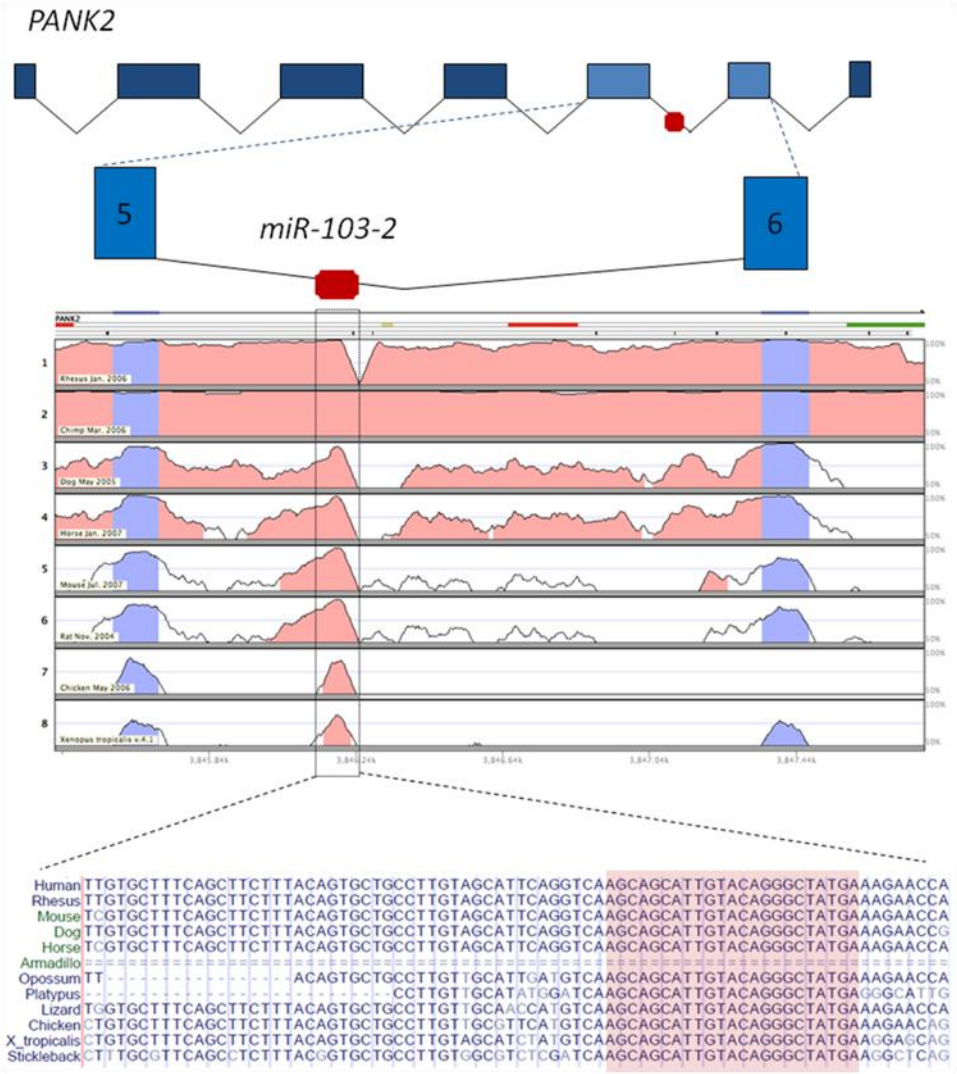

Figure 1.9: miR-103-2 conservation within *PANK2* intron 5

Conservation diagrams are adjusted from rVista Genome Browser (Ovcharenko et al., 2004) and UCSC Human Genome Browser (Rhead et al., 2010). The miR-103-2 nucleotide sequence is shown and mature miR-103 sequence is highlighted.

recommended miR-103 as a suitable reference gene for miRNA qRT-PCR due to its high and consistent expression across 13 human normal tissues and 5 pair of distinct tumor/normal adjacent tissue (miR-107 had similar expression, but at lower levels) (Peltier and Latham, 2008). However, differential expression and functional roles for miR-103 and miR-107 have been reported in a variety disease and cellular contexts.

As predicted by their conservation within pantothenate kinase genes (Wilfred et al., 2007), miR-103/7 show dynamic expression in cells governing lipid and energy metabolism. In particular, miR-103/7 expression is induced during adipogenesis and ectopic miR-103 expression in preadipocytes results in accelerated adipogenesis (Xie et al., 2009). In addition, miR-103/7 expression is up-regulated in the presence of high glucose in pancreatic β cells (Tang et al., 2009) and in the liver of rats with increased susceptibility to diabetes (Herrera et al., 2010).

Differential miR-103/7 expression has also been detected in many cancers, including pancreatic, lung, breast, colon and prostate cancer (Roldo et al., 2006; Volinia et al., 2006; Yamakuchi et al., 2010). Takahshi et al. recently reported that miR-103/7 expression is lower in lung tumors and lung cancer cell lines than in normal lung, and overexpression of miR-107 induces G1 cell cycle arrest (Takahashi et al., 2009). However, miR-103/7 levels are also reported to be increased (Volinia et al., 2006) or unchanged (Peltier and Latham, 2008) in lung cancer, making it difficult to draw general conclusions on miR-103/7 expression. Likewise, elevated miR-103/7 has been detected in pancreatic tumors (Roldo et al., 2006), but another report suggests that miR-107 is epigenetically inactivated in pancreatic cancer cell lines (Lee et al., 2009). Notably, miR-103/7 expression is also responsive to estrogen (Cicatiello et al., 2010), hypoxia

(Yamakuchi et al., 2010) and hot and cold stress (Marsit et al., 2006), which may influence miR-103/7 expression in oncogenesis.

In contrast to cancer, in neurological disease miR-103/7 is clearly down regulated. Nelson et al. have recently demonstrated by *in situ* hybridization that miR-103/7 are found in human entorhinal cortex (EC) and transentorhinal cortex (TEC), two regions that are often impacted by neurodegeneration (Nelson et al., 2010). Interestingly, there is a correlation of decreased miR-103/7 expression and increased neurotic plaques and neurofirillary tangles in Alzheimer's disease (AD) brains (Nelson and Wang, 2010; Wang et al., 2008). Notably, miR-103/7 are also down regulated in mouse hippocampus following traumatic brain injury (Redell et al., 2009) and in human fetuses with anencephaly (Zhang et al., 2010), indicating that expression is affected by a range of neuronal insults.

The differential expression of miR-103/7 in these physiological contexts begs the question: what regulates miR-103/7 expression? In addition, are miR-103 and miR-107 co-regulated with their host genes? There is precedence to think not. Several reports conclude that ~30% of intronic microRNA are transcriptionally regulated independently of their host promoters (Monteys et al., 2010; Ozsolak et al., 2008; Wang and Li, 2009). Indeed, there is low correlation of miR-103 expression with *PANK2* and *PANK3* or miR-107 with *PANK1* on miRNA and mRNA microarrays (Baskerville and Bartel, 2005; Wang et al., 2008). Likewise, co-expression is not predicted *in silico,* based on the host genes' intron size and miR-103/7 location within introns (Wang et al., 2009).

Recently, Monteys et al. have described an independent miR-107 promoter (Monteys et al., 2010). They identified a putative transcriptional start site (TSS) ~1kb

upstream of miR-107 (within *PANK1* exon 5) that is sufficient to drive miR-107 expression in a promoterless plasmid (Monteys et al., 2010). In addition, p53 and C/EBPalpha binding sites are located near the putative TSS (Monteys et al., 2010). This finding is significant because recent studies have also shown that miR-107 expression is up regulated by p53 following cellular exposure to etoposide, a telomerase II inhibitor (Yamakuchi et al., 2010). A functional p53 binding site within the *PANK1* promoter has been credited with p53 mediated miR-107 regulation (Yamakuchi et al., 2010); however, future studies will be necessary to differentiate p53 regulation through *PANK1* and the intronic miR-107 promoter.

In contrast to miR-107, miR-103 may be dependent on *PANK2* and *PANK3* promoters for transcription. Interestingly, Monteys et al. did not identify a transcriptional start site or transcriptional regulatory elements upstream of miR-103-1 or miR-103-2 (Monteys et al., 2010). Likewise, Ozsolak et al. predict that miR-103-1 relies on the *PANK3* promoter for expression (Ozsolak et al., 2008). If miR-103 transcription is dependent on host gene transcription, differential expression of the microRNA and host gene may also be explained by post-transcriptional regulation.

1.3.4 miR-103/7 targets

Several microRNA target prediction programs are available for *in silico* identification of putative miR-103/7 MREs (Yue et al., 2009). These programs predict hundreds of possible miR-103/7 targets. However, three targets with possible roles in neurodegeneration have recently been experimentally validated (Wang et al., 2008; Wang et al., 2010; Yamakuchi et al., 2010).

In 2008, Wang et al. identified β-site precursor protein cleaving enzyme (BACE1) as a miR-103/7 target (Wang et al., 2008). BACE1 cleaves β-amyloid precursor protein to generate the neurotoxic β-amyloid peptide Aβ (Haniu et al., 2000) and its dysregulation may play a role in AD pathogenesis (Guo and Hobbs, 2006). BACE1 mRNA levels are inversely proportional to miR-103/7 expression in Alzheimer's brains (Nelson and Wang, 2010; Wang et al., 2008) and putative miR-103/7 microRNA recognition elements (MRE) are predicted within the BACE1 3'UTR (Wang et al., 2008). miR-103/7 regulation through the MRE was validated by inserting it in the 3'UTR of a luciferase reporter and measuring change in activity compared with a mutant MRE in HeLa cells (Wang et al., 2008).

In April 2010, Yamakuchi et al. identified hypoxia inducible factor 1β as a miR-103/7 target (Yamakuchi et al., 2010). HIF-1β and HIF-1α make the heterodimer HIF-1, which is a transcription factor that mediates cellular response to hypoxia (Pugh and Ratcliffe, 2003). HIF-1β has a highly conserved miR-107 recognition element in its 3'UTR and down regulation of HIF-1β results in a block of hypoxic signaling within the cells (Yamakuchi et al., 2010). miR-107 overexpression and inhibition experiments confirm that it inhibits HIF-1β expression (Yamakuchi et al., 2010). In addition, miR-107 overexpression in mice results in decreased tumor size and number of vessels (Yamakuchi et al., 2010). Interestingly, HIF has also recently been proposed as target for neuroprotective therapies due to its roles in cellular survival (Correia and Moreira, 2010).

In July 2010, Wang et al. identified a third miR-103/7 target: granulin (GRN) (Wang et al., 2010). Granulin is an extracellular glycoprotein that plays a role in cell growth, inflammation and wound repair (Bateman and Bennett, 2009). In addition, *GRN*

mutations lead to neuronal atrophy and frontotemporal lobar dementia, an autosomal dominant disease (Snowden et al., 2006). This target was identified by overexpressing miR-107 in H4 cancer cells, which have a partial glial/neuronal phenotype, immunoprecipitating microribonuclear particles (mRNPs) and identifying bound mRNA transcripts by microarray (Wang et al., 2010). GRN regulation was confirmed by luciferase reporter assays and GRN protein levels following miR-107 overexpression and inhibition in cell culture (Wang et al., 2010). In addition, an increase in GRN expression correlated with miR-107 down regulation following cortical brain injury in mouse (Wang et al., 2010).

1.4 Phospholipase A2 group VIA

In 2006, *PLA2G6* was identified as the INAD causative gene by linkage analysis of a large consanguineous Pakistani family with NBIA and 12 smaller families with INAD (Morgan et al., 2006). *PLA2G6* encodes calcium-independent phospholipase A_2 group VIA ($iPLA_2$-VIA).

1.4.1 Gene and protein structure

The large phospholipase A_2 superfamily can be subdivided into four major families: secreted PLA_2s, cytosolic calcium-dependent PLA_2s, platelet activating factor acetylhydrolases, and calcium-independent PLA_2 ($iPLA_2$) (Six and Dennis, 2000). As the name implies, the $iPLA_2$ family is unique because its family members do not require Ca^{2+} for enzyme activity. The $iPLA_2$ family has six members: $iPLA_2$-VIA (also called $iPLA_2\beta$), $iPLA_2$-VIB ($iPLA_2\gamma$), $iPLA_2$-VIC (neuropathy target esterase (NTE)), $iPLA_2$-

VID (adiponutrin), iPLA$_2$-VIE (TTS-2.2) and iPLA$_2$-VIF (GS2) (Ackermann et al., 1994; Mancuso et al., 2000; Schaloske and Dennis, 2006). cPLA$_2\gamma$ is also a calcium-independent PLA$_2$, however it is not included in the phospholipase A2 VI group because it has greater sequence homology with group IV phospholipases (Balboa and Balsinde, 2002). Of note, iPLA$_2\alpha$ is a non-mammalian glycoprotein of the patatin family and was named based on sequence similarity to a cytosolic calcium-dependent PLA$_2$ but does not belong in the iPLA$_2$ family (Andrews et al., 1988).

Human *PLA2G6* includes 17 exons spanning over 69 kb on chromosome 22 and gives rise to multiple splice variants (Figure 1.10) (Larsson Forsell et al., 1999; Larsson et al., 1998). iPLA$_2$-VIA-1 (A-1) encodes a cytosolic ~85 kDa enzyme with eight ankyrin-like repeats, a lipase consensus sequence motif (Gly-X-Ser-X-Gly), calmodulin binding domain, ATP-binding domain, bipartite nuclear localization sequence and caspase cleavage sites (Atsumi et al., 2000; Lauber et al., 2003; Ma and Turk, 2001). iPLA$_2$-VIA-2 (A-2) is identical to A-1 with the exception of an insertion within the eighth ankyrin repeat that adds a proline-rich 54-amino acid stretch upstream of the lipase consensus sequence (Ma et al., 1999). iPLA$_2$-VIA-3 (A-3) is identical to A-2 except that a C-terminal 158 nucleotide insertion introduces a premature stop codon; the enzymatic activity of this truncated isoform has not been investigated (Balsinde and Balboa, 2005). Finally, two catalytically inactive iPLA$_2$-VIA variants (Ank-1 and Ank-2) contain only the ankyrin repeats and lack an active site.

iPLA$_2$-VIA and iPLA$_2$-VIB are the predominant iPLA$_2$ family members. However, iPLA$_2$-VIB lacks ankyrin repeats and contains competing mitochondrial and peroxisomal localization signals (Mancuso et al., 2000; Mancuso et al., 2004).

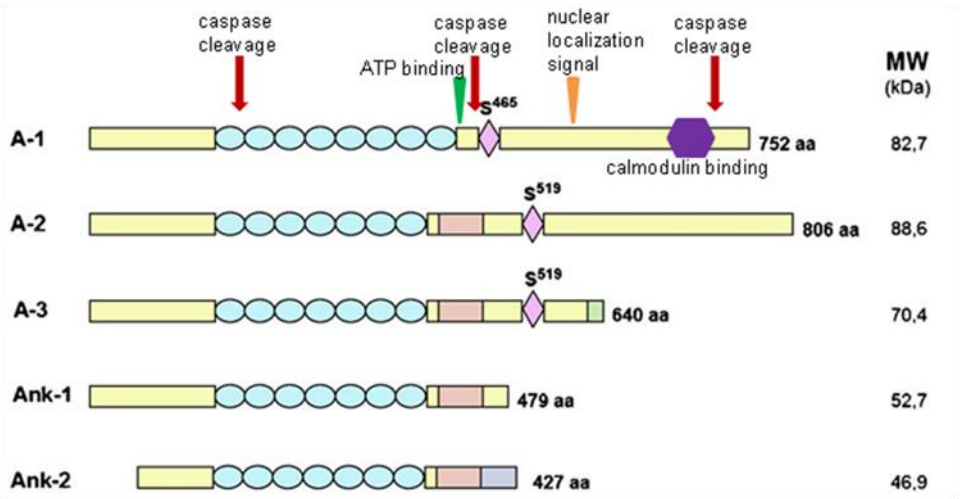

Figure 1.10: iPLA$_2$-VIA splicing variants

Identical sequences in all variants are shown in yellow. Sequence changes with respect to iPLA2-VIA-1 are shown as pink, green, and blue rectangles. The ankyrin repeats are represented as blue circles, and the catalytic serines within the lipase consensus sequence motif (Gly-X-Ser-X-Gly) are shown as pink diamonds. The relative location of caspase cleavage sites (red arrow), ATP binding domain (green wedge), nuclear localization signal (orange wedge) and the calmodulin binding site (purple hexagon) are also shown. Amino acid number and the calculated molecular mass of each variant are indicated. Figure adapted and used with permission from (Balsinde and Balboa, 2005).

Historically, the $iPLA_2$ inhibitor bromoenol lactone (BEL) has been used to study these proteins; however, the selectivity of BEL *in vivo* is unclear (Balsinde and Dennis, 1996). In 2002, Jenkins et al. found that $iPLA_2$-VIA and $IPLA_2$-VIB show different sensitivities towards the BEL enantiomers, which has enabled some dissection of $iPLA_2$ function (Jenkins et al., 2002). In addition, recent studies using antisense technologies have begun to clarify $iPLA_2$-VIA cellular roles.

1.4.2 Function and regulation

Phospholipase A_2 enzymes catalyze the hydrolysis of sn-2 ester bonds of glycerophospholipids, producing free fatty acids and lysophospholipids (Figure 1.11) (Dennis, 1994). $iPLA_2$-VIA can cleave any phospholipid because it lacks specificity for the fatty acid at the sn-2 position (Ackermann et al., 1994; Tang et al., 1997). Therefore, $iPLA_2$-VIA is implicated in multiple cellular processes. $iPLA_2$-VIA is important for membrane homeostasis and remodeling (Balsinde et al., 1997; Balsinde et al., 1995). In addition, $iPLA_2$-VIA has been implicated in apoptosis (Balsinde et al., 2006), inflammation (Sun et al., 2009), cell growth (Sun et al., 2009), chemotaxis (Carnevale and Cathcart, 2001) and secretion (Balboa et al., 2003).

$iPLA_2$-VIA regulation involves ankyrin domain-regulated oligomerization, calmodulin binding and caspase cleavage (Balsinde and Balboa, 2005). $iPLA_2$-VIA functions as a tetramer, and deletion of its ankyrin repeats, which may facilitate protein-protein interactions, results in an inactive enzyme (Tang et al., 1997). Interestingly, splice variants comprised solely of ankyrin repeats may regulate $iPLA_2$ activity by interfering with oligomerization of the active proteins (Larsson et al., 1998).

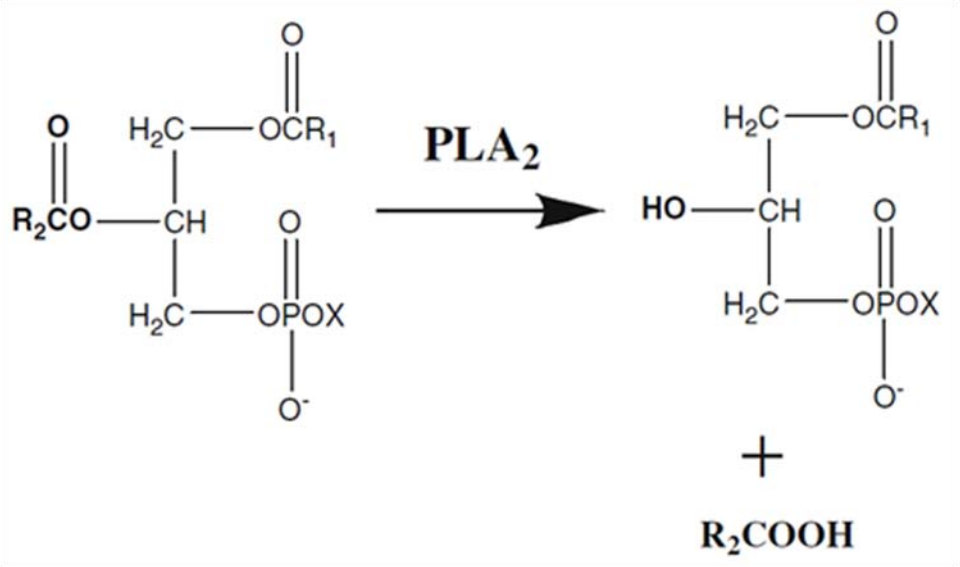

Figure 1.11: Phospholipase A_2 activity

Phospholipid on the left is hydrolyzed at the sn-2 position to yield lysophospholipid and free fatty acid on the right. Figure adapted and used with permission from (Burke and Dennis, 2009)

Additionally, calmodulin reversibly binds and inhibits iPLA$_2$-VIA in the presence of Ca^{2+} (Jenkins et al., 2001). By this mechanism, iPLA$_2$-VIA may trigger Ca^{2+} entry following depletion of intracellular Ca^{2+} stores (Smani et al., 2003). Finally, caspase cleavage has been found to increase iPLA$_2$-VIA activity; this increase may accelerate phospholipid turnover and lead to apoptotic membranous changes (Atsumi et al., 2000).

iPLA$_2$-VIA is ubiquitously expressed. In the original *PLA2G6* gene characterization, iPLA$_2$-VIA expression was present in all 23 tissues examined by Northern blot although each splice variant had a unique tissue distribution (Larsson Forsell et al., 1999). iPLA$_2$-VIA expression has also been detected in numerous cell lines including the human retinal pigment epithelium (RPE) cell line ARPE-19 (Kolko et al., 2009), murine macrophages cell line P388D1(Ackermann et al., 1994), pancreatic cells (Ma et al., 1997; Ramanadham et al., 2004), human astrocytic cells (A172) (Peterson et al., 2007) and renal cells (Cummings et al., 2004). In addition, iPLA$_2$-VIA, as well as iPLA$_2$-VIB, expression has been detected in the adult human eye, rat brain and monkey brain by immunohistochemistry (Kolko et al., 2007; Ong et al., 2005a; Ong et al., 2005b; Shirai and Ito, 2004).

1.4.3 Mutations and hypotheses of disease

In INAD, defects in iPLA2-VIA may disrupt phospholipid membrane homeostasis and a number of signaling pathways, leading to pathological changes. *PLA2G6* deletion, missense, splice site and nonsense mutations are found in INAD patients (Morgan et al., 2006). However, homozygous null mutations are only found in classic INAD patients, suggesting that complete lack of iPLA$_2$-VIA may cause early

onset disease (Morgan et al., 2006). Deletion, missense or splice site *PLA2G6* mutations may cause less severe disease by having a limited effect on iPLA2-VIA enzymatic activity, regulation or cellular localization.

1.5. Objectives of current study and approach

The long term goal of the Hayflick laboratory is to develop effective treatment for NBIA. In the past ten years, significant strides toward this goal have been made by the *PANK2* and *PLA2G6* gene discoveries. However, much remains unclear about these genes and the mechanism by which their mutation causes neurodegeneration. Characterizing the expression and function of *PANK2* and *PLA2G6* informs the difficult task of developing and testing potential treatments. Toward this goal, my thesis projects focus on three questions. First, what controls the transcriptional regulation of *PANK2*? Second, is the miR-103/7 family co-expressed with pantothenate kinases? Third, is *PLA2G6* expressed in prenatal human neuronal development?

Chapter 2

Transcriptional regulation of *PANK2*

Chapter 2.1

Characterization of the human *PANK2* promoter

*manuscript in press in *Gene* (Polster et al., 2010)

Brenda J Polster[1*], Moon Y Yoon[1], and Susan J Hayflick[1]

[1] Molecular and Medical Genetics, Oregon Health and Science University, Portland OR.

3181 SW Sam Jackson Park Rd, Portland OR 97239, USA

[*]corresponding author
Phone: 503 494 5326
Fax: 503 494 4411
Email: polsterb@ohsu.edu

ABSTRACT

Pantothenate kinase 2 **(**PANK2) is an essential regulatory enzyme in coenzyme A biosynthesis. *PANK2* mutations cause pantothenate kinase-associated neurodegeneration (PKAN), which leads to pigmentary retinopathy, progressive dystonia and other abnormalities. Two nearly identical PANK2 isoforms have been described: short PANK2 and mature PANK2, which are processed from a precursor isoform. Since the biological relevance of these isoforms remains unclear, we sought to explore their transcriptional regulation. Here we show that their regulation is distinct and describe a promoter for the short isoform of PANK2. Moreover, we identify potential regulators of *PANK2* expression, including NF-Y, FOXN4 and the human heterogeneous nuclear ribonucleoprotein A/B family. These findings validate expression of the short PANK2 isoform and enable predictions about potentially deleterious sequence variants in the regulatory region of this human disease gene.

Keywords: pantothenate kinase, hnRNPA/B, FOXN4, NF-Y, PKAN

Abbreviations: PKAN, pantothenate kinase-associated neurodegeneration; PANK, pantothenate kinase; EMSA, electrophoresis mobility shift assay.

1. INTRODUCTION

Pantothenate kinase (PANK) is the rate limiting enzyme in the biosynthesis of coenzyme A. The pantothenate kinase gene family includes *PANK1*, *PANK2*, *PANK3* and *PANK4*, which give rise to five functional isoforms; PANK1a, PANK1b, PANK2, PANK3 and PANK4 (Rock et al., 2002; Zhou et al., 2001). *PANK1*, *PANK2* and *PANK3* are functional kinases encoded from six conserved core exons preceded by differing initiation exons (Zhou et al., 2001). Also, PANK2 differs from other pantothenate kinases in its mitochondrial localization and its regulation by acyl-CoA and palmitoylcarnitine (Hortnagel et al., 2003; Johnson et al., 2004; Leonardi et al., 2007a; Rock et al., 2000).

We investigated the transcriptional regulation of *PANK2*, the causative gene for pantothenate kinase-associated neurodegeneration (PKAN), an autosomal recessive disease characterized by dystonia and retinal degeneration (Zhou et al., 2001). A critical question in PKAN pathogenesis is why disruption of a ubiquitously expressed gene causes a neurological-specific disease. Thus we sought to identify regulatory factors controlling *PANK2* expression.

Multiple PANK2 isoforms have been identified (Hortnagel et al., 2003; Kotzbauer et al., 2005; Zhou et al., 2001). Initially, we described a mitochondrial 50.6 kDa PANK2 isoform with a leucine initiation codon (CTG) (Zhou et al., 2001). This protein has become known as the PANK2 short form (sPANK2) (Zhang et al., 2006). Subsequently, a larger precursor isoform (pPANK2) was identified that begins translation 330 nucleotides upsteam with a methionine initiation codon (ATG) (Hortnagel et al., 2003). This precursor isoform is sequentially cleaved at two sites by the mitochondrial processing peptidase, yielding intermediate (iPANK2) and mature (mPANK2, 48 kDa)

isoforms (Kotzbauer et al., 2005). sPANK2 and mPANK2 both localize to mitochondria, although they utilize different localization signals and may be subject to distinct transcriptional, translational and post-translational regulation (Hortnagel et al., 2003; Johnson et al., 2004; Kotzbauer et al., 2005).

In this work, we sought to characterize the transcriptional regulation of *PANK2*. These studies advance our understanding of the regulation of short and mature PANK2 isoforms and allow us to test, for the first time, whether sequence variants in the region affect transcription.

2. MATERIALS AND METHODS

2.1 Database Searches

Human *PANK2* genomic organization was obtained from the UCSC Human Genome Browser (Kent et al., 2002) and sequence comparisons were performed using the ECR Browser (Ovcharenko et al., 2004) , Mulan (Ovcharenko et al., 2005) and ClustalW2 (Larkin et al., 2007). The transcription factor binding sites in the promoter region were analyzed using MatInspector (Cartharius et al., 2005). Prediction of CpG islands and TATA-dependent transcription initiation sites were generated by CpG Island Searcher and CorePromoter (Takai and Jones, 2003; Zhang, 2005).

2.2 Plasmid Construction

We employed three methods for constructing plasmids. The *PANK2* promoter fragments in plasmids -2351/-301, -2351/+13, -1332/+13, -1332/-301, -633/+13, -327/+13, -102/+13, -327/-76, -180/-76, -327/-144, -327/-217 and -247/-144 were

amplified from human genomic DNA by PCR using primers (Table 2.1) containing *NheI* (forward primers) or *HindIII* (reverse primers) recognition sites. The promoter fragments were cloned into a promoter-less luciferase reporter vector, pGL3-Basic (Promega). We created additional reporter plasmids (-262/+13, -216/+13, -162/+13) using the Erase-a-Base Kit (Promega). Briefly, the -633/+13 plasmid was linearized with *NheI* and *SacI* and digested with Exonuclease III. The digestion was stopped by S1 Nuclease, treated with Klenow DNA polymerase, ligated and transformed into competent cells. To create the -254/-76, -237/-76, and -211/-76 truncation plasmids, we generated novel *NheI* restriction sites (GCTAGC) in the -327/-76 plasmid with the QuikChange Site-Directed Mutagenesis Kit (Stratagene). Briefly, we designed oligonucleotides with our desired nucleotide change (Table 2.2), annealed the oligonucleotides to the plasmid template (-327/-76), transcribed with *PfuTurbo* polymerase, treated with *DpnI* endonuclease and transformed into competent cells. *NheI* digestion and re-ligation of the plasmids generated the truncated plasmids. We also used the QuikChange Site-Directed Mutagenesis Kit to alter putative transcription factor binding sites (Ets1, IRF4, NF-Y, FOXN4, NFkB) with the -327/-76 plasmid.

2.3 RNA Ligase-mediated Rapid Amplification of cDNA Ends (RACE)

Total RNA from human brain (Ambion) was used to identify the transcriptional start points with the GeneRacer Kit (Invitrogen). Briefly, 5 mg RNA was treated with calf intestine alkaline phosphatase and tobacco acid pyrophosphatase, ligated with an RNA adapter oligonucleotide using T4 RNA ligase, and random-primed for reverse

Table 2.1
PCR primer sequences for plasmid construction

Name	Sequence
Hp2prom5F (-2351)	AGGCTAGCGATTACAGGCACGCACCACTACGCCCAGCTAAG
Hp2prom6F (-1332)	AGGCTAGCCACAAGCGAAGCTCAACCTTTTTGTTCAGCC
Hp2prom3F (-633)	AGGCTAGCTCTCTCCAACGCAGGCGGAAAGGAGG
Hp2prom2F (-327)	AGGCTAGCAGGAGGCTCGGGCCCTTCCACCCACG
Hp2prom9F (-247)	AGGCTAGCCCTCCGCGGAACCCGGATCCCCTCCTCCACCACCC
Hp2prom10F (-180)	AGGCTAGCGACGGAGGCACGGTCAATCCTCCTCGAGTTAGGGAG
Hp2prom1F (-102)	AGGCTAGCGATTGGCTTCCTGCGCGTTGGCGCAAC
Hp2prom7R (-217)	GCAAGCTTGGGTGGAGGAGGGGATCCGGGTTCCGCGGAGG
Hp2prom8R (-144)	GCAAGCTTGCTCCCTAACTCGAGGAGGATTGACCGTGCCTCCGTC
Hp2prom4R (-76)	GCAAGCTTGGTTGCGCCAACGCGCAGGAAGCCAATC
Hp2prom3R (-301)	GCAAGCTTGGCGTGGGTGGAAGGGCCCGAGCCTCCTCAT
Hp2prom1R (+13)	GCAAGCTTGCAAGCCCCCCAGCGTCGGATTCCTTCTCGCC

Table 2.2
Oligonucleotides for QuikChange Site-Directed Mutagenesis

Plasmid	Primer	Sequence*
-254/-76	hp2promqct3F	CCATCACTCTCTTCTGGGCTACGCTAGCTTCTCTTCCTCCGC
	hp2promqct3R	GCGGAGGAAGAGAAGCTAGCGTAGCCCAGAAGAGAGTGATGG
-237/-76	hp2promqct4F	GGGCTACACCGCCTTCTCTTCCTCGCTAGCACCCGGATCCCC
	hp2promqct4R	GGGGATCCGGGTGCTAGCGAGGAAGAGAAGGCGGTGTAGCCC
-211/-76	hp2promqct6F	CGGATCCCCTCCTCCACGCTAGCCTCCCCGCCCCGTCAC
	hp2promqct6R	GTGACGGGGCGGGGAGGCTAGCGTGGAGGAGGGGATCCG
Ets1	hp2promETS_mt1f	CTACACCGCCTTCT*ctt**aa*TCCGCGGAACCCGG
	hp2promETS_mt1r	CCGGGTTCCGCGGA*tt**aag*AGAAGGCGGTGTAG
IRF4	hp2promIRF4_mt1f	CTCTTCCTCCGCG*a**aat*CCGGATCCCCTCCTC
	hp2promIRF4_mt1r	GAGGAGGGGATCCGG*a**ttt*CGCGGAGGAAGAG
5' NF-Y	hp2promNFY_mt1f	CACGATAGCCTCTC*atgtg*ACGGAGGCACGGTC
	hp2promNFY_mt1r	GACCGTGCCTCCGT*cacat*GAGAGGCTATCGTG
FOXN4	hp2promWHN_mt1f	GTTAGGGAGCCGACTGG*aatc*GAGGCCTTTGGG
	hp2promWHN_mt1r	CCCAAAGGCCTC*gatt*CCAGTCGGCTCCCTAAC
NfkB	hp2promNFk_mt1f	GGCCTTTGGGCCG*taac*CAGCCTCGTCGG
	hp2promNFk_mt1r	CCGACGAGGCTG*gtta*CGGCCCAAAGGCC
3' NF-Y	hp2promNFY2_mt1f	CAGCCTCGTCGG*atgtg*CTTCCTGCGCGTTG
	hp2promNFY2_mt1r	CAACGCGCAGGAAG*cacat*CCGACGAGGCTG

*Nucleotide changes are underlined and putative transcription factor binding sites are in lowercase italics.

transcription. cDNA was amplified by nested PCR. The PCR products were cloned into pCRII TOPO TA cloning vector (Invitrogen) and sequenced.

2.4 Cell Culture, Transient Transfections and Luciferase Assays

Human neuroblastoma (SH-SY5Y) cells were cultured in RPMI with 10% FBS, 10 ng/ml human neuron growth factor, non-essential amino acids and penicillin/streptomycin antibiotics at 37ºC and 5% CO2. Cells were seeded in 12-well plates, grown to 90% confluency, and transfected using Lipofectamine 2000 (Invitrogen) according to manufacturer's instructions. Each well was transfected with 0.4 µg CMV-β-galactosidase and 0.4 µg of pGL3-Basic or luciferase reporter plasmids containing the 5'flanking fragments of human *PANK2* gene. Cells were harvested in 100 µl Passive Lysis Buffer (Promega) 24 hours after transfection. To assay for β-galactosidase activity, 50 µl of cell lysate was combined with 60 µl Z buffer (60mM Na_2HPO_4, 40mM NaH_2PO_4, 10 mM KCl, 1 mM $MgSO_4$, 50mM 2-Mercaptoethanol, pH 7.5) and 40 µl ONPG substrate (Sigma) (4 mg/ml in 60 mM Na_2HPO_4, 40mM NaH_2PO_4, pH 7.5 buffer) and incubated at 30ºC for 30 minutes. The reaction was quenched by adding 100 µl of 1 M Na_2CO_3 and measured at A420. To assay for luciferase activity, 20 µl of cell lysate was combined with 300 µl of GlyGly-ATP (25mM Glycylglycine, 15 mM $MgSO_4$, 5 mM ATP) and 100 µl of luciferin (Promega) (300 µg/ml) and measured on a luminometer. The luciferase values were normalized to β-galactosidase activity. Each transfection was performed in triplicate and repeated at least 3 times.

2.5 Electrophoresis Mobility Shift Assay (EMSA)

Nuclear extracts were prepared from SH-SY5Y cells. Briefly, ~2 x 10^7 cells were washed with ice cold PBS, harvested in CE buffer (1 mM HEPES KOH, 6 mM KCl, 100 µM EDTA, 100 µM DTT, 100 µM PMSF, Complete Protease Inhibitors EDTA-free (Roche)) plus 0.5% NP-40 and centrifuged to pellet the nuclei. The pellet was washed in CE buffer, resuspended in 200ul NE buffer (250 µM Tris HCl, 60 µM KCl, 1 mM DTT, 1 mM PMSF, Complete Protease Inhibitors EDTA-free (Roche)), lysed by freeze/thaw cycles in liquid nitrogen, and centrifuged. The final supernatant was frozen in liquid nitrogen and stored at -80ºC.

Single stranded probes labeled with IRDye-700 were designed to contain the putative binding sites for predicted transcription factors within the *PANK2* promoter (Table 3).The probes were annealed at 95ºC, cooled to room temperature, and used in DNA-protein binding reactions according to the Odyssey Infrared EMSA Kit (LiCor Biosciences). Briefly, the labeled oligonucleotides were incubated with ~10ug SH-SY5Y nuclear extract at room temperature for 20 minutes and resolved on a 4% TBE native acrylamide gel at 4ºC, avoiding light exposure. For competitor assays, oligonucleotides with identical sequence to EMSA1, EMSA2, EMSA3, EMSA4 and EMSA5 forward and reverse oligonucleotides were ordered from Invitrogen. Additional competitor oligonucleotides were designed (Table 2.3) to contain putative or mutated binding sites for NF-Y and FOXN4 (Schlake et al., 1997; Zhu et al., 2004). The oligonucleotides were annealed at 95ºC, cooled to room temperature, and added in to the DNA-protein binding reaction in 200-fold excess of IRDye-700 labeled probes. For antibody binding, the

Table 2.3
Oligonucleotides for EMSA

EMSA probe	oligonucleotide	Sequence
EMSA1	hp2promEMSA1F	GACTGGACGCGAGGCCTTTGGGCCGTCCCCAGCCTCGTCG
	hp2promEMSA1R	CGACGAGGCTGGGGACGGCCCAAAGGCCTCGCGTCCAGTC
EMSA2	hp2promEMSA2F	TCGTCGGATTGGCTTCCTGCGCGTTGGCGCAAC
	hp2promEMSA2R	GTTGCGCCAACGCGCAGGAAGCCAATCCGACGA
EMSA3	hp2promEMSA3F	CGCCTTCTCTTCCTCCGCGGAACCCGGATC
	hp2promEMSA3R	GATCCGGGTTCCGCGGAGGAAGAGAAGGCG
EMSA4	hp2promEMSA4F	AGCCTCTCATTGGACGGAGGC
	hp2promEMSA4R	GCCTCCGTCCAATGAGAGGCT
EMSA5	hp2promEMSA5F	GGGAGCCGACTGGACGCGAGGCCTTTGGGC
	hp2promEMSA5R	GCCCAAAGGCCTCGCGTCCAGTCGGCTCCC
FOXN4	FOXN1siteF	ATAGGGCGAATTGGGTACCAAAGGGACGCTATCGAGCTCCAGCTTT
	FOXN1siteR	AAAGCTGGAGCTCGATAGCGTCCCTTTGGTACCCAATTCGCCCTAT
NF-Y	NFYsiteF	AGACCGTACGTGATTGGTTAATCTCTT
	NFYsiteR	AAGAGATTAACCAATCACGTACGGTCT
FOXN4 mt	FOXN1mt1F	ATAGGGCGAATTGGGTACCAAAGGGAGCCTATCGAGCTCCAGCTTT
	FOXN1mt1R	AAAGCTGGAGCTCGATAGGCTCCCTTTGGTACCCAATTCGCCCTAT
NF-Y mt	NFYmt1F	AGACCGTACGTGATCAGTTAATCTCTT
	NFYmt1R	AAGAGATTAACTGATCACGTACGGTCT

reaction mixture was incubated with 2 µg of hnRNPA/B (Santa Cruz Biotechnology, cs-15385) or STAT3 (kind gift from Dr. David Farrell, OHSU) antibody prior to addition of labeled oligonucleotides. As a control for binding conditions, the reaction was also incubated with labeled oligonucleotides prior to the addition of 2 µg of antibody. The gels were imaged at 700 nm using the LiCor Odyssey Imaging System.

2.6 Proteomic Analysis

We submitted native 4% acrylamide TBE gel slices to the OHSU Proteomics Shared Resource for analysis. The samples were digested with trypsin and analyzed by LC-MS using an Agilent 1100 series capillary LC system (Agilent Technolgies) to elute

the peptides from a Zorbax SB-C18 column (Agilent Technologies, cat. No. 5064-8258) into an LTQ linear ion trap mass spectrometer (ThermoFisher). Electrospray ionization was performed with an ion max source fitted with a 34 gauge metal needle (ThermoFisher, cat. No. 97144-20040). Peptides were identified by comparing the observed MS/MS spectra to theoretical MS/MS spectra of peptides using the program Sequest (Version 27, rev. 12, ThermoFisher). Lists of identified proteins were assembled using the program Scaffold (version 2_06_00, Proteome Software).

3. RESULTS

3.1 In silico analysis of PANK2

28 out of 39 *PANK2* spliced expressed sequence tags (ESTs) correspond to the initiating exon of *PANK2* transcript variant 1 (NM_153638) in the UCSC Human Genome Browser (Figure 2.1a). This transcript gives rise to the mitochondrial PANK2 isoforms sPANK2 and pPANK2. The less abundant *PANK2* transcript variants 2 (NM_153640) and 3 (NM_024960) are predicted to encode a non-functional cytosolic PANK2 isoform (Zhang et al., 2006). The dominance of variant 1 expression is supported by the mitochondrial localization of PANK2 in human brain sections and tissue culture models (Hortnagel et al., 2003; Johnson et al., 2004; Kotzbauer et al., 2005). *In silico* analysis of the *PANK2* 5' region reveals the presence of a large CpG island spanning the initiating exons for *PANK2* transcript variants 1, 2 and 3, suggesting that *PANK2* expression is driven by a TATA-less promoter (Takai and Jones, 2003).

In addition, there is a lack of sequence conservation in the 5'end of *PANK2* transcript variant 1(Figure 2.1a) (Ovcharenko et al., 2004). Overall, *PANK2* variant 1 has

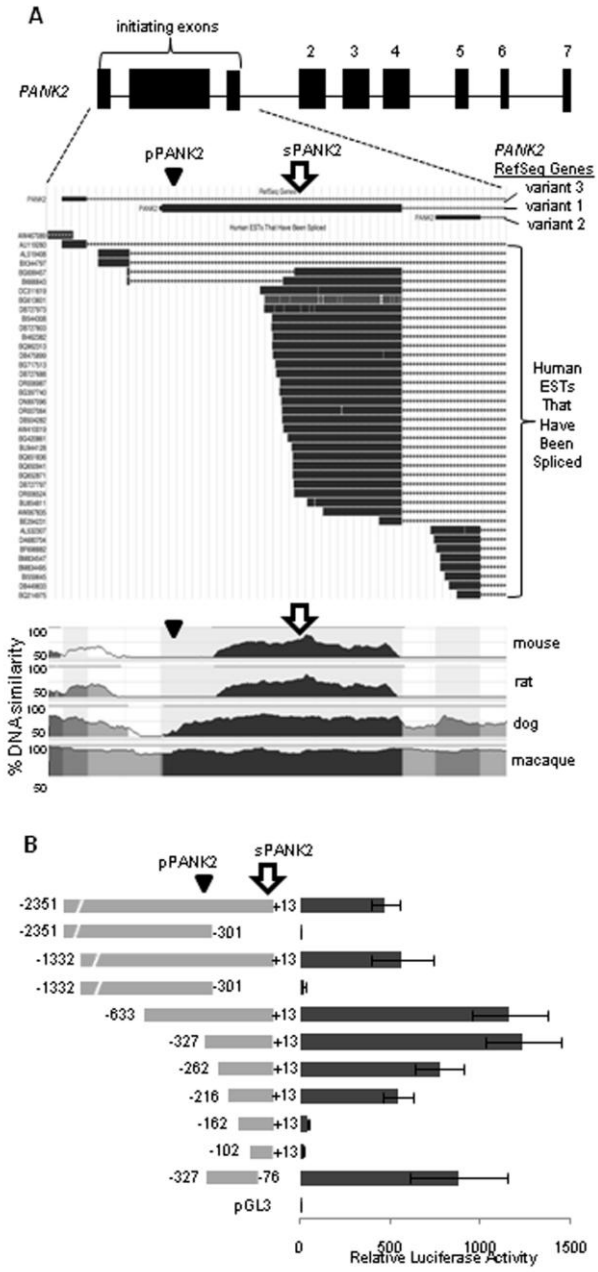

Figure 2.1: ***PANK2* structure and transcriptional activity**

(A) *PANK2* genomic structure, RefSeq mRNA variants, human spliced ESTs and sequence conservation. The sPANK2 leucine initiation codon (arrow) and pPANK2 methionine initiation codon (triangle) are designated. The enhanced region is adapted from the UCSC Human Genome Browser (*http://genome.ucsc.edu)* and corresponds to chr20:3869450-3870650 on Human GRCh37 Assembly (hg19)(Kent et al., 2002). The conservation summary is adapted from the ECR Browser (ecrbrowser.dcode.org) (Ovcharenko et al., 2004).

(B) Luciferase activity in SH-SY5Y cells driven by serial truncation of *PANK2*. Luciferase activity was normalized to β-galactosidase activity and results are shown as fold change from the empty pGL3 vector. The error bars represent standard error of three independent experiments.

87% identity to mouse *Pank2* cDNA, although the sequence conservation ends downstream of the pPANK2 translation initiation site. In fact, mouse, cat, dog and cow *PANK2* transcripts do not contain the pPANK2 mitochondrial localization signal and are predicted to initiate translation near the 5' end of exon 1 (Leonardi et al., 2007b).

3.2 Identification of a promoter for sPANK2 expression

In search of a promoter, we analyzed the transcriptional activity of DNA fragments from the 5' end of *PANK2* in the human neuroblastoma cell line, SH-SY5Y. We designated nucleotide numbering with +1 corresponding to the cytosine in the sPANK2 translation initiation codon (CTG) (chr20:3870078 on Human GRCh37). We found that the -2351/+13 and -1332/+13 fragments showed strong promoter activity, while -2351/-301 and -1332/-301 fragments did not demonstrate promoter activity (Figure 2.1b).

To further characterize this region, we tested truncations of the 2.3 kb fragment (Figure 2.1b). The -2351/+13 and -1332/+13 fragments produced half the transcriptional activity of -633/+13 fragments, indicating that the DNA upstream of -633 may contain negative regulatory elements. In contrast, 5' truncations of the region downstream of -327 resulted in decreasing promoter activity, suggesting that the sequence contains essential positive regulatory elements. We also assayed the luciferase activity of a 3'truncation construct (-327/-76), which demonstrated similar promoter activity to the -327/+13 fragment. To identify transcription initiation sites for the *PANK2* gene, 5'RACE was performed. We identified three sites (-78, -87, -122) upstream of the sPANK2 translational start site (Figure 2.2). The -327/-76 promoter region has 62.9% identity to mouse, with the highest sequence conservation centering around the transcription

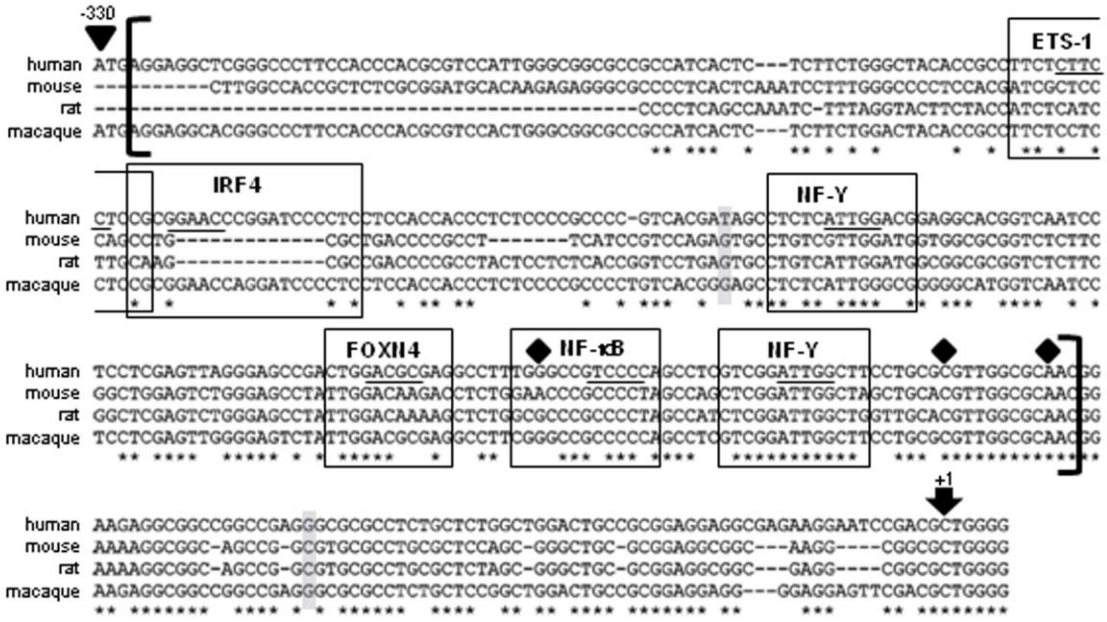

Figure 2.2: Mammalian conservation of *PANK2* 5'genomic sequence.

The cytosine of the sPANK2 leucine initiation codon (CTG) is labeled as +1. The sPANK2 leucine initiation (arrow) and the pPANK2 methionine initiation codon (triangle) are designated. Transcriptional start sites identified by 5'RACE are marked by diamonds and boundaries of the -327/-76 promoter region are indicated with brackets. The locations of putative binding sites for transcription factors are boxed and the core binding regions are underlined. *PANK2* sequence variants are highlighted in grey. The sequence corresponds to chr20:3869748-3870083 on Human GRCh37 Assembly (hg19). The sequence alignment was created with Mulan (mulan.dcode.org) and ClustalW2.

initiation sites and sPANK2 leucine initiation codon (Figure 2.2) (Ovcharenko et al., 2005).

3.3 Analysis of PANK2 promoter for potential transcription factors

We performed additional truncation analysis of the -327/-76 *PANK2* region, which revealed several potential regulatory elements within the promoter. The -180/-76, -247/-144 and -327/-217 fragments displayed less than 50% of the transcriptional activity of -327/-76 (Figure 2.3a). We used MatInspector to identify factors that may interact with these promoter elements (Cartharius et al., 2005). Putative ETS1 and IRF4 sites (disrupted in -180/-76), NF-Y, FOXN4 and NF-κB sites (eliminated in -327/-217) and a second NF-Y (disrupted in -247/-144) were identified (Figure 2.2, 2.3b). The FOXN4 site was described as a WHN (FOXN1) binding site in MatInspector; however, we were able to detect *FOXN4*, but not *FOXN1*, mRNA in SH-SY5Y cells (data not shown). FOXN1 and FOXN4 share a similar DNA binding domain, which is distinct from the rest of the FOX family members (Katoh, 2004). Two NF-Y sites were identified and we reference them as the 5' or 3' NF-Y sites within the promoter. The NF-Y sites are highly conserved in mammals, although the binding sites for ETS1, IRF4, FOXN4 and NF-κB are less conserved (Figure 2.2).

We created constructs with point mutations in these predicted regulatory elements and assayed the effect on promoter activity. Disruption of the ETS1 and NF-κB binding sites caused an increase in promoter activity, while disruption of IRF4, FOXN4 and the 5' residing NF-Y binding sites caused a decrease in promoter activity (Figure 2.3c).

Next, we performed electrophoresis mobility shift assays (EMSA) to investigate whether SH-SY5Y nuclear proteins could bind to the regulatory elements in the

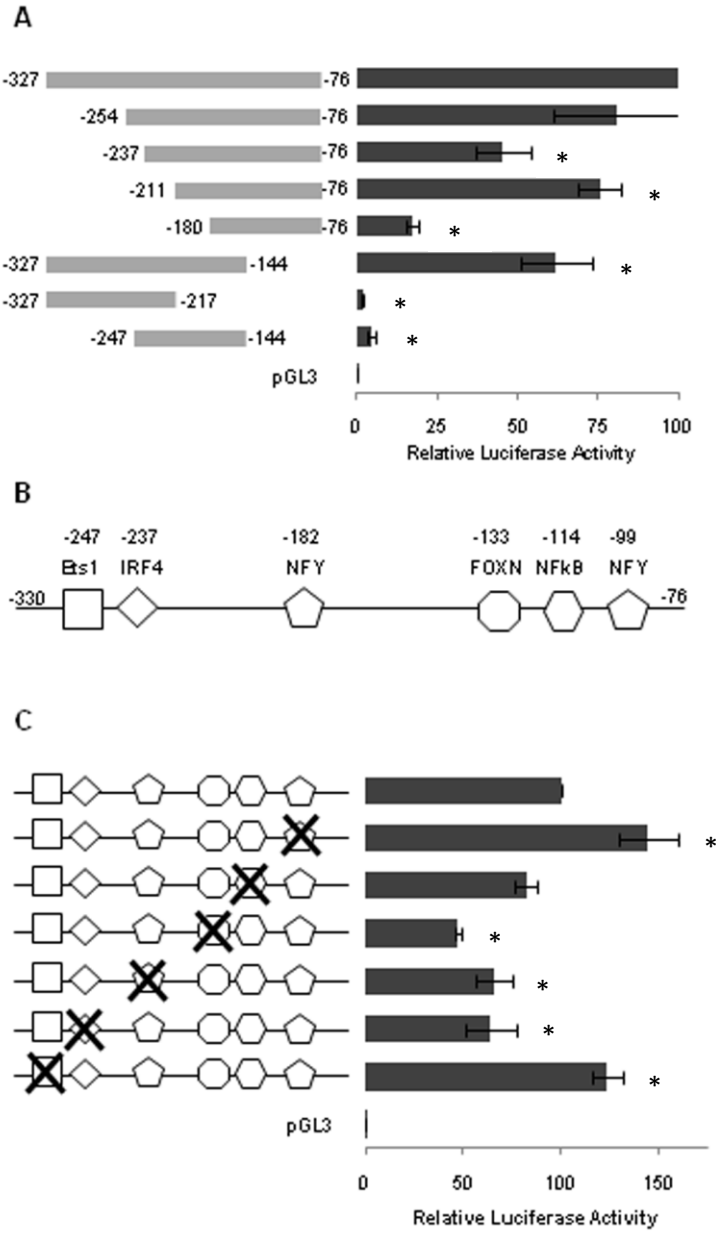

Figure 2.3: Deletion and mutational analysis of the *PANK2* minimal promoter.

(A) Luciferase activity in SH-SY5Y cells driven by fragments of the -327/-76 minimal promoter region. (B) Diagram of predicted transcription factor binding sites within the *PANK2* minimal promoter. (C) Luciferase activity in SH-SY5Y cells driven by constructs containing mutant transcription factor binding sites. Luciferase activity was normalized to β-galactosidase activity and results are shown relative to -327/-76 activity. Error bars represent standard error of three independent experiments. *Not included in published manuscript: Groups were tested and compared using ANOVA and Bonferroni post-hoc test. P values <0.05 were taken as significant and (*) indicates a significant change from the wildtype -327/-76 construct in (A) and (C).*

promoter. We designed probes to contain the predicted transcription factor binding sites within the *PANK2* promoter (Figure 2.4a) and found that the probes containing IRF4/ETS1 sites (EMSA3), 3'NF-Y site (EMSA4) and FOXN4 site (EMSA5) form DNA-protein complexes and cause a band shift upon gel electrophoresis (Figure 2.5).

We chose to further examine the EMSA4 and EMSA5 regions because NF-Y is a common regulator of CG rich promoters and FOXN4 plays a role in neuronal tissues. We found that 200-fold excess of unlabeled oligonucleotides containing NF-Y or FOXN4 binding sites competes with the EMSA4 and EMSA5 probes, respectively (Figure 2.4b,c). We investigated the specificity of this competition by adding 200-fold excess of unlabeled oligonucleotides containing mutated NF-Y or FOXN4 binding sites, and found they did not compete with the EMSA4 and EMSA5 probes (Figure 2.4b,c). These results suggest that NF-Y and FOXN4 are responsible for the shifted EMSA4 and EMSA5 bands upon electrophoresis, and may bind the *PANK2* promoter.

Interestingly, upon attempting to confirm FOXN4 binding to the EMSA5 probe, we identified hnRNPA/B as an additional potential regulator of the *PANK2* promoter. The addition of a FOXN4 antibody to the DNA-protein binding reaction did not result in additional shifting of the EMSA5 band (data not shown). Therefore, we excised the shifted EMSA5 band following gel electrophoresis and analyzed the protein content by mass spectrometry; FOXN4 was not found in the sample. However, one protein was identified in two replicate EMSA5 analyses: the heterogeneous Nuclear Ribonucleoprotein A/B (hnRNPA/B) family. The binding of hnRNPA/B to the EMSA5 oligo was confirmed by addition of hnRNPA/B antibody to the DNA-protein binding reaction, which caused a supershift of the EMSA5 band upon electrophoresis (Figure

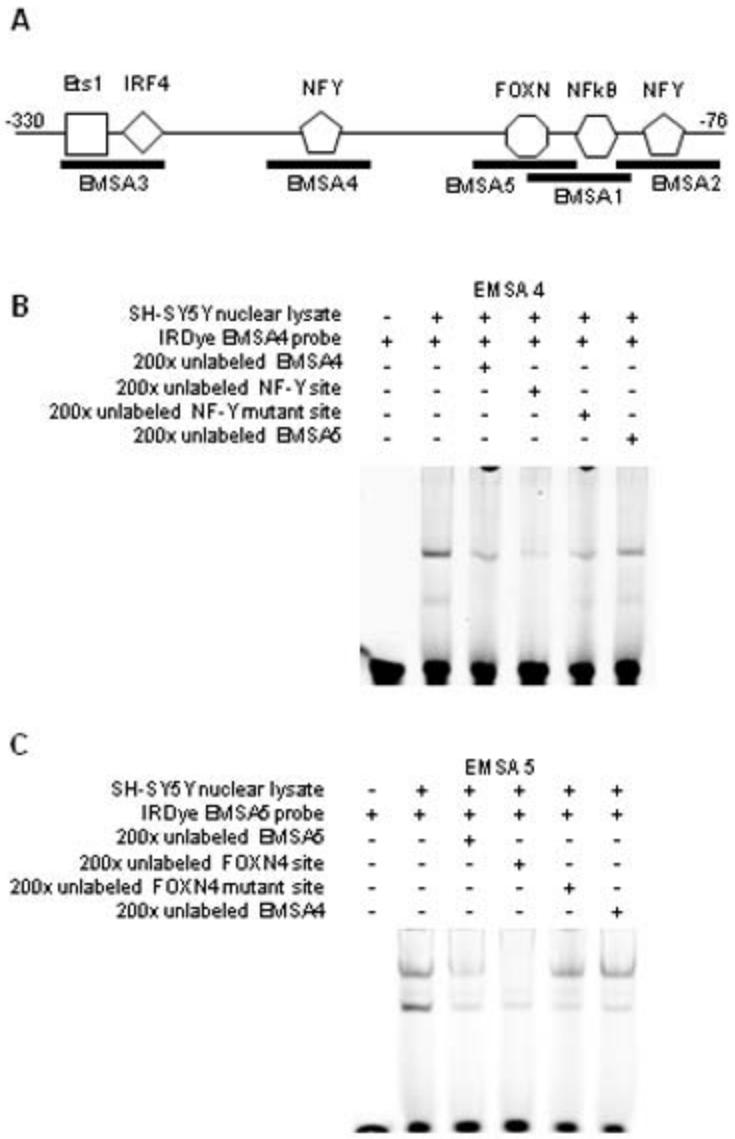

Figure 2.4: Binding of SH-SY5Y nuclear proteins to DNA probes EMSA4 and EMSA5

(A)Diagram of predicted transcription factor binding sites within the *PANK2* minimal promoter and relative location of EMSA probes.

(B, C)Binding of SH-SY5Y nuclear proteins to DNA probes EMSA4 and EMSA5. Unlabeled oligonucleotide competitors were added to the reactions, as indicated. The reactions were resolved on a 4% TBE native acrylamide gel at 4ºC.

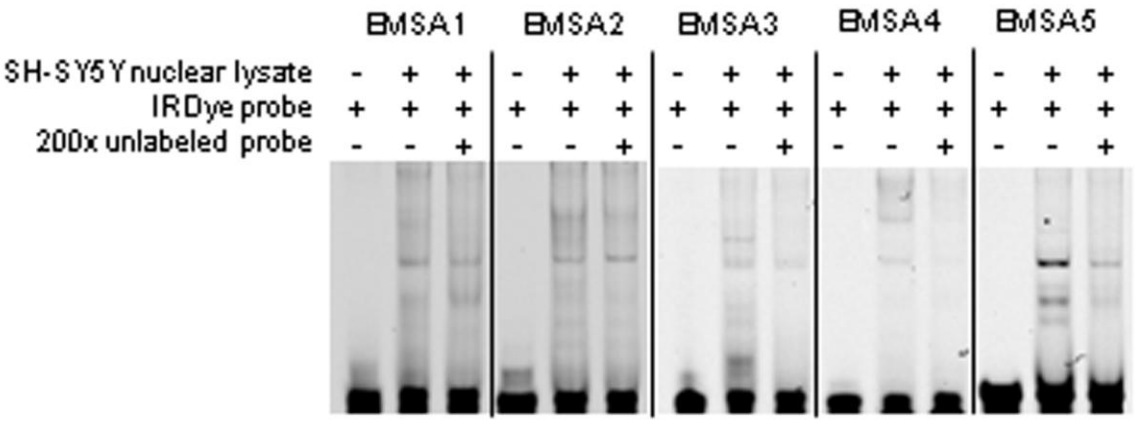

Figure 2.5: Binding of SH-SY5Y nuclear proteins to DNA probes EMSA1, EMSA2, EMSA3, EMSA4 and EMSA5.

Unlabeled oligonucleotide competitors were added to the reactions, as indicated. The reactions were resolved on a 4% TBE native acrylamide gel at 4ºC. *(Supplemental Figure 1 in published manuscript***)**

2.6). Of note, the STAT3 antibody negative control for the EMSA5 supershift inhibits protein binding to the EMSA5 probe when added after lysates. Therefore, the antibody may interfere with protein-DNA binding, either non-specifically or by disrupting STAT3 protein associations.

3.4 Predicting the effect of PANK2 sequence variants on promoter activity

We also investigated the effects of two *PANK2* sequence variants found in patients with brain iron accumulation. One sequence variant located -55 relative to the leucine initiation codon (276G>A in NM_153639) was found in a PKAN patient with only one identified *PANK2* mutant allele (785-788del in exon 3)(Zhou et al., 2001). A second variant located at -193 (138A>T in NM_153639) was identified in a patient with a related disorder being tested for PKAN. *In silico* analysis reveals that these variants do not reside in *PANK2* promoter regulatory elements and are not conserved in mouse and rat. Indeed, neither variant had a demonstrable effect on *PANK2* promoter activity (data not shown).

4. DISCUSSION

Our results describe a GC-rich *PANK2* promoter that drives expression of the sPANK2 isoform. Most of the *PANK2* spliced ESTs listed in the UCSC Genome Browser overlap with the sPANK2 transcript and support the presence of a promoter in the region we identified. The -327/-76 promoter region has 62.9% identity to mouse, which is typical for core promoter elements conserved in human and mouse orthologs (Jin et al., 2006). In contrast, PANK2 transcript has ~87% identity to mouse PANK2 cDNA.

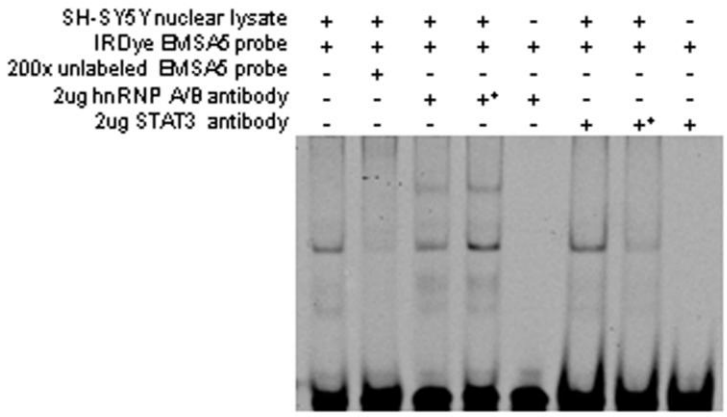

Figure 2.6: **Binding of SH-SY5Y nuclear proteins to EMSA5 probe and supershift by hnRNPA/B antibody.**

2 µg of antibody was added before or after (*) the binding reaction. A STAT3 antibody was included as a control and unlabeled oligonucleotide competitors were added to the reactions, as indicated. The reactions were resolved on a 4% TBE native acrylamide gel at 4ºC.

Although an alternate promoter for pPANK2 may exist, we were unable to identify one within the 2 kb region we studied. TATA sites are predicted further than 2 kb upstream of the pPANK2 transcript, suggesting the presence of alternate promoters (Takai and Jones, 2003; Zhang, 2005). The presence of an additional TATA-dependent *PANK2* promoter would provide an intriguing mechanism for tissue specific expression of the pPANK2 isoform. This idea is not unprecedented, as recent studies have suggested that over half of RefSeq genes are regulated by alternative promoters, and in 17% of those genes a tissue specific alternative promoter was observed (Kimura et al., 2006). Interestingly, the long *PANK2* transcript encoding pPANK2 has been identified in human brain tissues, and a single 48 kDa PANK2 isoform (mPANK2) was detected in cortical brain extracts, raising the possibility of tissue specific expression (Hortnagel et al., 2003; Kotzbauer et al., 2005). In contrast, the 50.6 kDa sPANK2 isoform has only been reported in HeLa cell extracts (Johnson et al., 2004). A direct comparison of pPANK2 and sPANK2 expression across tissues has not been published, and further investigation would be necessary to clarify the biological significance of two putative mitochondrial PANK2 isoforms.

Our results suggest that the *PANK2* promoter may be regulated by NF-Y. MatInspector predicted two highly conserved CCAAT boxes in the *PANK2* minimal promoter, although only one site affected promoter activity and was able to bind SH-SY5Y nuclear lysates (Figure 2.4). This CCAAT-box is located 58-100 nucleotides upstream of the *PANK2* transcriptional start sites, which is typical for a functional NF-Y binding site (Figure 2.3)(Bucher, 1990). NF-Y is composed of three subunits (NF-YA, NF-YB and NF-YC) and is implicated in the regulation of 30% of eukaryotic promoters

(Bucher, 1990; Sinha et al., 1995). CCAAT boxes are found in the promoters of several types of genes, including those that are developmentally controlled, tissue specific, housekeeping, inducible and cell cycle regulated (Mantovani, 1999). Although NF-Y is a major CCAAT box recognizing protein, numerous other transcription factors can also regulate gene expression through this common regulatory element (Mantovani, 1998). Therefore, further investigation is necessary to characterize the regulation of *PANK2* through the CCAAT box.

We also identified FOXN4 as a potential regulator of *PANK2* transcription. FOXN4 is a forkhead/wing helix transcription factor with a role in the specification of cells in retinogenesis and spinal neurogenesis in mouse (Gouge et al., 2001; Li et al., 2005). Interestingly, recent studies have also shown that Foxn4 regulates the expression of Nr4a2, a nuclear receptor that is associated with familial Parkinsons disease (Jiang and Xiang, 2009). We were unable to confirm FOXN4 binding to the *PANK2* promoter by EMSA supershift or mass spectrometry. In addition, the FOXN4 core binding site is not well conserved in mouse and rat. However, these results do not eliminate FOXN4 as a potential *PANK2* transcriptional regulator and further investigation is warranted.

While not predicted *in silico*, our proteomic analysis revealed that the hnRNPA/B family may regulate *PANK2* expression. The hnRNPA/B family of proteins play a role in RNA processing/trafficking, telomere maintenance, and transcriptional regulation (He and Smith, 2009). hnRNPA1 has been identified by mass spectrometry as a transcriptional regulator for several genes, including *gamma-fibrinogen*, *thymidine kinase*, *apoE* and *vitamin D receptor* (Campillos et al., 2003; Chen et al., 2003; Lau et al., 2000; Xia, 2005). Recently, hnRNPA2 was found to function as a transcriptional

activator in response to mitochondrial respiratory stress (Guha et al., 2009). A possible link between mitochondrial stress and *PANK2* expression is intriguing in light of current hypotheses of PKAN pathogenesis(Johnson et al., 2004; Zhou et al., 2001).

Finally, characterization of the *PANK2* promoter enables prediction of the consequences of *PANK2* sequence variants on transcriptional activity. We did not detect any consequence of two *PANK2* sequence variants that lie outside key promoter regulatory elements. However, we predict that sequence variants disrupting key regulatory elements or a transcriptional start site would alter *PANK2* expression and could cause PKAN.

5. CONCLUSION

Our work provides the first description of *PANK2* transcriptional regulation. We conclude that sPANK2 and pPANK2 are controlled by distinct promoters. The sPANK2 promoter may be regulated by NF-Y, FOXN4 and hnRNPA/B. These findings validate the biological relevance of sPANK2, serve as a reference for interpreting regulatory sequence variants, and provide insight to the regulation of this disease-associated gene.

ACKNOWLEDGEMENTS

This work was supported by the National Institute of Child Health and Human Development, National Eye Institute, NBIA Disorders Association and Huebner Family Pediatric Neurobiology of Disease Fellowship. This work was also supported by the Proteomics Shared Resource generously funded by the Oregon Opportunity, and NIH

center grants 5P30CA069533 and 5P30EY010572. We are grateful to Dr. Richard Mauer's laboratory for use of their luminometer, and members of the Hayflick laboratory, Dr. Shawn Westaway and Dr. Jayme Gallegos for critical reading of the manuscript.

Chapter 2.2

Additional *PANK2* transcriptional regulation studies

Unpublished Results

2.2.1 Effects of cellular stress and PPAR agonists on *PANK2* expression

In addition to the promoter characterization described in Chapter 2.1, I conducted preliminary investigations into the regulation of *PANK2* expression by cellular stress and peroxisome proliferator-activated receptor (PPAR) agonists. A limited number of experiments were conducted and the preliminary results did not inspire further investigation. However, I have included these experiments for discussion.

Experimental Rationale

Oxidative stress and iron overload/depletion

Two hallmarks of neurodegenerative disease are oxidative damage and disrupted metal homeostasis (Calabrese et al., 2010). Accordingly, altered expression of genes that regulate oxidative stress and brain iron metabolism often correlates with neuronal pathogenesis. For example, changes in LfR (lactotransferrin receptor), MTf (melanotransferrin), CP (ceruloplasmin) and DCT1 (divalent cation transporter) expression correlate with brain iron accumulation (Qian and Wang, 1998). In addition, Gao et al. have shown that increased susceptibility to oxidative stress in primary cultured neurons is induced, in part, by downregulation of thioredoxin, an enzyme that helps maintain the redox homeostatic state of cells (Gao et al., 2005). Changes in the expression of these genes may be mediated by cells' transcriptional response to intracellular iron (Eisenstein, 2000) and oxidative stress (Ma, 2010).

Our current hypothesis for PKAN pathogenesis involves iron and oxidative stress; *PANK2* mutations are predicted to cause mitochondrial CoA deficiency and disruption of fatty acid β-oxidation, leading to oxidative stress that is exacerbated by high iron content

in the globus pallidus (Johnson et al., 2004). Indeed, a drosophila *PANK2* mutant, *dPANK/fumble,* is hyper-sensitive to cysteine, paraquat, dithiothreitol (DTT) and H_2O_2 compared with wildtype, which supports a role for *PANK2* in mediating oxidative stress (Bosveld et al., 2008). Oxidative stress triggers a range of adaptive responses as a result of cellular damage (Ma, 2010). Perhaps, in response to oxidative stress, increased *PANK2* expression may boost mitochondrial CoA production and provide a cellular defense against mitochondrial dysfunction and stress. Toward investigating this hypothesis, I measured *PANK2* promoter activity and *PANK2* mRNA levels in neuroblastoma cell lines following treatment with H_2O_2.

In addition, due to the association of *PANK2* mutation with brain iron accumulation, we were interested in confirming whether *PANK2* expression correlates with cellular iron levels. Excess iron can be a source of oxidative stress because free iron catalyzes the formation of highly reactive radicals that damage membranes and DNA. Accordingly, the genes involved in iron metabolism are under tight regulation. Specifically, iron responsive elements (IREs) in mRNA are recognized by iron-regulatory proteins (IRPs) that control the rate of mRNA translation or stability (Eisenstein, 2000). I did not identify an IRE within the *PANK2* promoter; regardless, we decided to conduct preliminary investigations into the effects of iron overload and chelation on *PANK2* expression with the hypothesis that oxidative stress induced by iron perturbations may affect *PANK2* expression.

PPAR agonist experiments

Upon *in silico* analysis of the 5' flanking region of *PANK2,* I observed a PPAR response element located within 1kb of the *PANK2* transcriptional start sites. The PPAR family of ligand-dependent transcription factors includes PPARα, δ (also called β) and γ. Upon binding with fatty acids, PPARs bind as a heterodimer with the retinoid X receptor (RXR) to a PPAR response element in the enhancer regions of genes, resulting in regulation of gene transcription (Bragt and Popeijus, 2008). Although all PPAR isoforms recognize the same basic PPAR response element, the consensus sequence can differ slightly for each PPAR (Heinaniemi et al., 2007).

In general, PPAR gene targets belong to pathways of lipid transport and metabolism (Kersten et al., 2000). Pantothenate kinases, which regulate the rate limiting step of coenzyme A biosynthesis, easily fit the description of a predicted PPAR target based on cellular function. Indeed, *PANK1α* expression is regulated by PPAR activation in human hepatoblastoma (HepG2) cells; however, *PANK1β, PANK2* and *PANK3* regulation is not observed in the cells (Ramaswamy et al., 2004). Despite the lack of *PANK2* regulation by PPARs in these liver-derived cells, I hypothesized that *PANK2* may be regulated by PPARs in neuronal cells.

The rationale for my hypothesis is that PPAR isoforms are differentially expressed in various tissues and stages of development, which may cause tissue specific regulation of target genes. For example, PPARα is predominately expressed in the liver (Auboeuf et al., 1997), while all three PPAR isoforms are expressed in the central nervous system (Heneka and Landreth, 2007). As a pilot study, I treated neuroblastoma

cells with bezafibrate (PPARα, ε, γ agonist), fenofibrate (PPARα agonist) or troglitazone (PPARγ agonist) and measured promoter activity and *PANK2* mRNA.

Materials and Methods

Cell culture

Human neuroblastoma (SH-SY5Y) cells were cultured in RPMI with 10% FBS, 10 ng/ml human neuron growth factor, non-essential amino acids and penicillin/streptomycin antibiotics at 37ºC and 5% CO2. Mouse neuroblastoma (N2a) cells were cultured in MEM with L-glutamine + Earle's BSS, 1.5 g/L sodium bicarbonate, 0.1 mM non-essential amino acids, 1 mM sodium pyruvate, 10% FBS and penicillin/streptomycin antibiotics at 37ºC and 5% CO_2.

Cell transfections and treatments

For H_2O_2 experiments, SH-SY5Y cells were plated at 7 x 10^5 cells/ml in 6 and 12 well plates. The 6 well plates were grown for ~48 hours, treated with H_2O_2 dissolved in SH-SY5Y media and RNA was harvested in RNA-STAT60. Final concentration of H_2O_2 and duration of treatment are as indicated in Figures 2.7 and 2.8. For *PANK2* promoter assays, the 12 well plates were grown for ~24 hours and transfected with Lipofectamine 2000 according to the manufacturer's instructions. Each well was transfected with 0.8μg of luciferase reporter plasmid containing a 2kb fragment of the *PANK2* 5' region (construct -2351/+13 in Chapter 2.1). The cells were grown for another 24 hours, treated with H_2O_2 dissolved in SH-SY5Y media and harvested in 100 μl Passive Lysis Buffer (Promega) for luciferase and β-galactosidase assays or RNA-STAT60 for gene

expression assays. Final concentration of H_2O_2 and duration of treatment are as indicated in figures 2.7 and 2.8.

For iron overload and depletion experiments, N2a cells were plated at 2.7 x 10^5 cells/ml in 12 well plates. For RNA harvest, 12 well plates were grown for ~48 hours, treated with 100μg/ml FAC (Ammonium Iron (III) Citrate, Sigma #F5879) or 0.5mM DFO (deferozamine mesylate, Sigma #D9533) for 24 hours and RNA was harvested in RNA-STAT60. For *PANK2* promoter assays, the 12 well plates were grown for ~24 hours and transfected with Lipofectamine 2000 according to the manufacturer's instructions. Each well was transfected with 0.5μg of pRSV-βgal and 0.5μg of luciferase reporter plasmid containing a 2kb fragment of the *PANK2* 5' region (construct -2351/+13 in Chapter 2.1). The cells were grown for another 24 hours, treated with 100μg/ml FAC (Ammonium Iron (III) Citrate, Sigma #F5879) or 0.5mM DFO (deferozamine mesylate, Sigma #D9533) for 19 hours and harvested in 100 μl Passive Lysis Buffer (Promega) for luciferase and β-galactosidase assays or RNA-STAT60 for gene expression assays.

For PPAR agonist experiments, SH-SY5Y and N2a cells were plated and transfected as described in oxidative stress and iron overload/depletion experiments. For N2a experiments, 48 hours after plating the cells in 12 well plates (or 24 hours after transfection), the cells were treated with various doses of bezafibrate (BF) for 24 hours. For SH-SY5Y experiments, 48 hours after plating the cells in 12 well plates, the cells were treated with 750μM bezafibrate (BF), 250μM fenofibrate 100μM troglitazone (TG) or DMSO (as a control) for 24 hours. All cells were harvested in Passive Lysis buffer (Promega) for luciferase and β-galactosidase assays or RNA-STAT60 for gene expression assays.

Luciferase and β-galactosidase assays

To assay for luciferase activity, 20 µl of cell lysate was combined with 300 µl of GlyGly-ATP (25mM Glycylglycine, 15 mM $MgSO_4$, 5 mM ATP) and 100 µl of luciferin (Promega) (300 µg/ml) and measured on a luminometer. To assay for β-galactosidase activity, 50 µl of cell lysate was combined with 60 µl Z buffer (60mM Na_2HPO_4, 40mM NaH_2PO_4, 10 mM KCl, 1 mM $MgSO_4$, 50mM 2-Mercaptoethanol, pH 7.5) and 40 µl ONPG substrate (Sigma) (4 mg/ml in 60 mM Na_2HPO_4, 40mM NaH_2PO_4, pH 7.5 buffer) and incubated at 30ºC for 30 minutes. The reaction was quenched by adding 100 µl of 1 M Na_2CO_3 and measured at A_{420}. To assay for luciferase activity, 20 µl of cell lysate was combined with 300 µl of GlyGly-ATP (25mM Glycylglycine, 15 mM $MgSO_4$, 5 mM ATP) and 100 µl of luciferin (Promega) (300 µg/ml) and measured on a luminometer. The luciferase values were normalized to β-galactosidase activity and shown as relative light units. However, a β-galactosidase control was not used for the H_2O_2 experiments in SH-SY5Y cells and the results are shown as raw light units.

TaqMan Gene Expression Assays

For each sample, 200ng of total RNA was reverse transcribed using the SuperScript First-Strand Synthesis System (Invitrogen) and TaqMan Gene Expression Assays for *Pank2*, *TfR*, *Hprt*, *HPRT*, *GAPDH*, *RPLP0*, *PANK2*, and *TfR* were ran using TaqMan Universal Master Mix, according to the manufacturer's instructions. *Hprt* was used to normalize all TaqMan Gene Expression Assays on N2a RNA. For SH-SY5Y RNA, *GAPDH*, *RPLP0* and *HPRT* were used to normalize data in Figures 2.7a, 2.8a and 2.11, respectively.

Results and Conclusions

H_2O_2

To investigate the effect of oxidative stress on *PANK2* expression, I exposed SH-SY5Y cells to hydrogen peroxide and measured *PANK2* promoter activity and *PANK2* mRNA expression at select time points. Treating cells with brief and low doses of hydrogen peroxide is an established model system to investigate neuronal cell death via oxidative damage and stress. For example, treating primary cortical neurons with 100 μM H_2O_2 for 3 hours is sufficient to induce apoptotic mechanisms (Whittemore et al., 1995). In SH-SY5Y cells, 2.5 hour treatment with 100 μM H_2O_2 is sufficient to activate caspase-3 (a key player in intrinsic and extrinsic apoptotic pathways (Ghavami et al., 2009)), and cell death is prominent after 8 hours of 100 μM H_2O_2 treatment (De Sarno et al., 2003). I hypothesized that *PANK2* expression may be induced in the early stages of cellular stress. Therefore, I treated SH-SY5Y cells with 10-250 μM H_2O_2 for 2-9 hours and assayed the effects on *PANK2* expression.

I failed to see a robust change in *PANK2* expression with the brief and low H_2O_2 treatments. *PANK2* mRNA levels were not affected by 2 hour treatment with 10μM-250μM H_2O_2 and *PANK2* promoter activity was not affected ($p > 0.05$) by 2 hour treatment with 10μM, 50μM or 150μM H_2O_2 (Figure 2.7). Interestingly, I did see a suggestion of increased *PANK2* expression following 3 hour treatment with 100μM H_2O_2 ($p=0.05$), and a ~20% increase in *PANK2* promoter activity after 5 hours of 100μM H_2O_2 treatment ($p=0.05$)(Figure 2.8). However, I did not follow up with investigation of these later time points.

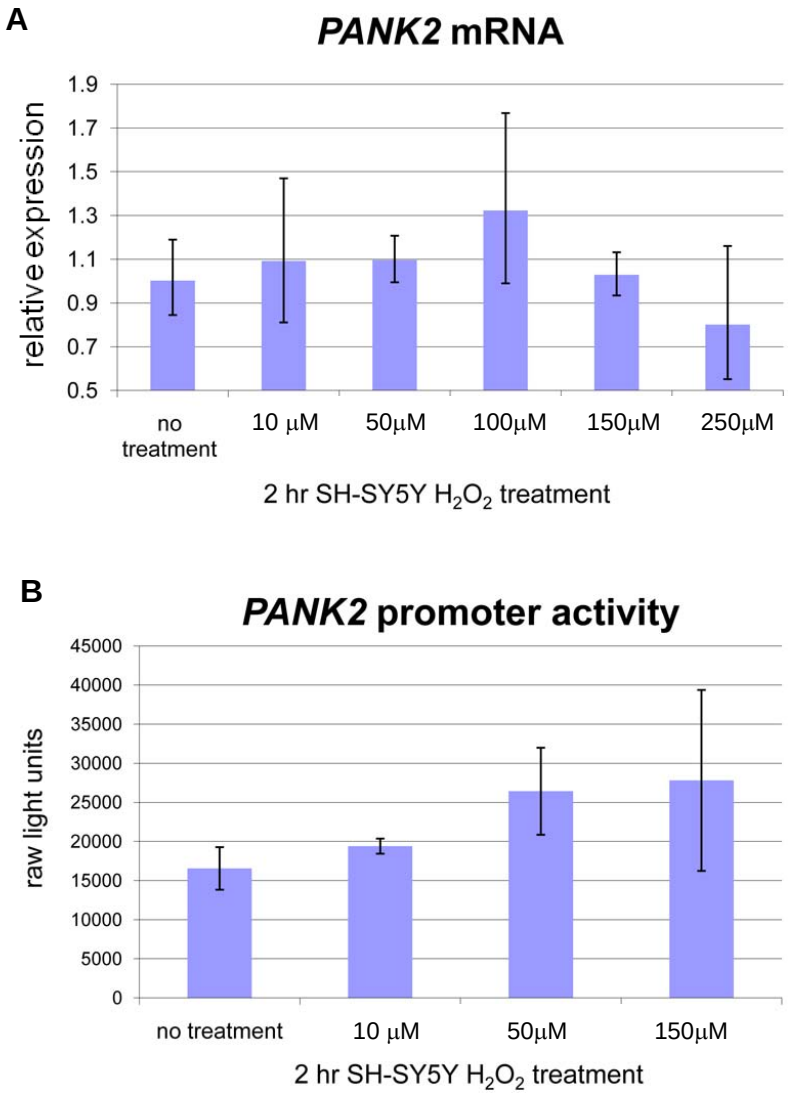

Figure 2.7: *PANK2* expression and *PANK2* promoter activity following 2 hour treatment with various doses of H_2O_2 in SH-SY5Y cells.

A) SH-SY5Y cells were exposed to varying doses of H_2O_2 for 2 hours. RNA was harvested and analyzed with Gene Expression Assays. The data is normalized to *GAPDH* and error bars represent standard deviation. B) SH-SY5Y cells were transfected with a luciferase reporter construct containing 2kb of the *PANK2* 5' region and exposed to varying doses of H_2O_2 for 2 hours. Luciferase activity was determined for each treatment and error bars represent standard deviation. Changes in expression were not significant ($p>0.05$) by student t-test.

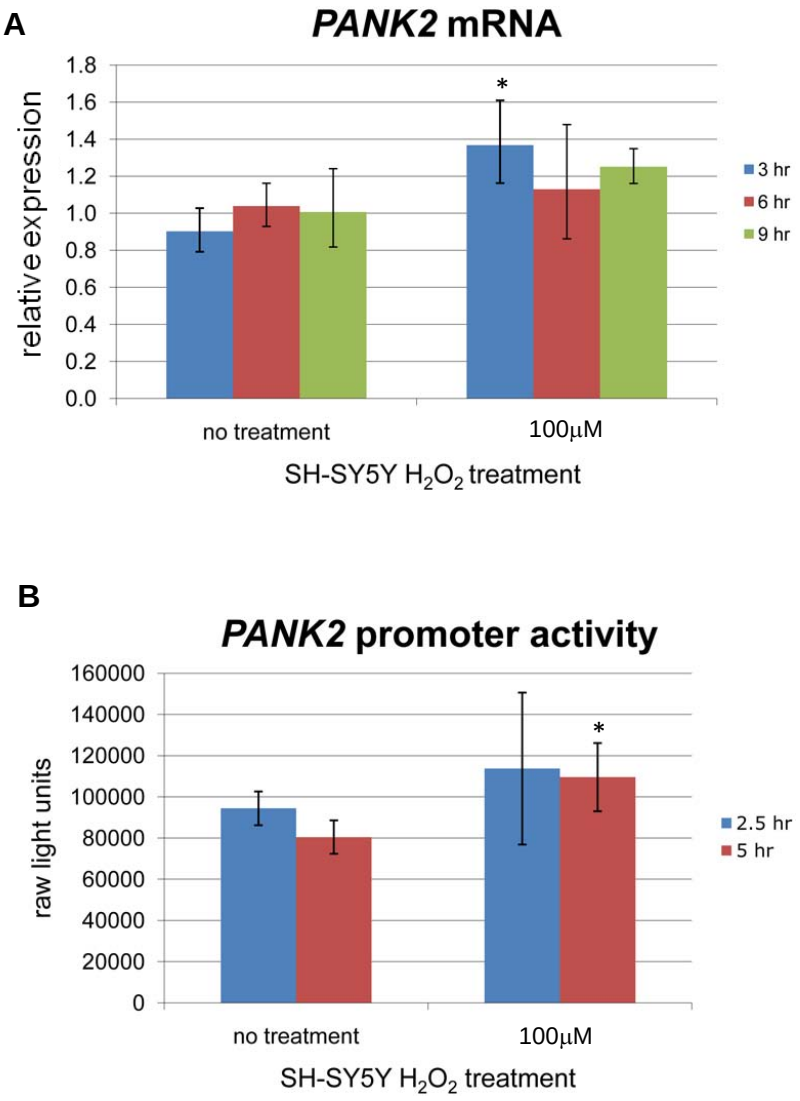

Figure 2.8: *PANK2* expression and *PANK2* promoter activity following 100μM H_2O_2 treatment for various lengths of time in SH-SY5Y cells.

A) SH-SY5Y cells were exposed to 100μM H_2O_2 for 3, 6 or 9 hours. RNA was harvested and analyzed with Gene Expression Assays. The data is normalized to *RPLP0* and error bars represent standard deviation. B) SH-SY5Y cells were transfected with a luciferase reporter construct containing 2kb of the *PANK2* 5' region and exposed to 100μM H_2O_2 for 2.5 or 5 hours. Luciferase activity was determined for each treatment and error bars represent standard deviation. * p=0.05 by student t-test.

Although I did not observe a change in *PANK2* transcription with low, brief H_2O_2 treatments, *PANK2* could still be regulated by oxidative stress. Recently, induction of the p63 transcription factor (Heo et al., 2009) and down regulation of thioredoxin (Ding et al., 2008) has been observed in SH-SY5Y cells following treatment with 400-750μM H_2O_2. Therefore, there is precedence for investigating *PANK2* transcriptional regulation under additional experimental parameters using H_2O_2. Further investigation of *PANK2* expression and function following oxidative damage or stress may be interesting, in light of our hypotheses of PKAN pathogenesis.

Iron

To investigate the effect of iron on *PANK2* expression, I measured *PANK2* promoter activity and *Pank2* mRNA expression in mouse neuroblastoma (N2a) cells following treatment with 100μg/ml FAC (ammonium iron (III) citrate) or 0.5mM DFO (deferozamine mesylate). The experiments were conducted in N2a cells for two reasons. First, established experimental protocols for N2a iron overload (Fernaeus and Land, 2005) and iron depletion (Chang et al., 2007) were available. Second, at the time of experiments I was encountering repeated technical difficulties with the SH-SY5Y cells.

I did not observe a correlation between cellular iron levels, *Pank2* expression and *PANK2* promoter activity. In the *PANK2* luciferase reporter assay, there was a significant decrease in promoter activity following iron overload; however I did not observe a significant effect on relative *Pank2* mRNA levels (Figure 2.9). For the gene expression assays, the transferrin receptor (*Tfr*) was included as a control. Low iron levels promote increased *Tfr* expression, while excess iron leads to *Tfr* mRNA degradation

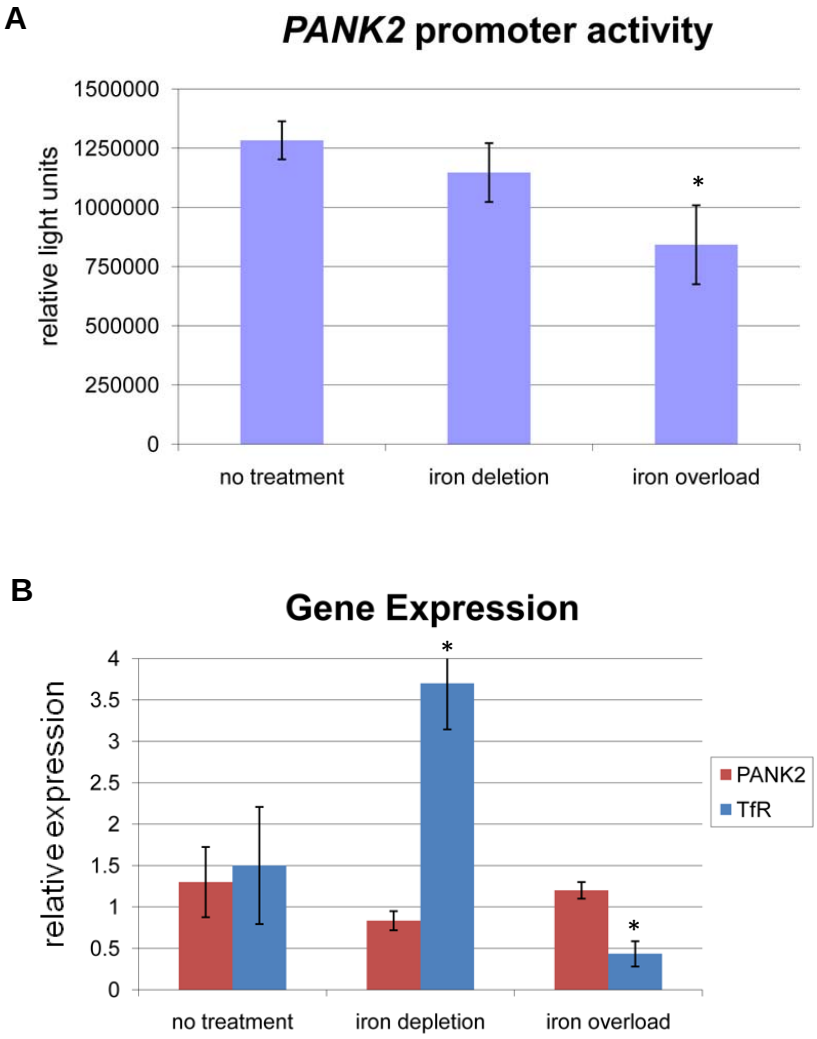

Figure 2.9: *PANK2* expression and *PANK2* promoter activity following iron depletion and overload in N2a cells.

A) N2a cells were transfected with a β-galactosidase reporter construct and a luciferase reporter construct containing 2kb of the *PANK2* 5' region, and exposed to 100μg/ml FAC (iron overload) or 0.5mM DFO (iron depletion) for 24 hours. Luciferase activity was normalized to β-galactosidase activity and error bars represent standard deviation. B) N2a cells were exposed to 100μg/ml FAC (iron overload) or 0.5mM DFO (iron depletion) for 24 hours. RNA was harvested and analyzed with Gene Expression Assays. Transferrin receptor (*TfR*) was included as a positive control for iron mediated gene regulation. The data is normalized to *Hprt* and error bars represent standard deviation. *$p<0.05$ by student t-test.

(Casey et al., 1988). Therefore, iron was successfully overloaded and deleted in N2a cells, and *PANK2* does not appear to be regulated by iron.

PPAR

I used three PPAR agonists to investigate PPAR regulation of *PANK2*: bezafibrate, fenofibrate and troglitazone. Bezafibrate is a widely used PPAR agonist, which activates all three PPAR isoforms (Tenenbaum et al., 2005). Fenofibrate, in contrast, is an agonist specific for PPARα (Schoonjans et al., 1996). Troglitazone, a thiazolidinedione derivative, is a PPARγ specific agonist (Lehmann et al., 1995). Doses and duration of treatment were selected based on previous cell culture studies, which have demonstrated PPAR regulation of target genes (Martin et al., 1997; Ramaswamy et al., 2004) or effects of PPAR agonists on cell growth in neuroblastoma cell lines (Valentiner et al., 2005).

Initial experiments in mouse neuroblastoma (N2a) cells suggested that *PANK2* may be regulated by PPAR. For these experiments, I treated N2a cells with 250-750μM bezafibrate treatment for 24 hours. This pan-PPAR agonist caused a significant increase in *PANK2* promoter activity at 750μM (Figure 2.10). In addition, endogenous levels of *Pank2* increased 2 fold with 750μM bezafibrate treatment and 2.5 fold with 1.25mM bezafibrate treatment (Figure 2.10). In comparison, Ramasway et al. had observed a 5.5 fold increase in *PANK1α* expression following 24 hour treatment with 700μM bezafibrate treatment in HepG2 cells (Ramaswamy et al., 2004). Therefore, these results

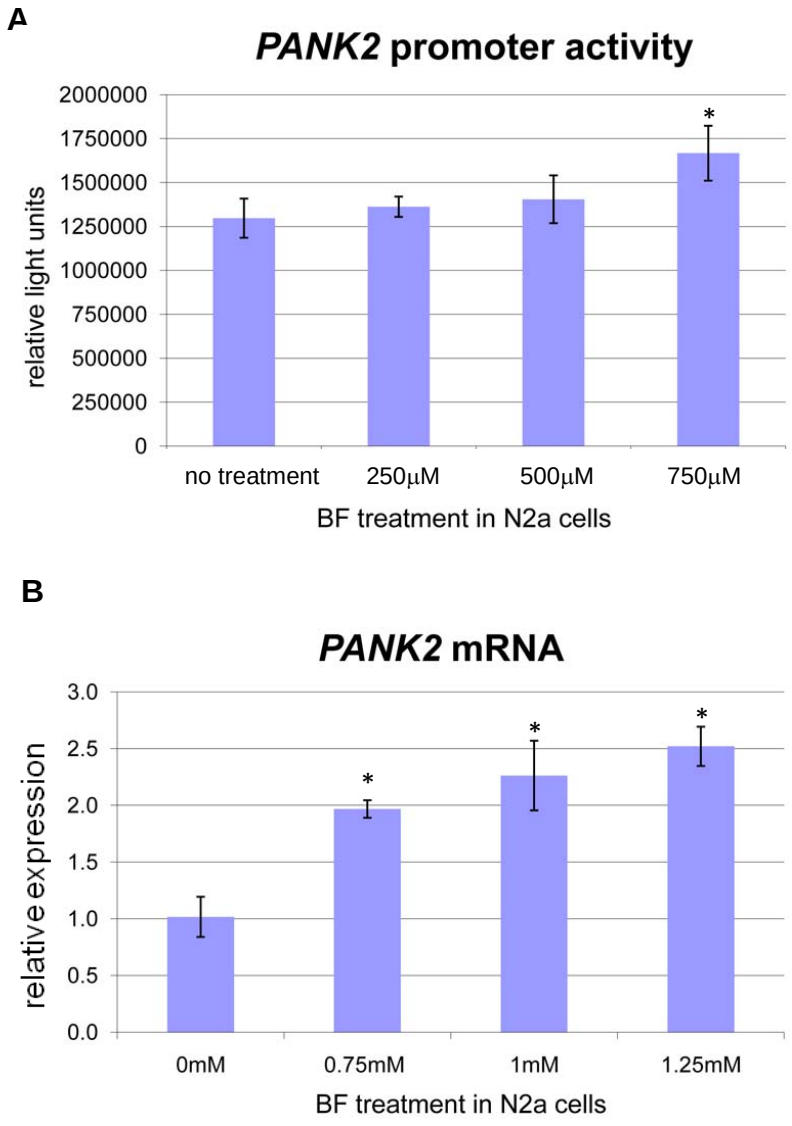

Figure 2.10: *PANK2* expression and *PANK2* promoter activity and relative expression following bezafibrate treatment in N2a cells

A) N2a cells were transfected with a β-galactosidase reporter construct and a luciferase reporter construct containing 2kb of the *PANK2* 5' region, and exposed to various doses of bezafibrate (BF) for 24 hours. Luciferase activity was normalized to β-galactosidase activity and error bars represent standard deviation. B) N2a cells were exposed to various doses of bezafibrate (BF) for 24 hours. RNA was harvested and analyzed with Gene Expression Assays. The data is normalized to *Hprt* and error bars represent standard deviation. *$p<0.05$ by student t-test.

were suggestive of *PANK2* regulation by PPAR, but with less sensitivity than *PANK1α* regulation.

However, I was unable to detect PPAR regulation of *PANK2* in SH-SY5Y cells. For these experiments, I treated cells with bezafibrate, as well as fenofibrate (PPARα specific agonist) and troglitazone (PPARγ specific agonist) and investigated the effect on endogenous *PANK2* expression by TaqMan Gene Expression Assays. Due to the regulation of *PANK1α* in HepG2 cells by bezafibrate, I also measured *PANK1* expression in these experiments. However, I did not observe a change in *PANK2* or *PANK1* expression following 24 treatment with the PPAR agonists (Figure 2.11). The lack of *PANK1* regulation may be due to differential regulation of *PANK1α* in SH-SY5Y cells compared with HpG2 cells. However, the *PANK1* gene expression assay used for these experiments detects α and β forms of *PANK1*, and this non-specificity may also mask the regulation of *PANK1α*. Regardless, the lack *PANK2* regulation in these preliminary SH-SY5Y experiments persuaded us to discontinue the investigation.

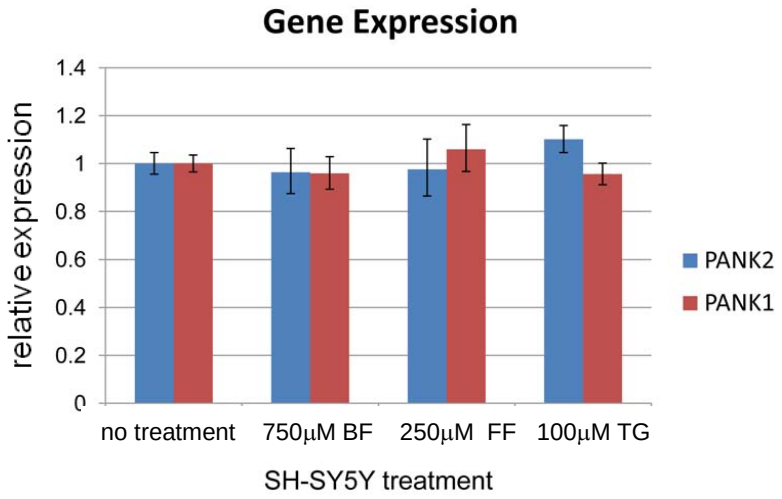

Figure 2.11: *PANK2* and *PANK1* expression following treatment with PPAR agonists in SH-SY5Y cells.

SH-SY5Y cells were exposed to 750μM bezafibrate (BF), 250μM fenofibrate (FF) or 100μM troglitazone for 24 hours. RNA was harvested and analyzed with Gene Expression Assays. The data is normalized to *HPRT* and error bars represent standard deviation.

2.2.2 Investigating *PANK2* regulation by hnRNPA/B

Experimental Rationale

As described in Chapter 2.1, the hnRNPA/B family was identified as a potential *PANK2* transcription regulator. The hnRNPA/B proteins are among the most abundant RNA-binding proteins (Steiner et al., 1996), although they also bind to double stranded DNA (Kumar et al., 1986). Similar to the experimental journey that lead to our identification of hnRNPA/B proteins as potential *PANK2* transcriptional regulators, proteomic analysis of proteins bound to various other gene promoters have identified hnRNPA/B proteins. In particular, hnRNPA1 has been identified as binding the promoter regions of *c-myc* (Takimoto et al., 1993), *APOE* (Campillos et al., 2003), thymidine kinase (Lau et al., 2000), γ-fibrinogen (Xia, 2005) and vitamin D receptor (Chen et al., 2003). hnRNPA2 has been identified as binding *BRCA1* (Thakur et al., 2003) and *GnRH1* promoters (Zhao et al., 2008), and hnRNPA3 binds regulatory regions of the *Hoxc8* gene (Makeyev et al., 2005). However, a consistent DNA binding motif for hnRNPA/B proteins has not been identified, and direct and indirect mechanisms of hnRNPA/B mediated transcriptional regulation have been proposed (He and Smith, 2009).

To further investigate the proposed regulation of *PANK2* by hnRNPA/B proteins, I conducted several experiments. First, I investigated the effect of overexpressing hnRNPA1 on *PANK2* promoter activity. In addition, I inhibited expression of three hnRNPA/B family members (hnRNPA1, A2 and A3) by transient transfection of shRNA and determined the effect on *PANK2* promoter activity. Finally, I investigated the binding of hnRNPA/B proteins to the *PANK2* promoter by chromatin immunoprecipitation.

Materials and Methods

Cell culture and transfections

The hnRNPA1 overexpression construct (SC321092) and pCMV6-AC control vector (PS100020) were purchased from Origene. shRNA constructs to knockdown hnRNPA1 (psA1), hnRNPA2 (psA2) and hnRNPA2 (psA3) and an empty vector control (psEMPTY) were received as a kind gift from Dr. Lexie Friend at the University of Queensland .

SH-SY5Y cells were cultured as described in Ch2.2.1 materials and methods. Cells were seeded in 24-well plates, grown to 80% confluency, and transfected using Lipofectamine 2000 (Invitrogen) according to manufacturer's instructions. For shRNA experiments, each well was transfected with 0.8μg psA, psA2, psA3 or psEMPTY, 0.1μg of the *PANK2* minimal promoter (hp2prom2F/4R) and 0.1 μg CMV-β-galactosidase. For hnRNPA1 overexpression, each well was transfected with 0.8μg of hnRNPA1 or pCMV6-AC, 0.1μg of the *PANK2* minimal promoter (the -327/-76 reporter construct, as described in Chapter 2.1) and 0.1 μg CMV-β-galactosidase. Cells were harvested in 100 μl Passive Lysis Buffer (Promega) 48 hours after transfection. β-galactosidase and luciferase activity were assayed as described in Ch2.2.1 materials and methods. The luciferase values were normalized to β-galactosidase activity. Each transfection was performed in triplicate and repeated 3 times.

Chromatin immunoprecipitation

Chromatin immunoprecipitations were performed using the EZ-ChIP^{TM} kit (Upstate/Millipore). Briefly, SH-SY5Y cells were plated in a T75 flask, grown to ~90%

confluence, rinsed with PBS and crosslinked in 1% formaldehyde for 10 minutes. Unreacted formaldehyde was quenched by the addition of glycine. The cells were washed with cold PBS (containing protease inhibitors) and harvested. The cells were sonicated on wet ice (8-10 pulses using 30% max power, 3.5 output on Branson Sonifier 450) and stored at -80°C. A portion of the sample was uncrosslinked and the DNA was ran on a 1% agarose gel to confirm sheering to ~600-1500bp. The crosslinked protein/DNA was immunoprecipitated with 3μg (rabbit) hnRNPA/B antibody, 3μg rabbit IgG, 1μg (mouse) RNA polymerase II antibody or 1μg mouse IgG. Then, the crosslinks were reversed by addition of NaCl and incubation overnight at 65°C. Finally, the DNA was purified using a spin column and stored at -20°C. The process was repeated three times (beginning with plating cells) to yield three SH-SY5Y harvests that represent three biological replicates. The DNA was amplified using a variety of *PANK2* promoter primers surrounding the predicted hnRNPA/B binding region (Table 2.4, Figure 2.14).

Results and Conclusions

I investigated the effect of hnRNPA1 overexpression on *PANK2* promoter activity because it is the hnRNPA/B family member that has been identified most frequently to function as a transcriptional regulator. Successful overexpression of hnRNPA1 was confirmed by RT-PCR (data not shown). However, hnRNPA1 overexpression did not have an effect on *PANK2* promoter activity in SH-SY5Y cells (Figure 2.12).

As a complementary approach to identifying an hnRNPA/B protein that regulates *PANK2* transcription, I knocked down hnRNPA1, hnRNPA2 or hnRNPA3 by shRNA and determined the effect on *PANK2* promoter activity. In agreement with the hnRNPA1

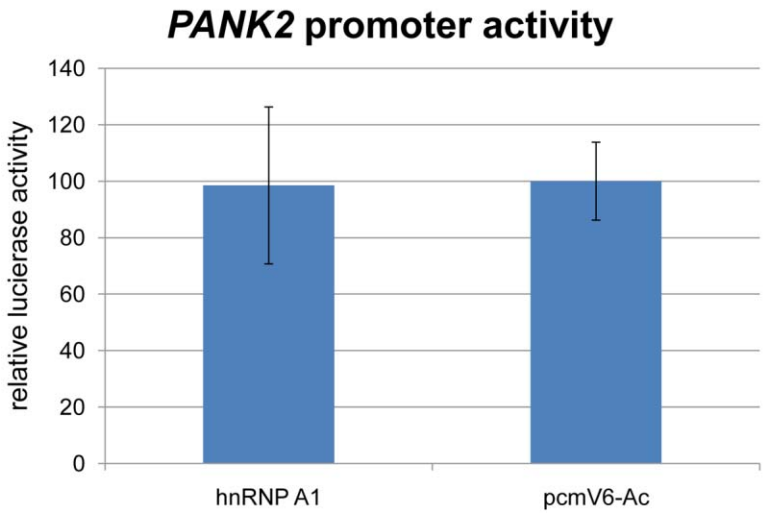

Figure 2.12: ***PANK2* promoter activity following transient transfection with hnRNPA1.**

SH-SY5Y cells were so-transfected with hnRNPA1 or empty vector control (pcmV6-Ac), a β-galactosidase reporter construct and a luciferase reporter construct containing the minimal *PANK2* promoter. Luciferase activity was normalized to β-galactosidase activity and error bars represent standard deviation.

overexpression experiments, hnRNPA1 knockdown did not have an effect on *PANK2* promoter activity (Figure 2.13). In contrast, knockdown of hnRNPA2 and hnRNPA3 resulted in a 50% increase in activity of the *PANK2* promoter , although only the hnRNPA3 result was significant by student t-test (Figure 2.13). Unfortunately, I cannot interpret these results with confidence because I was unable to confirm that the shRNA transfections successfully knocked down hnRNPA1, hnRNPA2 or hnRNPA3. I saw no change in expression of these isoforms by RT-PCR and I was unsuccessful in monitoring expression of the proteins by western blot. Therefore, the results suggest that hnRNPA2 and hnRNPA3 may negatively regulate *PANK2* expression, but confirmation of knockdown is required to validate the findings.

Finally, chromatin immunoprecipitation experiments to detect interaction of hnRNPA/B with the *PANK2* promoter were also inconclusive. For these experiments, I immunoprecipitated SH-SY5Y protein/DNA with an hnRNPA/B (rabbit) antibody, a control IgG rabbit antibody, a DNA polymerase II (mouse) antibody and a control IgG mouse antibody. Immunoprecipitation with the RNA polymerase II antibody repeated ly pulled down more *PANK2* promoter sequence than an IgG mouse control antibody (Figure 2.15a). This result suggests that RNA polymerase II binds to the *PANK2* minimal promoter region, as we would predict. However, I obtained inconsistent results from hnRNPA/B immunopreciptiations. Initially, I did two immunopreciptiations on the same SH-SY5Y DNA-protein harvest and saw enrichment of the *PANK2* promoter (using hp2prom10F/1R primers) in the first, but not the second experimental attempts (Figure 2.15a). Therefore, I expanded my ChIP analysis to include three independent SH-SY5Y protein-DNA harvests and analyzed the immunoprecipitated DNA with four *PANK2*

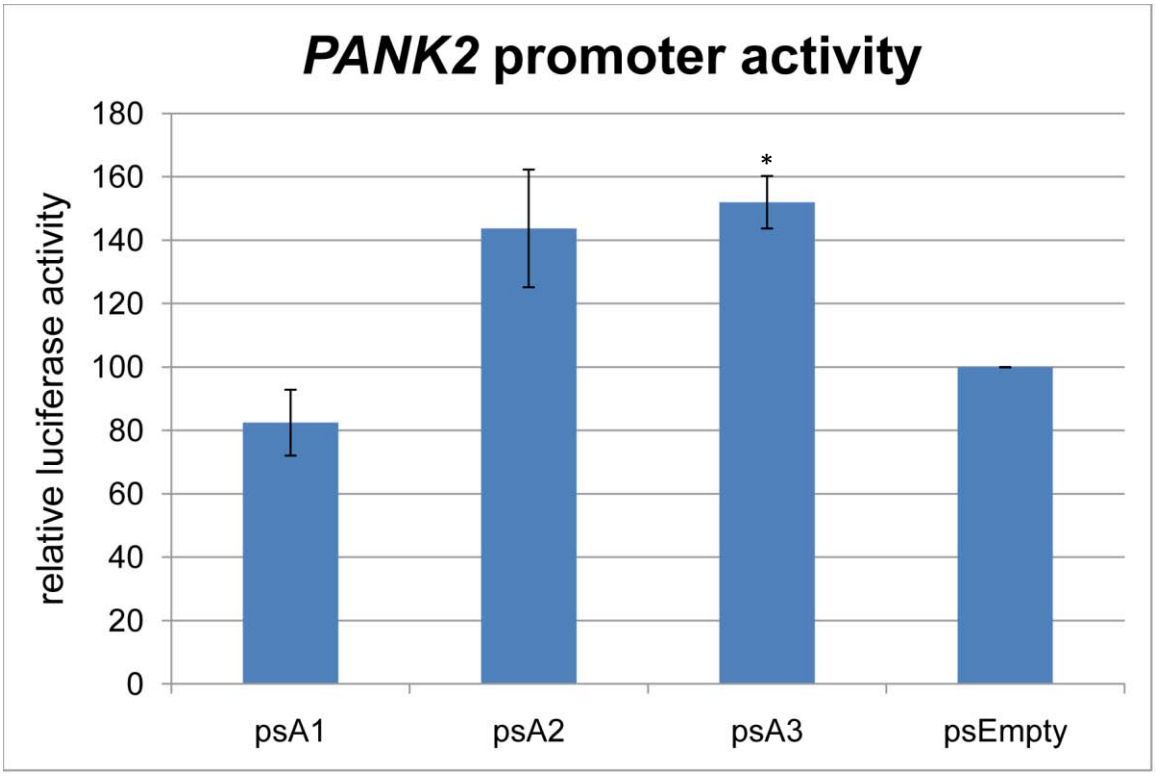

Figure 2.13: *PANK2* promoter activity following transfection with hnRNPA1, hnRNPA2 and hnRNPA3 shRNA.

SH-SY5Y cells were so-transfected with shRNA plasmids against hnRNPA1 (psA1), hnRNPA2 (psA2), hnRNPA2 (psA3) or empty vector control (psEmpty), a β-galactosidase reporter construct and a luciferase reporter construct containing the minimal *PANK2* promoter. Luciferase activity was normalized to β-galactosidase activity and error bars represent standard error. *$p<0.05$ by student t-test.

Table 2.4: primers for DNA ChIP PCR

Name	Sequence
Hp2prom2F	AGGCTAGCAGGAGGCTCGGGCCCTTCCACCCACG
Hp2prom9F	AGGCTAGCCCTCCGCGGAACCCGGATCCCCTCCTCCACCACCC
Hp2prom10F	AGGCTAGCGACGGAGGCACGGTCAATCCTCCTCGAGTTAGGGAG
Hp2prom4R	GCAAGCTTGGTTGCGCCAACGCGCAGGAAGCCAATC
Hp2prom1R	GCAAGCTTGCAAGCCCCCCAGCGTCGGATTCCTTCTCGCC

Figure 2.14: Location of *PANK2* primers for ChIP PCR within the *PANK2* promoter.

PANK2 5'genomic sequence with primer locations marked with blue arrows and *PANK2* EMSA5 probe sequence highlighted in orange. The sequence corresponds to chr20:3,869,746-3,870,125 on Human GRCh37 Assembly (hg19).

A

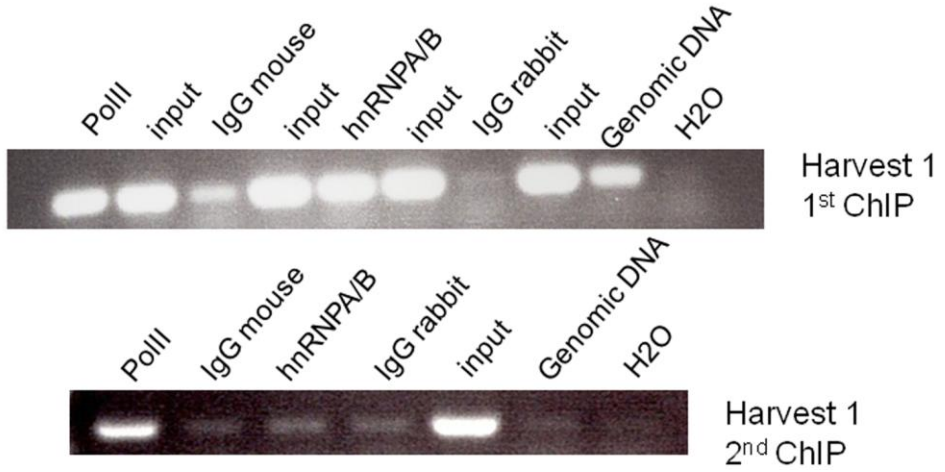

B

	10F/1R	9F/4R	2F/4R	9F/1R
SH-SY5Y Harvest 1	positive negative	positive	positive	positive
SH-SY5Y Harvest 2	negative	positive	negative	negative
SH-SY5Y Harvest 3	positive	negative	negative	positive

Figure 2.15: Summary of ChIP experiments to detect hnRNPA/B proteins bound to the *PANK2* promoter in SH-SY5Y cells.

A) Representative PCR result of two separate chromatin immunoprecipitations performed on SH-SY5Y cell harvest 1 with 10F/1R primers. B) Summary of hnRNPA/B ChIP results from three independent SH-SY5Y platings and crosslinking. "Positive" results indicate that more DNA was amplified from hnRNPA/B immunoprecipitation than the IgG rabbit immunoprecipitation, while "negative" indicates that equal or less DNA was amplified from hnRNPA/B immunoprecipitation than the IgG rabbit immunoprecipitation.

promoter primer sets. As summarized in Figure 2.15b, I continued to obtain inconsistent results from these experiments.

The inconsistent ChIP results, combined with my failure to validate hnRNPA/B knockdown by shRNA, resulted in our decision to publish the *PANK2* promoter characterization studies without conclusive evidence of *PANK2* transcriptional regulation by hnRNPA/B proteins.

Chapter 3

Expression and function of miR-103/7

Chapter 3.1

Discordant expression of miR-103/7 and pantothenate kinase host genes in mouse

*manuscript in press as a Brief Communication to *Molecular Genetics and Metabolism*

Brenda J Polster[1*], Shawn K Westaway[2], Thuy M Nguyen[1] and Susan J Hayflick[1]

[1] Molecular and Medical Genetics, Oregon Health and Science University, Portland OR.

[2] Neurology, Oregon Health and Science University, Portland OR.

3181 SW Sam Jackson Park Rd, Portland OR 97239, USA

[*]corresponding author
Phone: 503 494 2449
Fax: 503 494 6886
Email: polsterb@ohsu.edu

Abstract

miR-103 and miR-107, microRNAs hosted by pantothenate kinase genes, are proposed to regulate cellular lipid metabolism. microRNA-mediated regulation is complex, potentially affecting expression of the host gene, related enzymes within the same pathway, or apparently distinct targets. Using qRT-PCR, we demonstrate that miR-103 and miR-107 expression does not correlate with expression of host pantothenate kinase genes in mouse tissues. The miR-103/7 family thus provides an intriguing model for dissecting microRNA transcription, processing and coordinated function within host genes.

Keywords: intronic microRNA, pantothenate kinase

Abbreviations: miRNA, microRNA; PANK, pantothenate kinase; PKAN, pantothenate kinase-associated neurodegeneration; preliminary microRNA, pre-miRNA; UTRs, untranslated regions.

1. Introduction

Mammalian microRNAs (miRNAs) are post-transcriptional regulators that bind to complementary regions generally within 3' untranslated regions (UTRs) of messenger RNA transcripts (mRNAs), forming double-stranded RNA complexes that ultimately result in gene silencing. Approximately 37% of mammalian miRNAs are located within the introns of protein-coding genes (Griffiths-Jones et al., 2006).. Initially, intronic miRNAs were predicted to be co-transcribed with their host transcript because many miRNAs and their host genes have been shown to have similar expression patterns (Rodriguez et al., 2004). However, not all miRNA expression correlates with host gene expression (Baskerville and Bartel, 2005; Liang et al., 2007). miRNAs thus likely represent an integral part of a complex regulatory network controlling many key cellular pathways, including metabolism. Differential miRNA expression may be governed by post-transcriptional regulation (Obernosterer et al., 2006), independent promoters (Monteys et al., 2010) or disparate transcript stabilities (Jung et al., 2010).

miR-103 and miR-107 are highly conserved miRNAs that map to intron 5 of three distinct pantothenate kinase (*PANK*) genes. *PANK2* and *PANK3* host the preliminary miRNA (pre-miRNA) sequences miR-103-2 and miR-103-1, respectively, which are processed into miR-103. *PANK1* encodes miR-107, which differs from miR-103 by a single nucleotide. Pantothenate kinase is the rate limiting enzyme in the biosynthesis of coenzyme A, a cofactor that is involved in over 100 metabolic reactions (Robishaw and Neely, 1985). In addition, *PANK2* is the causative gene in pantothenate kinase-associated neurodegeneration (PKAN), which is characterized by dystonia, brain iron accumulation and neuroaxonal spheroid deposition (Zhou et al., 2001).

The conservation of miR-103/7 within pantothenate kinase genes suggests a role for these miRNAs in metabolism and neurodegeneration. miR-103 and miR-107 are both ubiquitously expressed, with relative abundance in the brain (Babak et al., 2004; Baskerville and Bartel, 2005). However, differential expression of miR-103 and miR-107 has been reported in adipogenesis (Xie et al., 2009), models of diabetes (Herrera et al., 2010) and following glucose treatment in a pancreatic β cell line (Tang et al., 2009), as well as in neurological disease (Nelson and Wang, 2010; Wang et al., 2008) and cancer (Lee et al., 2009; Roldo et al., 2006; Takahashi et al., 2009; Volinia et al., 2006; Yamakuchi et al., 2010). Functionally, miR-103/7 are predicted to target many enzymes that are important in regulating metabolism (Wilfred et al., 2007). Moreover, experimentally validated miR-103/7 targets include β-site amyloid precursor protein-cleaving enzyme 1 (BACE1) (Wang et al., 2008), granulin (GRN) (Wang et al., 2010) and hypoxia inducible factor-1β (HIF-1β) (Yamakuchi et al., 2010), which have all been implicated in neurodegeneration.

Microarray analyses of miRNA and mRNA profiles in human tissues previously revealed a low correlation between the ubiquitously expressed miR-103/7 family and their host genes (Baskerville and Bartel, 2005; Liang et al., 2007). However, in cell culture, correlated expression has been observed. For example, there is similar induction of miR-103/7, *Pank1*, *Pank2* and *Pank3* expression during differentiation of 3T3-fibroblasts to adipocytes (Xie et al., 2009). Also, p53 can induce expression of *PANK1* and miR-107; presumably, through a p53 element located ~1kb upstream of the *PANK1* transcriptional start site (Yamakuchi et al., 2010). Finally, studies in a pancreatic cancer

cell line suggest that miR-107 expression can be regulated through epigenetic silencing of the *PANK1* promoter (Lee et al., 2009).

However, evidence is also surfacing for independent transcription of miR-107 and *Pank1*. In particular, Monteys et al. recently described an independent miR-107 promoter that is sufficient to drive miR-107 expression in a promoterless plasmid (Monteys et al., 2010). In another study, Corcoran et al. also predicted miR-107 to have an independent promoter, based on RNA polymerase II chromatin immunoprecipitation experiments (Corcoran et al., 2009). Interestingly, however, miR-103-1 and miR-103-2 are not predicted to have promoters independent of *Pank3* and *Pank2*, respectively (Corcoran et al., 2009).

In this short report, we present the relative expression of the pantothenate kinase genes and their intronic miRNAs in various mouse tissues and discuss the relationship of these expression levels to the regulation and function of these miRNAs.

2. Material and Methods

qRT-PCR

Total RNA was harvested from three 100 day old C.D2 Es-Hba wildtype mice using RNAqueous-Micro kit (Ambion, Inc.) for retinal tissue and RNA-STAT60 (Tel-Test, Inc.) for all other tissue.

To quantify *Pank1*, *Pank2* and *Pank3* mRNA levels, cDNA was synthesized from 50ng total RNA using the High-Capacity cDNA Reverse Transcription Kit (Applied Biosystems, Inc.) according to the manufacturer's instructions. For PCR, cDNA was diluted using RNase free water, mixed with primer/probe sets for *Pank1*

(Mm00458408_m1), *Pank2* (Mm00463258_m1), *Pank3* (Mm00461298_m1) or *Gusb* (Mm03003537_s1) and 2× PCR Universal Master Mix (Applied Biosystems, Inc.). PCR reactions were performed in triplicate on an ABI Prism 7000 Sequence Detections System following the manufacturer's directions.

To quantify miRNAs, cDNA was reverse transcribed from 4ng total RNA using primers from miR-103 (assay ID 439), miR-107 (assay ID 443) or snoRNA234 (assay ID 1234) TaqMan MicroRNA Assays and reagents from the TaqMan MicroRNA Reverse Transcription kit (Applied Biosystems, Inc.). The resulting cDNA was amplified by PCR using primer/probe sets supplied with the TaqMan MicroRNA Assays and 2x TaqMan Universal PCR Master Mix (Applied Biosystems, Inc.). PCR reactions were performed in triplicate on an ABI Prism 7000 Sequence Detections System following the manufacturer's directions.

Gusb and snoRNA234 were endogenous controls for the analysis of *Pank* and miRNA expression, respectively. For each tissue, the mean $Ct_{control}$ value was subtracted from the mean $Ct_{experimental}$ value (ΔCt). Spleen was chosen as a reference tissue and the mean ΔCt value for spleen was subtracted from each tissue ΔCt value ($\Delta\Delta Ct$). Relative expression (RE) in each tissue was calculated as $RE = 2^{-\Delta\Delta Ct}$. The mean of the RE for three biological replicates is plotted in Figure 1 and error bars represent the standard error of the mean.

3. Results & Discussion

To determine whether miR-103 and miR-107 are co-expressed with their host genes in mouse, we measured relative miR-103, miR-107, *Pank1*, *Pank2* and *Pank3*

expression by qRT-PCR (Figure 3.1). We detected widespread expression of all pantothenate kinase genes. *Pank2* has highest expression in brain, retina and testis, three tissues that are affected by PKAN (Hayflick et al., 2003). *Pank3*, in contrast, is most abundantly expressed in the small intestine, and *Pank1* has relative abundance in the liver. Notably, the relative expression patterns of *Pank1*, *Pank2* and *Pank3* in testis, brain and liver differ from a previously published report (Leonardi et al., 2007b). miR-103 is broadly expressed across mouse tissues with highest relative expression in brain and lung, consistent with previous findings using microarrays (Babak et al., 2004). In contrast, miR-107 was most abundant in brain and kidney.

Despite the shared characteristic of ubiquitous expression, miR-103 and miR-107 expression profiles poorly correlate with that of their host genes. For miR-107, this result supports the recent model of transcription from an independent promoter (Monteys et al., 2010). For miR-103, the discordant expression is likely attributed, at least in part, to its redundant expression from *Pank2* and *Pank3* transcripts. However, post-transcriptional factors may also play a role in controlling the relative abundance of the mature transcript. In support of this concept, Lee et al have demonstrated that regulation at the level of microRNA processing is common and often controls tissue-specific regulation of ubiquitously expressed miRNA precursor transcripts (Lee et al., 2008).

The miR-103/7 family represents an intriguing model of disease-associated intronic microRNA. They are highly conserved within pantothenate kinase genes; one of which, *PANK2*, is associated with a neurodegenerative disease. Moreover, miR-103/7 likely regulates proteins involved in acetyl-coA metabolism, as well as neurodegeneration. However, expression of the mature microRNAs is not synchronized

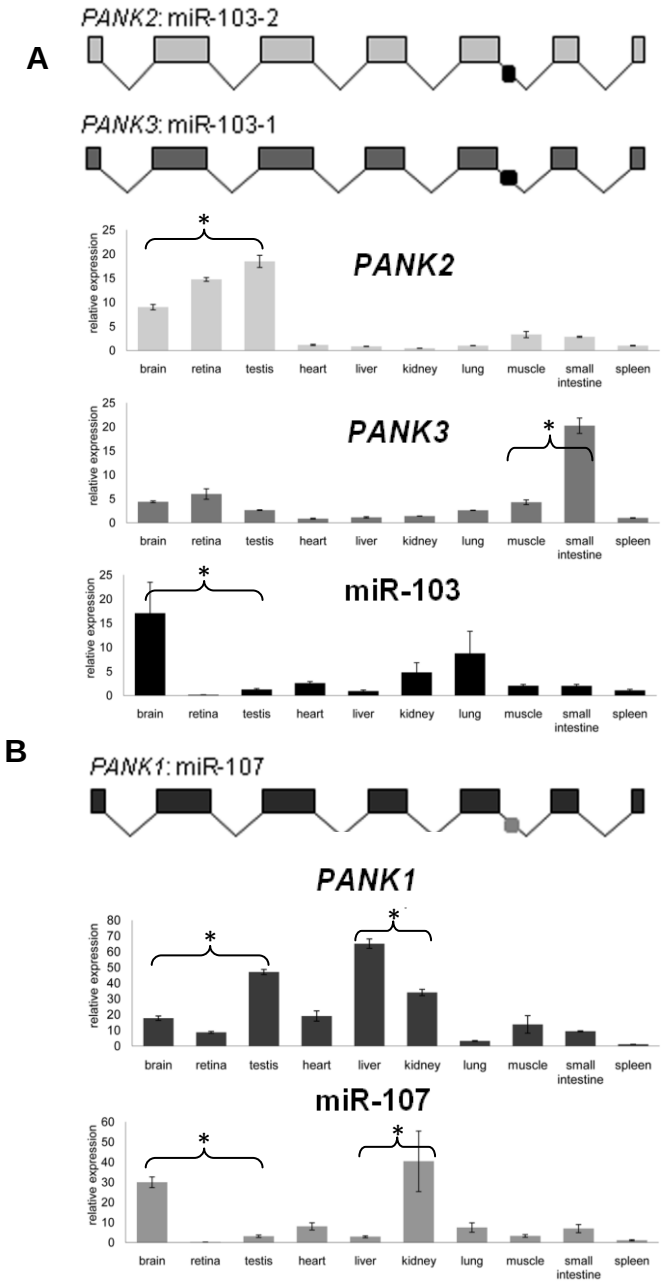

Figure 3.1: Relative expression of miR-103, miR-107 and their host genes in mouse tissues.

RNA was harvested from mouse tissues (n=3) and analyzed by qRT-PCR. Error bars represent standard error.
Not included in submitted manuscript: Groups were tested and compared using ANOVA and Bonferroni post-hoc test. P values <0.05 were taken as significant and (*) indicates a significant pairwise change. Select pairwise comparisons are shown to emphasize differences in expression patterns.

with that of the host genes. These distinct expression patterns are likely due to multiple factors, including the existence of alternate promoters, variable stabilities of the RNA transcripts and regulation of post transcriptional processing. Therefore, the miR-103/7 family provides an intriguing model for dissecting miRNA transcription, processing and coordinated function with host genes.

ACKNOWLEDGEMENTS

This work was supported by the Huebner Family Pediatric Neurobiology of Disease Fellowship (to B.P.).

Chapter 3.2

Additional miR-103 studies

unpublished results

3.2.1 Precursor and mature miR-103 expression in mouse

Experimental Rationale

In cases where intronic miRNA expression does not correlate with host gene expression, the differential expression may be governed by post-transcriptional regulation of miRNA processing. miRNA processing involves cleavage of the primary precursor transcript (pre-miRNA) to a ~70 nucleotide precursor (pre-miRNA) (Denli et al., 2004) within the nucleus. Then, the pre-miRNA is exported to the cytoplasm (Bohnsack et al., 2004), where it is further cleaved and processed to yield the mature miRNA (Chendrimada et al., 2005). In the past years, several instances of cell and tissue-specific regulation of this process have been observed (Lee et al., 2008; Michael et al., 2003; Obernosterer et al., 2006). Therefore, I hypothesized that the disparate expression profiles of miR-103/7 and pantothenate kinase genes observed in Chapter 3.1 may be caused by tissue specific regulation of miRNA processing. To test this hypothesis, I analyzed RNA from mouse tissues by Northern blot to visualize the relative expression of pre-miR-103-2, encoded by *PANK2* intron 5, and the mature miR-103.

Materials and Methods

Northern blot

Total RNA was harvested in Trizol from 100 day old Hba wildtype mouse tissues and stored at -20C. For Northern blot analysis, 5μg of RNA was run on a 15% denaturing polyacrylamide gel at 150V for ~1.5 hours. The RNA was transferred to a positively charged nylon membrane (BrightStar-Plus membrane (Ambion)) for 45 minutes at 200mA, using an Invitrogen XCellII Blot Module. The membrane was

crosslinked using the UV Stratalinker 1800, allowed to dry and prehybridized in ULTRAhyb-Oligo hybrdiziation buffer (Ambion) with rotation for 30 minutes at 42°C. Then, the membrane was hybridized with rotation at 42°C overnight in 100ng/ml 3'DIG labeled miRCURY probes (Exiqon) to detect mature miR-103 (5'TCATAGCCCTGTACAATGCTGCT 3') or miR-103-2 (5'GACCTGAATGCTACAAG 3'). The membrane was washed, twice, for 30 minutes in 2x SSC with 0.5% SDS at 42°C. Finally, the miRCURY probe was detected using the DIG Wash and Block buffer set (Roche), DIG Luminescent Detection kit (Roche) and exposure to film (X-Omat Blue XB-1 (Kodak)).

Results and Discussion

To investigate whether miR-103-2 is subject to post-transcriptional regulation, I compared miR-103-2 and miR-103 expression in mouse tissues by Northern blot (Figure 3.2). As expected, the pattern of miR-103 expression observed by Northern blot matched the expression pattern measured by qRT-PCR on the same tissues, with highest expression observed in brain and lung (Chapter 3.1, Figure 3.1). However, miR-103-2 had higher expression in all tissues that miR-103. Most strikingly, miR-103-2 expression was much higher in intestine, kidney, liver and spleen than miR-103. This result suggests that miR-103-2 may be post-transcriptionally regulated for tissue specific expression. However, as with the qRT-PCR results discussed in Chapter 3.1, interpretation of the results is complicated by the fact that two miR-103 precursor species (miR-103-2 from PANK2 and miR-103-1 from PANK1) give rise to the mature miR-103 sequence.

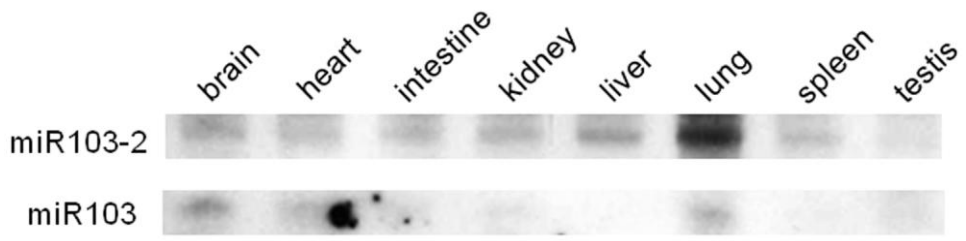

Figure 3.2: Discordant expression of precursor (*miR-103-2)* and mature (*miR-103*) transcripts in mouse tissue by Northern blot.

5μg of total RNA from each mouse tissue was loaded onto a 15% denaturing polyacrylamide, transferred to a positively charge nylon membrane and hybridized with DIG-labeled probes to pre-miR-103-2 and miR-103.

3.2.2 The search for miR-103 targets

Experimental Rationale

MicroRNAs function by imperfect pairing to nucleotide sequences, which can result in the inhibition of mRNA translation or affect mRNA transcript stability (Filipowicz et al., 2008). Therefore, a common approach to delineating miRNA function is to identify the proteins that it regulates. Soon after the identification of mammalian miRNAs, many microRNA target prediction programs became available to predict miRNA recognition elements (MREs) (John et al., 2004; Kiriakidou et al., 2004; Lewis et al., 2003). Common methods to experimentally validate regulation of the predicted miRNA targets include luciferase reporter assays and monitoring endogenous levels of the predicted targets following miRNA overexpression or inhibition. I used these two experimental approaches in attempt to confirm miR-103 regulation of predicted targets.

In total, I investigated nine predicted miR-103 targets. Initially, I investigated AXIN2, OTX1, SMYD5, ANXA11, FBXW1B, FMR2 and CKB by luciferase reporter assays. Next, I investigated PRPF4b and BDNF regulation by over expressing miR-103 in SH-SY5Y cells and monitoring the level of the endogenous targets by western blot.

Materials and Methods

microRNA target prediction

miR-103 target predictions were obtained from TargetScan (http://genes.mit.edu/targetscan) (Lewis et al., 2003), miRanda (www.microrna.org) (John et al., 2004) and DIANA-microT (http://diana.cslab.ece.ntua.gr/microT/) (Kiriakidou et al., 2004; Maragkakis et al., 2009) . Conservation of the miR-103

recognition elements was analyzed using the UCSC Human Genome Browser (Kent et al., 2002).

Plasmid Construction

For AXIN2, OTX1 and SMYD5 constructs, the genes' 3'UTR were amplified from human genomic DNA by PCR (primers in Table 3.1). For the Lin41 constructs, a 185 bp region of the Lin41 3'UTR was amplified from *C.elegans* genomic DNA using primers (Table 3.1) as previously described (Vella et al., 2004). The PCR products were purified and cloned into pCR-TOPO (Invitrogen), digested with NheI and SacI restriction enzymes and subcloned into pISO (kind gift from David Bartel) (Lewis et al., 2003). Identical reporter plasmids containing mutated MRE(s) were created by amplifying DNA from the Lin41, AXIN2, OTX1 and SMYD5 pCR-TOPO clones using primers that overlap the predicted MRE and contain mutated sequence (Table 3.1). Then, the PCR products containing mutations were purified and used as a template for PCR. The reconstructed mutant 3'UTR fragments were purified, cloned into pCR-TOPO, and subcloned into pISO using NheI and SacI restriction enzymes.

Reporter constructs for ANXA11, FBXW1B, FMR2, CKB , OTX1 and miR103T were created by embedding the predicted MRE (or mutated MRE) into a common DNA backbone containing restriction sites for Sac1, EcoR1, Pst1 and NheI. For each construct, complementary oligonucleotides (Table 3.2) were annealed and ligated into pISO that had been NheI/SacI digested and purified. The sequences of all constructs were confirmed by sequencing.

Table 3.1:
PCR primers for luciferase reporter constructs

Target	Primer name	sequence
Axin2	Axin2F	AAAGTGGAGCGGATCGATTGAG
	Axin2R	CTACATGAGGGGGAGCCTCAGT
	Axin2mt1f	GGCTATTGAAGAAGTTACCTGTATTTGAGAGAC
	Axin2mt1r	GTCTCTCAAATACAGGTAACTTCTTCAATAGCC
	Axin2mt2f	CAGTTTATGGATAAGTTACTTTAAACTTGG
	Axin2mt2r	CCAAGTTTAAAGTAACTTATCCATAAACTG
	Axin2mt3f	TCCTAAGTTACTCTGTTTTGTC
	Axin2mt3r	GGTCAACCCTCAAGACCTTTAAGACAAAACAGAGTAACTTAGGAAA
OTX1	OTX1F	CGTTGGAGCTCCTCTGGGCTTGCCTTCAACTCTG
	OTX1R	AGTTGGCTAGCGTATAGAATGTGTAGGCCAAGCCG
	OTX1MT1F	CCCGATCCTGTTGAAGTTACTGCACCGCCCG
	OTX1MT1R	CGGGCGGTGCAGTAACTTCAACAGGATCGGG
SMYD	SMYD5F	CGTTGGAGCTCCAGCTACTTGGACTGCTGTCAGCG
	SMYD5R	AGTTGGCTAGCGAAGAAACACTGTTAGGCCCTG
	SMYD5MT1	CATGCCCTGGACAAAGTTACTGAGTTGGCTC
	SMYD5MT1	GAGCCAACTCAGTAACTTTGTCCAGGGCATGAGG
LIN41	LIN41F	CGTTGGAGCTCTCTCACCATTTTAATGGTTTCCCA
	LIN41R	AGTTGGCTAGCGAGCTTAAATGAACACTGGGGACA
	LIN-41MT1R	TTGCGATATTTACATCGCGTTGAGTTGAGAACGGATGTATAA
	LIN-41MT2F	GTAAATATCGCAATCCCTTTTTATACATCCATTCTCGCTC

Table 3.2: Oligonucleotides for luciferase reporter constructs

TARGET	Oligonucleotide	Sequence
AXIN2	Anxa11mref	CACTAAATGACTCGAATTCACATCACAGCCTCTTGCTGCTACGCTGCAGG
	Anxa11mrer	CTAGCCTGCAGCGTAGCAGCAAGAGGCTGTGATGTGAATTCGAGTCATTTAGTGAGCT
	Anxa11mremtf	CACTAAATGACTCGAATTCACAACGCTGACTCGTACGGTTACGCTGCAGG
	Anxa11mremtr	CTAGCCTGCAGCGTAACCGTACGAGTCAGCGTTGTGAATTCGAGTCATTTAGTGAGCT
FBXW1B	Fbxw1bmref	CACTAAATGACTCGAATTCACATCATGACAGCTTTGTACTGTGGAATGTGCTACGCTGCAGG
	Fbxw1bmrer	CTAGCCTGCAGCGTAGCACATTCCACAGTACAAAGCTGTCATGATGTGAATTCGAGTCATTTAG TGAGCT
	Fbxw1bmremtf	CACTAAATGACTCGAATTCACATCATGACATCATCGGACTGTGGACTATTCAACGCTGCAGG
	Fbxw1bmremtr	CTAGCCTGCAGCGTTGAATAGTCCACAGTCCGATGATGTCATGATGTGAATTCGAGTCATTTAG TGAGCT
FMR2	Fmr2mref	CACTAAATGACTCGAATTCACATCCAGGCCCCTGACAGGATGCTGCACGCTGCAGG
	Fmr2mrer	CTAGCCTGCAGCGTGCAGCATCCTGTCAGGGGCCTGGATGTGAATTCGAGTCATTTAGTGAGCT
	Fmr2mremtf	CACTAAATGACTCGAATTCACAACCATGCATCGGTCGGGTTACGGAACGCTGCAGG
	Fmr2mremtr	CTAGCCTGCAGCGTTCCGTAACCCGACCGATGCATGGTTGTGAATTCGAGTCATTTAGTGAGCT
CKB	Ckbmref	CACTAAATGACTCGAATTCACAACCAGCCCTGCTGCTACGCTGCAGG
	Ckbmrer	CTAGCCTGCAGCGTAGCAGCAGGGCTGGTTGTGAATTCGAGTCATTTAGTGAGCT
	Ckbmremtf	CACTAAATGACTCGAATTCACAGCCTGGCATCCAGATACGCTGCAGG
	Ckbmremtr	CTAGCCTGCAGCGTATCTGGATGCCAGGCTGTGAATTCGAGTCATTTAGTGAGCT
OTX1	Otx1mref	CACTAAATGACTCGAATTCACATGGTCCCGATCCTGTTGCTGCTGCTACGCTGCAGG
	Otx1mrer	CTAGCCTGCAGCGTAGCAGCAGCAACAGGATCGGGACCATGTGAATTCGAGTCATTTAGTGAG CT
	Otx1mremt1f	CACTAAATGACTCGAATTCACATGGTCCCGATCCTGTTGAAGTTACTACGCTGCAGG
	Otx1mremt1r	CTAGCCTGCAGCGTAGTAACTTCAACAGGATCGGGACCATGTGAATTCGAGTCATTTAGTGAGC T
	Otx1mremt2f	CACTAAATGACTCGAATTCACATGGACCCTAGCATCTAGATACAGCAACGCTGCAGG
SMYD5	Smyd5mref	CACTAAATGACTCGAATTCACATCATGCCCTGGACACTGCTGCTACGCTGCAGG
	Smyd5mrer	CTAGCCTGCAGCGTAGCAGCAGTGTCCAGGGCATGATGTGAATTCGAGTCATTTAGTGAGCT
	Smyd5mremt1f	CACTAAATGACTCGAATTCACATCATGCCCTGGACAAAGTTACTACGCTGCAGG
	Smyd5mremt1r	CTAGCCTGCAGCGTAGTAACTTTGTCCAGGGCATGATGTGAATTCGAGTCATTTAGTGAGCT
	Smyd5mremt2f	CACTAAATGACTCGAATTCACATAAGGGCATTGCCTCTCCAGGTACGCTGCAGG
	Smyd5mremt2r	CTAGCCTGCAGCGTACCTGGAGAGGCAATGCCCTTATGTGAATTCGAGTCATTTAGTGAGCT
miR103T	Mir103targetf	CACTAAATGACTCGAATTCACATCATAGCCCTGTACAATGCTGCTACGCTGCAGG
	Mir103targetr	CTAGCCTGCAGCGTAGCAGCATTGTACAGGGCTATGATGTGAATTCGAGTCATTTAGTGAGCT

miR-103 over expression and inhibition reagents

Pre-miR™ miRNA Precursors were ordered from Ambion, Inc. (pre-miR™103, cat#17100; Pre-miR™ negative control #1, cat# 17110) and miRIDIAN™ MicroRNA Mimics were ordered from Dharmacon, Inc. (miR-103 Mimic, custom order C-300039-02-005; miRIDIAN™ microRNA Mimic Negative Control #1, CN-001000-01-05). 2'O methyl oligonucleotides were synthesized by the OSYN MMI Core facility at OHSU (2'OMe miR103 AS, 5'GCUUUCAGCUUCUUUACAGUGCUGCCUUGUA3'; 2'OMe miR103 S, CCAGUUCGUCGUAACAUGUCCCGAUACUUUC3')).

Cell culture and transfection

Human neuroblastoma (SH-SY5Y) cells were cultured in RPMI with 10% FBS, 10 ng/ml human neuron growth factor, non-essential amino acids and penicillin/streptomycin antibiotics at 37ºC and 5% CO2. Mouse neuroblastoma (N2a) cells were cultured in MEM with L-glutamine + Earle's BSS, 1.5 g/L sodium bicarbonate, 0.1 mM non-essential amino acids, 1 mM sodium pyruvate, 10% FBS and penicillin/streptomycin antibiotics at 37ºC and 5% CO_2. HeLa cells were cultured in high glucose DMEM with L-glutamine, 10% FBS and penicillin/streptomycin antibiotics at 37ºC and 5% CO_2.

To assay the activity of endogenous miR-103, HeLa cells were seeded in 12-well plates, grown to 90% confluency, and transfected with 0.4 µg CMV-β-galactosidase and 0.4 µg of pISO reporter plasmids using Lipofectamine 2000 (Invitrogen) according to manufacturer's instructions. Cells were harvested in 100 µl Passive Lysis Buffer (Promega) 24 hours after transfection.

To assay the activity of miR-103 following inhibition and over expression , HeLa cells were seeded in 24-well plates, grown to 80% confluency and transfected with 5nM pre-miR™103 or Pre-miR™ negative control #1 and 0.8μg RSV-βgal. Then, the cells were grown for 24 hours and re-transfected with 5nM 2'OMe miR103 AS or 2'OMe miR103 S and 0.8μg miR103T. Both transfections were conducted using lipofectamine 2000 according to the manufacturer's instructions. 24 hours after the second transfection, the cells were harvested in 100μl passive lysis buffer

To verify miR-103 overexpression by Northern blot, SH-SY5Y cells were seeded in 12-well plates, grown to 90% confluency and transfected with 1.6μg pISO and 1-20nM pre-miR™103 with lipofectamine 2000, according to the manufacturer's instructions . RNA was harvested 24 hours later using the *mir*Vana™ Paris Kit (Ambion).

To verify miR-103 over expression by qRT-PCR, N2a cells were seeded in 24-well plates, grown to 80% confluency and transfected with 0.8μg pISO and pre-miR™103, Pre-miR™ negative control #1, miR-103 Mimic, or miRIDIAN™ microRNA Mimic Negative Control #1. RNA was harvested in RNA-STAT60 24 hours later.

To assay the effect of miR-103 over expression on predicted targets, N2a cells were seeded in 60mm plates at $3x10^5$ cells/ml, grown 24 hours, and transfected with 8μg pISO and pre-miR™103, Pre-miR™ negative control #1, miR-103 Mimic, or miRIDIAN™ microRNA Mimic Negative Control #1. 24 hours later, protein was harvested for luciferase assays and western blot.

Luciferase and β-galactosidase assays

To assay for β-galactosidase activity, 50 µl of cell lysate was combined with 60 µl Z buffer (60mM Na_2HPO_4, 40mM NaH_2PO_4, 10 mM KCl, 1 mM $MgSO_4$, 50mM 2-Mercaptoethanol, pH 7.5) and 40 µl ONPG substrate (Sigma) (4 mg/ml in 60 mM Na_2HPO_4, 40mM NaH_2PO_4, pH 7.5 buffer) and incubated at 30ºC for 30 minutes. The reaction was quenched by adding 100 µl of 1 M Na_2CO_3 and measured at A_{420}. To assay for luciferase activity, 20 µl of cell lysate was combined with 300 µl of GlyGly-ATP (25mM Glycylglycine, 15 mM $MgSO_4$, 5 mM ATP) and 100 µl of luciferin (Promega) (300 µg/ml) and measured on a luminometer.

qRT-PCR

To quantify miR-103, cDNA was reverse transcribed from total RNA using specific miRNA primers from the hsa-miR-103 TaqMan MicroRNA Assay (Applied Biosystems) and reagents from the TaqMan MicroRNA Reverse Transcription kit (Applied Biosystems). The resulting cDNA was amplified by PCR using TaqMan MicroRNA Assay primers with the TaqMan Universal PCR Master Mix according to the manufacturer's instructions. The relative levels of miRNA expression were normalized to snoRNA135 and relative expression was calculated by the ΔΔCt method.

For *PRPF4b* detection in mouse tissues, 2µg of RNA was DNase treated and reverse transcribed using High-capacity cDNA Reverse Transcription kit (Applied Biosystems). Relative expression of *PRPF4b* mRNA was quantified using TaqMan Gene Expression Assays (Applied Biosystems). *TBP*, *HMBS* and *RPLP0* were used to

normalize *PRPF4b* expression across tissues. The data was analyzed using the comparative Ct method in the qBasePlus software.

Northern blot

RNA was harvested from each well of a 12 well plate of SH-SY5Y cells using the *mir*Vana™ Paris Kit (Ambion) and resuspended in a final volume of 100µl elution buffer. 20ml of each RNA sample was analyzed by Northern blot as described in Ch 3.2.1 Materials and Methods.

Western blot

N2a cells were transfected as described above. 24 hours after transfection, cells were washed with PBS and lysed in ice cold cell disruption buffer (Ambion PARIS™ kit) containing protease inhibitors (Complete Mini EDTA-free protein inhibitor cocktail, Roche). Equivalent volumes of cell lysates were separated using 10% (for PRPF4b) or 15% (for BDNF) SDS-PAGE. Protein was transferred to a nitrocellulose membrane and the membrane was probed using rabbit anti-human PRP4 (Abgent cat#AP7551b) or chicken anti-human BDNF (Promega cat#G1641) and mouse anti-β-Actin (Sigma, cat#A5441) antibodies. Goat anti-rabbit Alexafluor 680 (Molecular Probes cat#A21058), IRDye800 goat anti-mouse (Rockland code#610-131-121), and IRDye800 goat anti-chicken (Rockland code#603-132-126) secondary antibodies were used and membranes were imaged using the LiCor Odyssey Imaging System.

Results and Discussion

Investigation of predicted targets by luciferase reporter assays

Multiple prediction programs are currently available to identify miRNA targets (Yue et al., 2009). However, at the onset of this project, in 2004, only a few prediction programs for mammalian miRNA targets were available; using these tools, I identified seven targets for preliminary investigation. AXIN2 was predicted by TargetScan, which combined thermodynamics-based modeling of RNA:RNA interactions with comparative sequence analysis to predict miRNA targets conserved across multiple genomes (Lewis et al., 2003). ANXA11, FMR2, FBXW1B and CKB were predicted by Diana-microT, which predicted targets based on experimental evaluation of the significance of individual miRNA bases in target recognition (Kiriakidou et al., 2004). Finally, *OTX1* and *SMYD5* were investigated based on their co-expression with miR-103 in the brain and region of complementarities with miR-103 in their 3'UTRs (Krichevsky et al., 2003).

A luciferase reporter system was used to investigate miR-103 regulation of these targets (Figure 3.3). Briefly, I inserted predicted miR-103 MRE(s) downstream of a firefly luciferase gene and transfected the constructs into HeLa cells, which endogenously express miR-103 (Mourelatos et al., 2002). Luciferase activity was compared to that of an analogous reporter with point mutations within the MRE(s) to determine miR-103 regulation through the MRE. As a positive control, experiments were performed using a 124nt segment of *c.elegans lin-41* 3'UTR that contains two let-7 miRNA recognition elements (Lewis et al., 2003). Notably, I used two reporter construct designs for these assays (Figure 3.4). AXIN2, OTX1 and SMYD5 reporter constructs contain ~500-1000 nucleotides of the genes' 3'UTR. However, to increase efficiency of cloning, I created

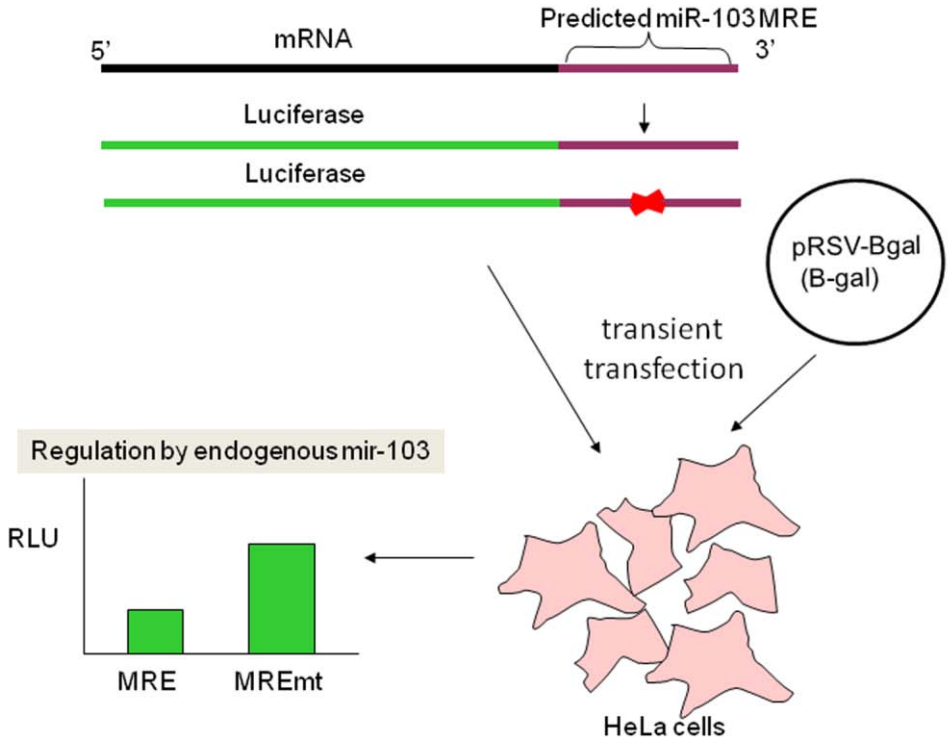

Figure 3.3: Luciferase reporter assay for miR-103 regulation of predicted miRNA recognition elements (MRE).

Luciferase reporter constructs containing wildtype or mutated miR-103 recognition elements were co-transfected with pRSV-βgal into HeLa cells, which endogenously express miR-103. miR-103 regulation through the predicted MRE was determined by comparing the relative luciferase activity (RLU) of wildtype and mutant reporter constructs.

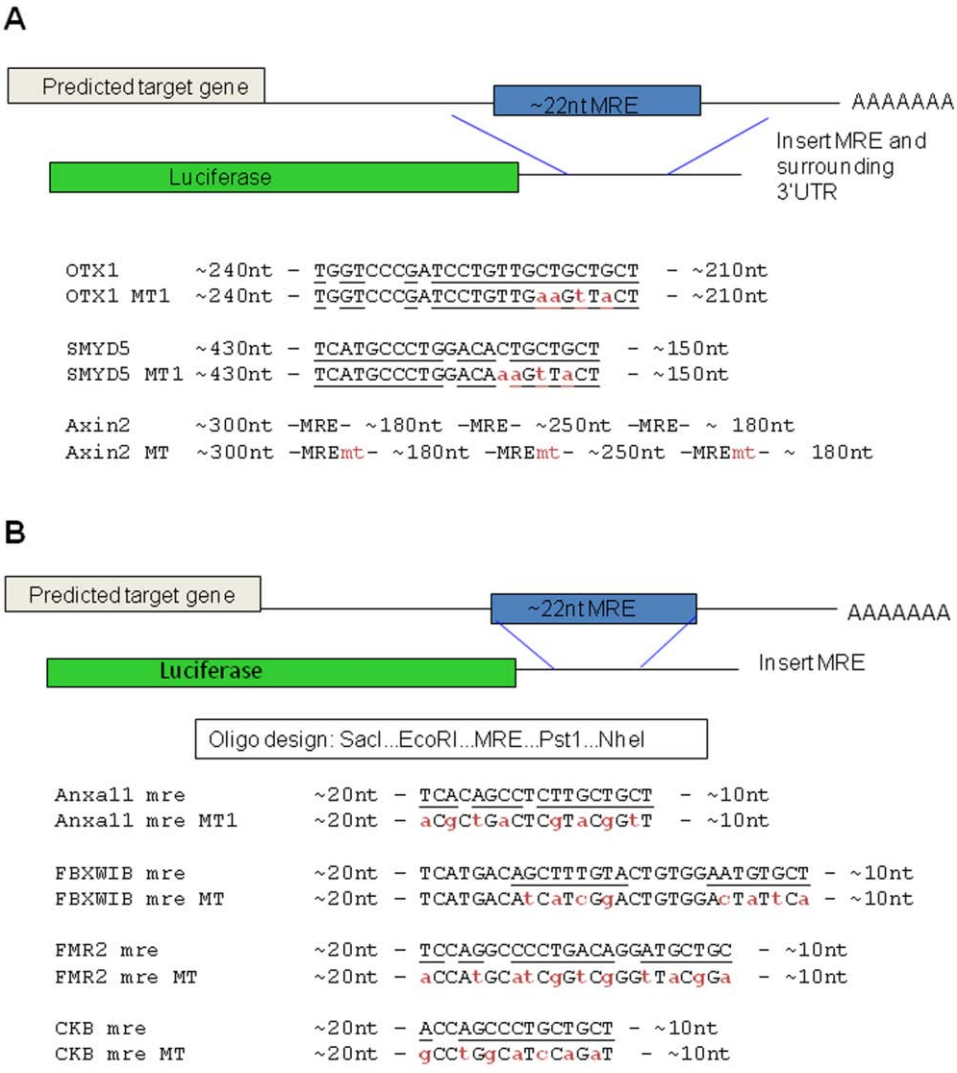

Figure 3.4: miR-103 MRE reporter construct design

A) Reporter constructs for AXIN2, OTX1 and SMYD5 were created to contain ~500-1000 nucleotides of the genes' 3'UTR.
B) Reporter constructs for ANXA11, FMR3, FBXW1B and CKB were created by inserting the predicted MRE sequence into a ~70 nucleotide common DNA backbone for direct cloning into the pISO 3'UTR.

reporter constructs for ANXA11, FMR3, FBXW1B and CKB by another established miRNA reporter assay protocol (Kiriakidou et al., 2004), which involves inserting the predicted MRE sequence into a ~70 nucleotide common DNA backbone for direct cloning into the pISO 3'UTR.

Mutation of the predicted MREs resulted in a significant increase in luciferase activity for the *Lin41* control, AXIN2 and OTX1, and a significant decrease in activity for SMYD5, FBXW1B and FMR2 (Figure 3.5). These results indicate that miR-103 down-regulates AXIN2 and OTX1 through the MRE(s) in their 3'UTRs, but increases cellular levels of SMYD5, FBXW1B and FMR2. However, while the results were statistically significant by a one sample t-test, I did not feel comfortable drawing conclusions from the very small changes in luciferase activity. Therefore, I tested additional reporter constructs to confirm miR-103 regulation of OTX1 and SMYD5 (Figure 3.6a). Briefly, I compared the results of the original experimental design (constructs containing ~500 nucleotide of the 3'UTR) with results generated with reporter constructs lacking the 3'UTR context ("mre" constructs) and containing different point mutations in the MRE.

For both OTX1 and SMYD5, the additional experiments did not confirm regulation by miR-103 (Figure 3.6b). OTX1mreMT1, which contains the same MRE point mutations as the original experimental design, caused a decrease in luciferase activity compared to OTX1mre. However, the differentially mutated OTX1mreMT2 construct did not demonstrate a significant change in luciferase activity from OTX1mre. For the SMYD5 constructs, SMYD5mreMT1 had similar luciferase activity as SMYD5mre, while SMYD5mreMT2 gave increased luciferase activity. Therefore,

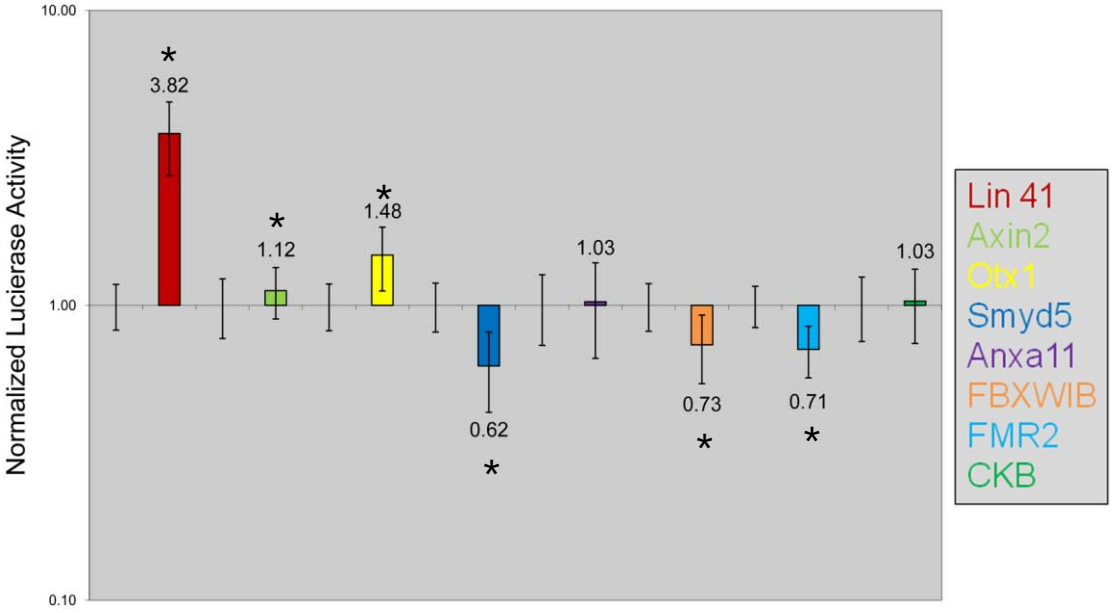

Figure 3.5: Regulation of predicted miR-103 targets.

Relative luciferase activity of MRE target constructs. For each predicted target, the colored bar represents the luciferase activity of the reporter construct containing the mutated miR-103 MRE. The wildtype MRE construct values were set to one and shown to the left of each mutant construct result. Luciferase activity was normalized to β-galactosidase activity and error bars represent standard deviation of three experiments performed in triplicate. *indicates a significant ($p<0.05$) change in wildtype versus mutant construct luciferase activity according to a one sample t-test.

A

```
OTX1           ~240nt - TGGTCCCGATCCTGTTGCTGCTGCT  - ~210nt
OTX1 MT1       ~240nt - TGGTCCCGATCCTGTTGaaGtTaCT  - ~210nt
OTX1 mre       ~20nt  - TGGTCCCGATCCTGTTGCTGCTGCT  - ~10nt
OTX1 mre MT1   ~20nt  - TGGTCCCGATCCTGTTGaaGtTaCT  - ~10nt
OTX1 mre MT2   ~20nt  - TGGaCCCtAgCaTcTaGaTaCaGCa  - ~10nt

SMYD5          ~430nt - TCATGCCCTGGACACTGCTGCT  - ~150nt
SMYD5 MT1      ~430nt - TCATGCCCTGGACAaaGtTaCT  - ~150nt
SMYD5 mre      ~20nt  - TCATGCCCTGGACACTGCTGCT  - ~10nt
SMYD5 mre MT1  ~20nt  - TCATGCCCTGGACAaaGtTaCT  - ~10nt
SMYD5 mre MT2  ~20nt  - TaAgGgCaTtGcCtCTcCaGgT  - ~10nt
```

B

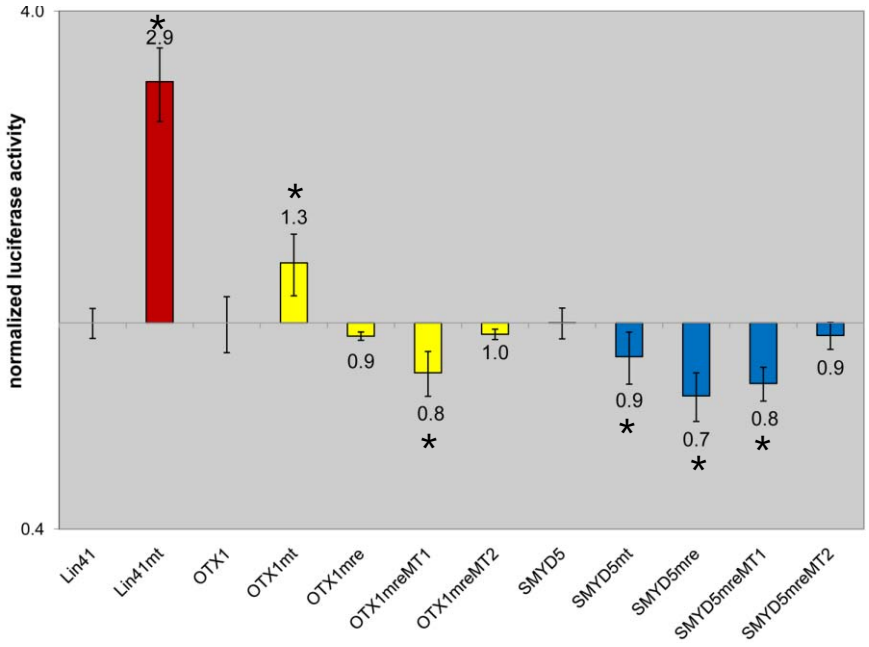

Figure 3.6: Effects of construct and mutation design on luciferase reporter assays

A) Comparison of MRE target construct and mutation designs
B) Relative luciferase activity of MRE target constructs. Luciferase activity is normalized to β-galactosidase activity and error bars represent standard deviation of two experiments performed in triplicate. *indicates a significant ($p<0.05$) change in luciferase activity from OTX1 or SMYD5 constructs according to a one sample t-test.

varying the reporter constructs' design induced changes in luciferase activities that are similar in magnitude to the changes seen for AXIN2,OTX1, SMYD5, FBXW1B and FMR2 (Figure 3.5).

As a result of these experimental inconsistencies, I am unable to confirm AXIN2, OTX1, SMYD5, ANXA11, FBXW1B, FMR2 or CKB as miR-103 targets.

miR-103 over expression and inhibition

In developing a new approach to identify miR-103 targets, I attempted to over express miR-103 and inhibit miR-103 activity in cell culture.

I used two reagents for miR-103 over expression: Pre-miR™ miRNA Precursor Molecules from Ambion, Inc. and miRIDIAN™ MicroRNA Mimic oligonucleotides from Dharmacon, Inc. Both of these reagents are advertised as double-stranded, chemically modified oligonucleotides designed to mimic the endogenous mature microRNAs (www.ambion.com, www.dharmacon.com). miR-103 over expression following transfection with pre-miR™103 was confirmed by Northern blot and qRT-PCR; miR-103 over expression following transfection with miR-103 Mimic was confirmed by qRT-PCR (Figure 3.7).

To inhibit miR-103 activity, I used 2'O-methyl oligoribonucleotides, which are nuclease resistant and function as irreversible, stoichiometric inhibitors of siRNA and miRNA function (Hutvagner et al., 2004; Meister et al., 2004). The miR-103 inhibitor, 2'OMe miR103 AS, is complementary to the mature miR-103 sequence, while a 2'O-methyl oligoribonucleotide identical to the mature miR-103 sequence (2'OMe miR103 S) serves as a negative control.

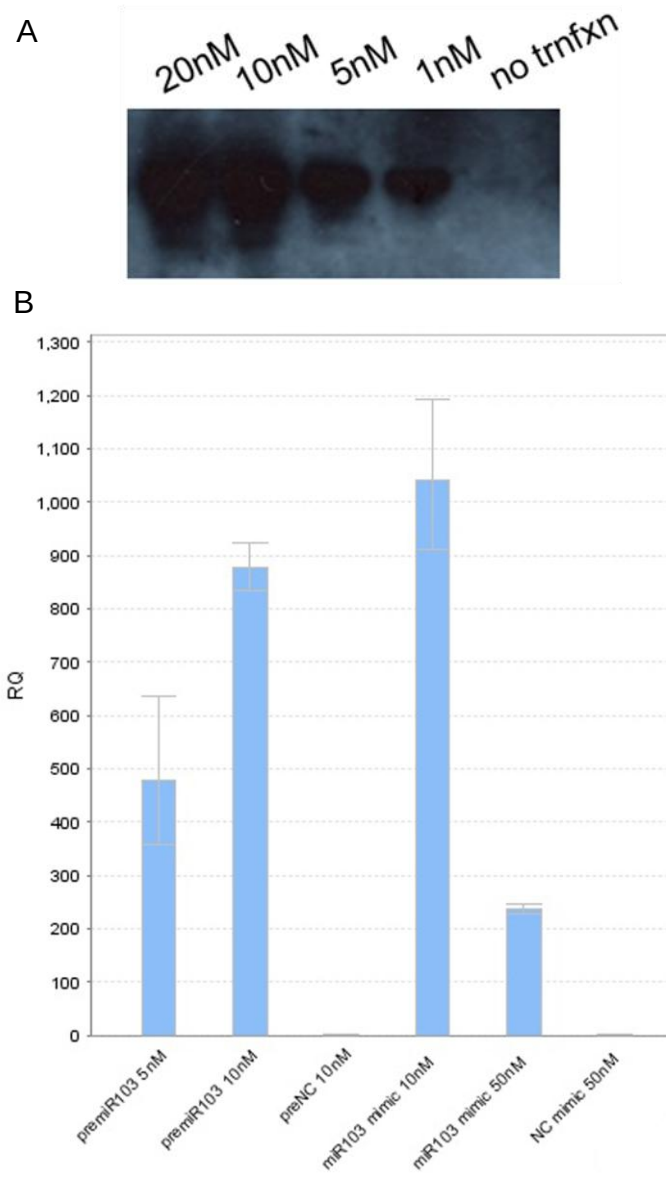

Figure 3.7: Evidence of miR-103 over expression

A) Northern blot analysis of SH-SY5Y cells transfected with 1-20nM of pre-miR™103. RNA was harvested from each well of a 12 well plate of SH-SY5Y cells using the *mir*Vana™ Paris Kit (Ambion) and resuspended in a final volume of 100µl elution buffer. 20ml of each RNA sample was loaded per well. B) Fold change (RQ) in the relative expression of miR-103 following transfection of N2a cells with pre-miR™103, pre-miR™NC, miR-103 Mimic and miRIDIAN mimic oligonucleotide negative control (NC). Error bars represent standard deviation.

To verify miR-103 inhibition, I sequentially transfected HeLa cells with 5nM pre-miR™103 or pre-miR™ negative control (NC), a luciferase reporter containing the miR103 complement sequence (mir103T) and 5nM 2'O-methyl oligonucleotides (Figure 3.8a). Cells that were transfected with pre-miR™103 had significantly less luciferase activity than cells transfected with a pre-miR™NC, indicating that miR-103 over expression caused significant degradation of the reporter transcript. However, 2'OMe103 AS did not inhibit the miR-103 activity (Figure 3.8b). Likewise, additional experiments with increasing ratio of 2'OMe103 AS to pre-miR™103 (2:1, 4:1, 10:1 and 50:1) did not demonstrate miR-103 inhibition (data not shown). Therefore, I was not able to verify miR-103 inhibition by 2'OMe103.

Investigation of highly conserved miR-103 MREs

Next, I identified miR-103 targets with near-perfect conservation of the MRE using miRanda target prediction software. miRanda prediction algorithms optimize sequence complementarity using position-specific rules and rely on strict requirements of interspecies conservation (John et al., 2004). However, only a handful of miRanda predicted recognition elements showed significant conservation in zebrafish, including p250-GAP, CPEB3, BDNF, PRPF4B, JARID2 and RUNX1T1. From this list, I investigated the effects of miR-103 over expression on BDNF and PRPF4B because antibodies for the proteins were commercially available.

Initially, I investigated miR-103 regulation of BDNF (brain-derived neurotrophic factor). The predicted BDNF miR-103 MRE is located 285 nucleotides from the translational stop codon and shows high conservation through zebrafish (Figure 3.9a).

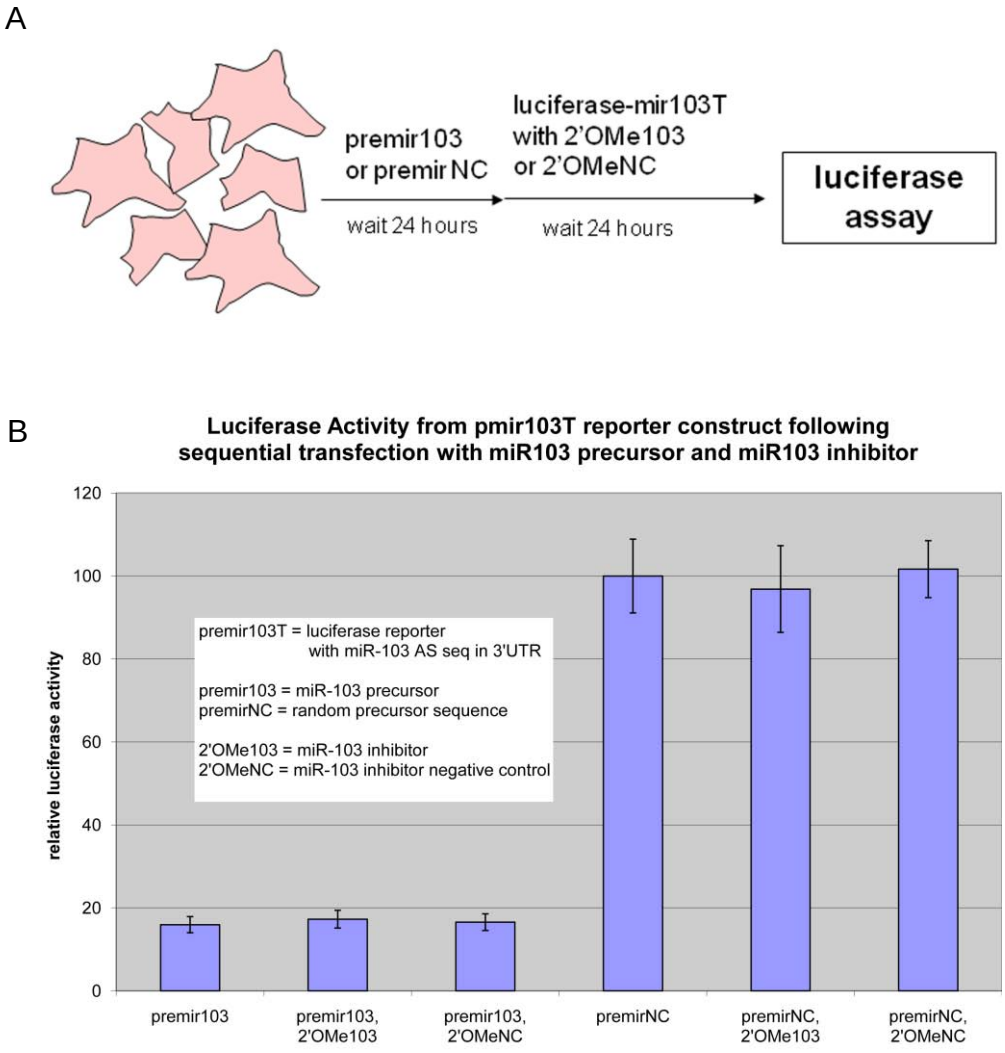

Figure 3.8: Functional assay to detect miR-103 over expression and inhibition

A) HeLa cells were transfected with RSV-βGal and pre-miR™103 or pre-miR™NC, allowed to grow for 24 hours, transfected with 2'OMe103(AS) or negative control (2'OMe103 S) and the premir103T luciferase reporter construct, grown another 24 hours and harvested for luciferase and β-galactosidase assays.
B) Relative luciferase activity of premir103T reporter construct. Luciferase activity is normalized to β-galactosidase activity and error bars represent standard deviation.

However, over expression of miR-103 in N2a cells did not change the abundance of pre-BDNF (37kDa) or mature BDNF (15kDa), as determined by western blot (Figure 3.9b). Interestingly, Mellios et al. also identified miR-103 as a potential regulator of BDNF, but were unable to validate the regulation by luciferase reporter assays (Mellios et al., 2008).

Next, I investigated miR-103 regulation of PRPF4B (serine/threonine-protein kinase PRP4 homolog). PRPF4b is involved in pre-mRNA splicing and signal transduction. It is not associated with disease; however, mutations in three other pre-mRNA-processing factor gene homologs (PRPF31, PRPF8 and HPRP3) are associated with familial retinitis pigmentosa (Chakarova et al., 2002; McKie et al., 2001; Vithana et al., 2001), a common feature of PKAN.

The predicted PRPF4B miR-103 MRE is located 357 nucleotides downstream of the translational stop codon and shows high conservation through zebrafish (Figure 3.10a). miR-103 over expression experiments suggest that PRPF4B may be regulated by miR-103, but the results from replicate experiments were inconsistent. Figure 3.10b is an example of western blots demonstrating down regulation of PRPF4B protein following transfection with 5nM pre-miR™103and 50nM miR-103 Mimic. However, significant PRPF4b down regulation was only observed in 2 out of 3 experimental replicates with pre-miR™103 and 1 out of 3 replicates with miR-103 Mimics (Figure 3.10c). Therefore, I was unable to confirm PRPF4B as a miR-103 target.

Despite this ambiguous result, I compared the relative expression of miR-103, miR-107 and PRPF4b in mouse tissues with the hypothesis that PRPF4b expression may be inversely correlated with miR-103/7. However, there was no obvious correlation between expression of miR-103/7 and this predicted target (Figure 3.11).

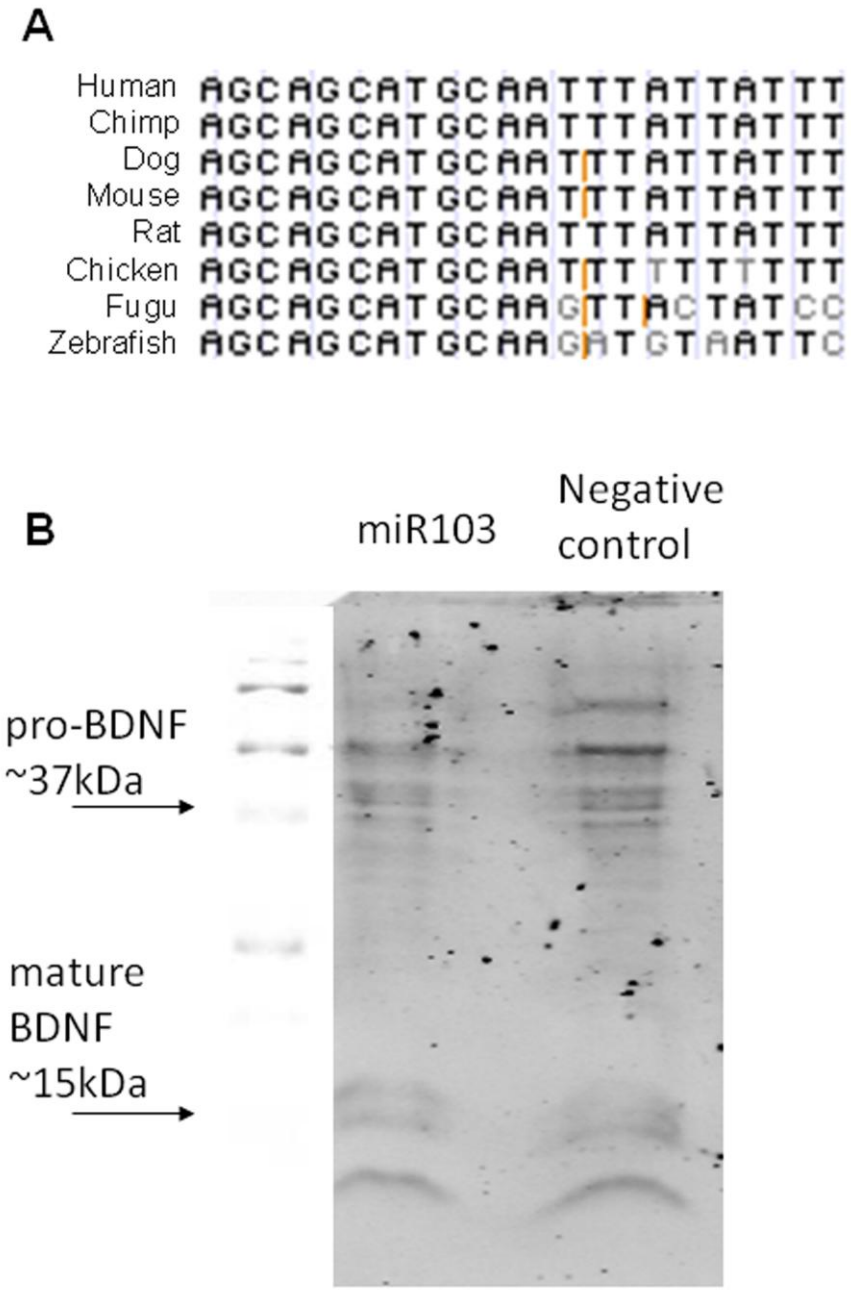

Figure 3.9: BDNF is a potential miR-103 target

A) Conservation of the predicted miR-103 MRE in the BDNF 3'UTR.
B) Western blot analysis of BDNF expression following transfection of N2a cells with 5nM pre-miR™103 or pre-miR™NC.

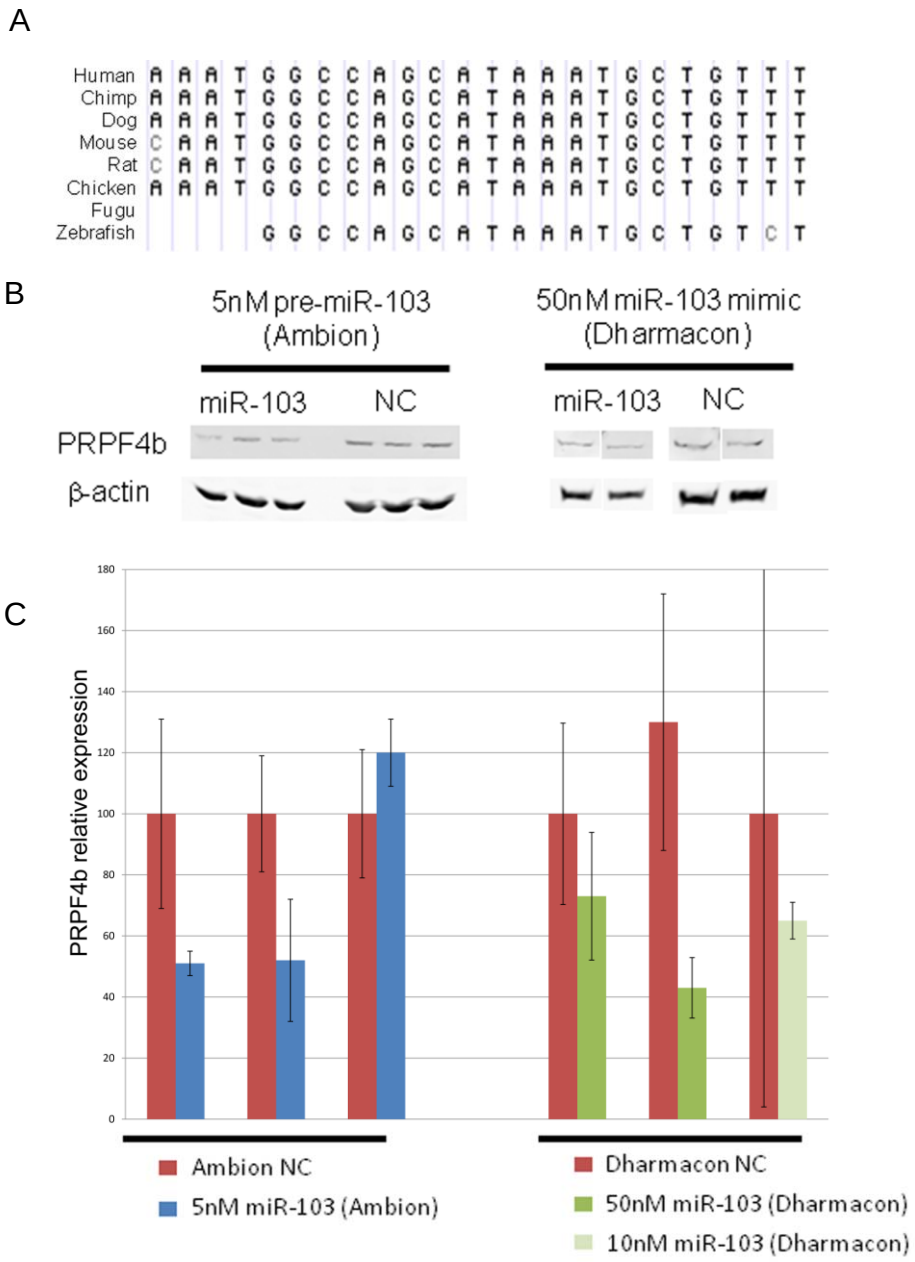

Figure 3.10: PRPF4b is a predicted target for miR-103

A) Conservation of the predicted miR-103 MRE in the PRPF4b 3'UTR.
B) Western blot analysis of PRPF4b expression following transfection of N2a cells with 5nM pre-miR™103 or pre-miR™NC and 50nM miR-103 Mimic or mirIDIAN mimic negative control.
C) Summary of six independent experiments to measure the effect of miR-103 over expression on PRPF4B expression. PRPF4b protein detected by western blot was quantified using the LiCor Odyssey Imaging system. Error bars represent standard deviation.

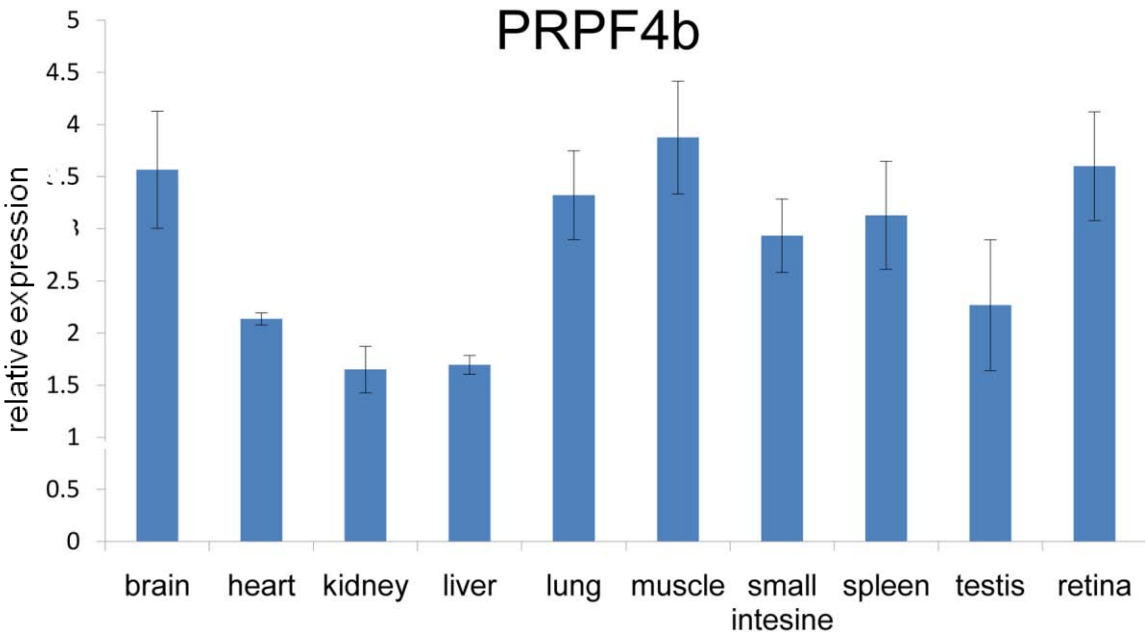

Figure 3.11: Relative expression of PRPF4b in mouse tissues.

RNA was harvested from mouse tissues (n=3) and analyzed by qRT-PCR. Error bars represent standard error.

Chapter 4

Expression of NBIA genes in human fetal development

Chapter 4.1

Expression of *PLA2G6* in human fetal development: Implications for infantile neuroaxonal dystrophy

*manuscript submitted to *Brain Research Bulletin*

Brenda Polster[1*], Moira Crosier[2], Susan Lindsay[2] and Susan Hayflick[1]

[1] Molecular and Medical Genetics, Oregon Health & Science University, Portland OR.

[2] MRC-Wellcome Trust Human Developmental Biology Resource, Institute of Human Genetics, Newcastle University, UK, NE1 3BZ

[*]corresponding author
Phone: 503 494 2449
Fax: 503 494 6886
Email: polsterb@ohsu.edu

ABSTRACT

Mutations in *PLA2G6*, which encodes calcium-independent phospholipase A_2 group VIA (iPLA2-VIA), underlie the autosomal recessive disorder infantile neuroaxonal dystrophy (INAD). INAD typically presents in the first year of life, and leads to optic atrophy and psychomotor regression. We have examined *PLA2G6* expression in early human embryonic development by *in situ* hybridization. At CS19 (approximately 7 post conception weeks [PCW]), strong expression is evident in the ventricular zone (VZ) of midbrain and forebrain, suggestive of expression in neural stem and progenitor cells. At CS23 (8 PCW) expression is also detectable in the VZ of the hindbrain and the subventricular zone (SVZ) of the developing neocortex, ganglionic eminences and diencephalon. By 9 PCW strong expression in the post-mitotic cells of the cortical plate can be seen in the developing neocortex. In the eye, expression is seen in the lens and retina at all stages examined. *PLA2G6* expression is also evident in the alar plate of the spinal cord, dorsal root ganglia, the retina and lens in the eye and and several non-neuronal tissues, including developing bones, lung, kidney and gut. These findings suggest a role for *PLA2G6* in neuronal proliferation throughout the developing brain and in maturing neurons in the cortical plate and hindbrain. Although widespread *PLA2G6* expression is detected in neuronal tissues, the pattern shows dynamic changes with time and indicates that INAD pathogenesis may begin prior to birth.

Keywords: PLA2G6, INAD, neurodegeneration, development, in situ hybridization

Abbreviations: INAD, infantile neuroaxonal dystrophy; NBIA, neurodegeneration with brain iron accumulation; PCW, post weeks conception;; PKAN, pantothenate-kinase associated neurodegeneration, SVZ, subventricular zone; VZ, ventricular zone.

1. INTRODUCTION

Infantile neuroaxonal dystrophy (INAD) is an autosomal recessive disease with early onset and rapid progression of hypotonia, hyperreflexia and tetraparesis. INAD belongs to a larger class of neuroaxonal dystrophies, which include pantothenate-kinase associated neurodegeneration (PKAN), idiopathic neurodegeneration with brain iron accumulation (NBIA), and Schindler disease. Within this group, INAD has the earliest onset, with motor and cognitive skill regression presenting at a median age of 15 months (Gregory et al., 2008; Kurian et al., 2008). Optic atrophy is also commonly observed. Historically, INAD was diagnosed from histological evidence of neuroaxonal spheroids in peripheral nerves (Nardocci et al., 1999). The detection of cerebellar atrophy and iron accumulation in the globus palidus by MRI is also diagnostic of INAD, although iron accumulation often is not observed until later in the disease (Gregory et al., 2008; Kurian et al., 2008; Morgan et al., 2006).

In 2006, the causative gene for INAD was identified as *PLA2G6*, which encodes a calcium-independent phospholipase (A_2 group VIA) (Morgan et al., 2006). *PLA2G6* mutations are found in the vast majority of INAD patients and have also been described in individuals previously diagnosed with idiopathic NBIA (Gregory et al., 2008), as well as individuals with adult-onset dystonia-parkinsonism (Paisan-Ruiz et al., 2009). Phospholipases A_2 comprise a large family of enzymes that catalyze the hydrolysis of sn-2 ester bonds of glycerophospholipids, producing free fatty acids and lysophospholipids (Dennis, 1994). Arachidonic acid and other fatty acids released by $iPLA_2$-VIA can initiate apoptosis, inflammation, and cell growth (Balsinde et al., 2006; Sun et al., 2009). The lysophospholipid remaining in the cell membrane can also trigger cellular processes,

including chemotaxis and fusion of biological membranes (Balboa et al., 2003; Carnevale and Cathcart, 2001).

The early presentation of INAD suggests that *PLA2G6* may have a developmental role. Malik and colleagues (Malik et al., 2008) showed that the *Pla2g6* knockout mouse (Bao et al., 2004) develops neurological impairments by 13 months and accumulates neuroaxonal spheroids similar to those in human INAD patients. In a second INAD mouse model, point mutations within *Pla2g6* result in moter dysfunction and neuroaxonal spheroids as early as 7 weeks of age (Wada et al., 2009). These studies, however, did not examine *Pla2g6* expression during mouse development. *Pla2g6* expression has been shown in mouse sagittal sections at embryonic day 14.5 as part of the high-throughput Eurexpress project (Visel et al., 2004). At this stage, the strongest expression seen in the brain is in the alar plate of the developing hindbrain with prominent expression also in an analogous region of the midbrain. *Pla2g6* also appears to be expressed weakly in the developing diencephalon and telencephalon of the forebrain. Expression was also detected in spinal cord and the bones of the developing skull, face, ribcage and limbs (EMAGE entry 18166; genex.hgu.mrc.ac.uk).

To better understand the potential role for *PLA2G6* in neuronal development and pathogenic mechanisms underlying disease, we examined *PLA2G6* expression, by *in situ* hybridization, across several stages of human embryonic and early fetal development.

2. MATERIALS AND METHODS

2.1 Human tissue collection and processing

Human embryonic and fetal tissues were obtained from the MRC-Wellcome Trust Human Developmental Biology Resource (www.hdbr.org), Institute of Human Genetics, Newcastle University. The samples were collected with appropriate maternal consents and ethical approval by the Newcastle and North Tyneside Research Ethics Committee. Tissue sections from 7 samples were analysed: Carnegie Stage (CS) 19 (~7 PCW, n=2), CS23 (8PCW, n=3) and 9 PCW (n=2). The stage of embryonic development (CS19 and CS23) was determined by assessment of external morphology as described (Bullen and Wilson, 1997; O'Rahilly et al., 1987). For fetal samples (9PCW) age was estimated from measurements of foot length and heel to knee length. These were compared with a standard growth chart (Hern, 1984).

2.2 In situ hybridization histochemistry

Three fragments of the cDNA for human *PLA2G6*; 453 bp of *PLA2G6* exon 2-exon4 (probe 1), 517 bp of *PLA2G6* exon 11-15 (probe2) and 557 bp of the *PLA2G6* 3'UTR (probe3) were amplified from homo sapiens *PLA2G6* mRNA (Accession: CU013143) and cloned into pCR-BluntII-TOPO (Invitrogen). The construct sequences were verified and prepared using HiSpeed Plasmid Midi kit (Qiagen). To create the *PLA2G6* antisense probe, the plasmid was linearized with SpeI and amplified from the T7 promoter. To create the *PLA2G6* control probe, the plasmid was linearized with Not1 and amplified from the Sp6 promoter. Probes were labeled with digoxygenin (DIG) using the DIG-RNA labeling kit (Roche Applied Science) according to manufacturer's instructions.

All probes were tested and *PLA2G6* probe 3 was selected for the studies subsequently described.

In situ hybridizations were preformed as previously described (Moorman et al., 2001) with some modifications. Briefly, sections were dewaxed in xylene, gradually hydrated in decreasing ethanol concentrations before incubation in Proteinase K (20μg/ml) at room temperature (RT), followed by fixation in 4% paraformaldehyde in PBS. Background was reduced by treating with 0.1M triethanolamine pH 8. Sections were air dried and probe added (300ng labeled probe per 100ul of Dig Easy Hyb mix (Roche)) at 68^{o}C overnight. The next day sections were washed once in 5x SSC then once in 2x SSC at 60^{o}C then incubated with Anti-digoxigenin AP Fab fragments (Roche) diluted 1:1000 at 4^{o}C overnight. Sections were then washed and expression detected using NBT/BCIP (20ul/ml Roche) in 0.1M Tris/0.1M NaCl (pH 9.5) in the dark at RT. Developing was stopped by rinsing slides first in 0.1M Tris/0.1M NaCl (pH 9.5) then in distilled H_2O. Sections were mounted using Aquamount and analyzed using a Zeiss Axioplan 2 microscope. Images were captured with a Zeiss Axiovision 4 imaging system.

3. RESULTS

In order to characterize the potential role of *PLA2G6* in fetal development, we examined *PLA2G6* expression by *in situ* hybridization during human embryonic (CS19 and CS23) and early fetal (9 PCW) development.

3.1 PLA2G6 expression in the brain

At CS19, *PLA2G6* expression was evident in the VZ of the pallium neuroepithelium (NEP) in the developing telencephalon (Figure 4.1A). The NEP is a pluripotent pseudostratified tissue of neural stem cells that extends from the frontal pole

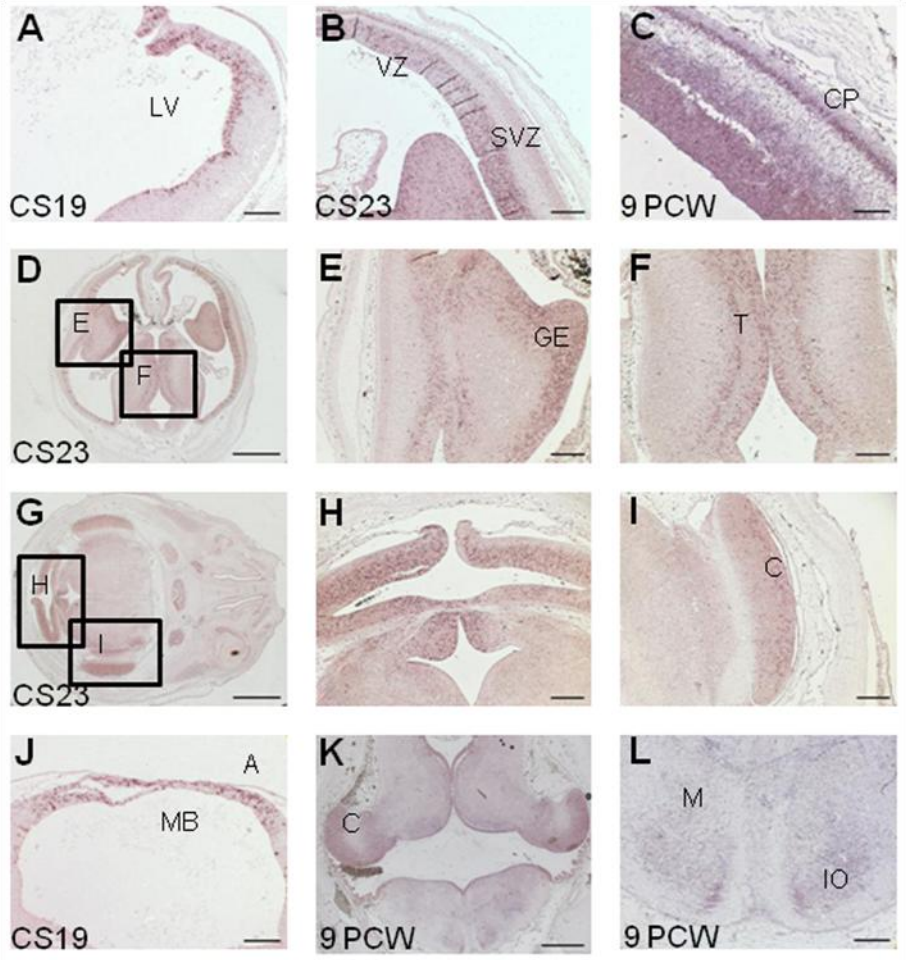

Figure 4.1: *PLA2G6* expression in human brain at CS19, CS23 and 9 PCW.

Panels A-L show images of i*n situ* hybridization with antisense probes for *PLA2G6* to sections at CS19 (A, J), CS23 (B, D-I) and 9PCW (C, K, L). Signal is detected as a purple stain. **A)-C)** *PLA2G6* staining in developing neocortex. At CS19 (A), expression can be seen close to the lateral ventricle (VZ), by CS23 (B) expression is in the VZ and SVZ and by 9PCW (C) expression is also seen in the CP. **D)** Low magnification image showing developing neocortex, ganglionic eminences and thalamus. The boxed areas are shown at higher magnification in panels **E** and **F**. **G)** Low magnification image showing developing midbrain, isthmus, cerebellum and pons. The boxed areas are shown at higher magnification in panels **H** and **I**. **J)** *PLA2G6* expression is seen in the alar plate of the developing midbrain. **K)** *PLA2G6* expression in the hindbrain is seen in the developing cerebellum, the VZ of medulla and neurons in developing nuclei (IO). Boxed area is seen at higher magnification in panel **L**. No signal was detected using sense control probes (Figure 4.2). A- alar plate C- cerebellum, CP- cortical plate; GE- ganglionic eminences, IO- inferior olive, I- isthmus, LV- lateral ventricle, M- medulla, MB- midbrain, NC- neocortex, P= pons, SVZ- subventricular zone, T- thalamus, VZ- ventricular zone. Scale bars are: 100μm in A.C.J.L; 200ɯm in B.E.F.H.I; 1000ɯm in D.G.K.

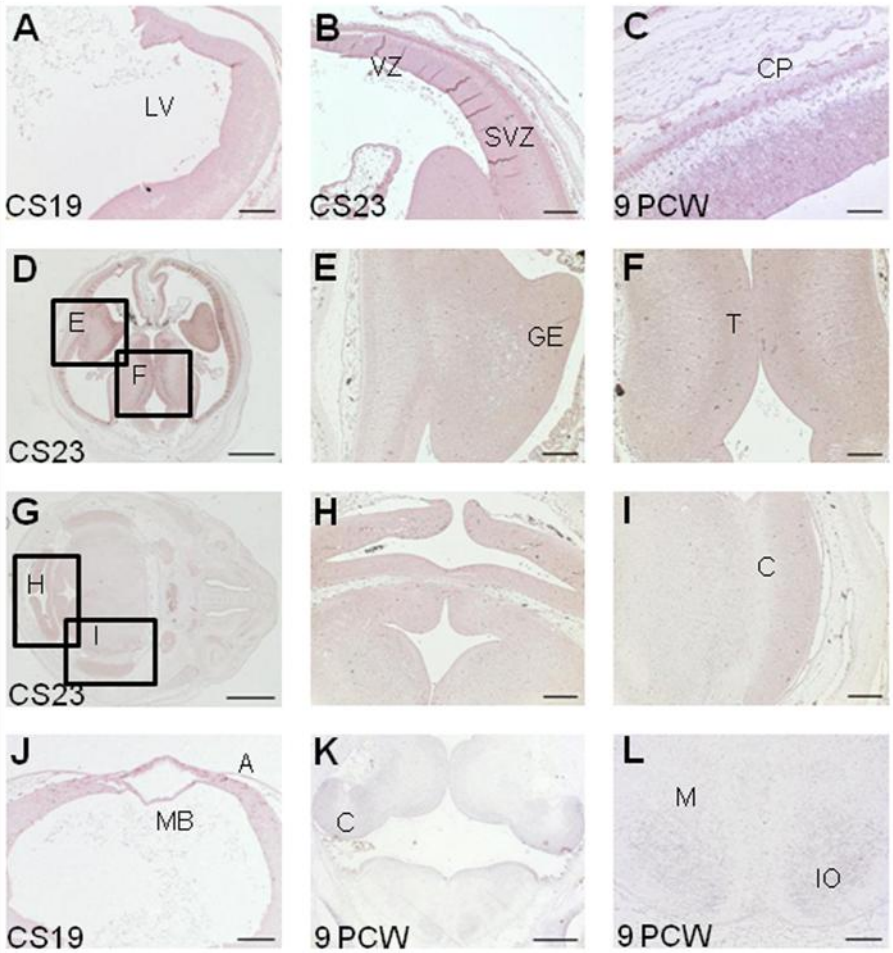

Figure 4.2 No signal is detected with *PLA2G6* sense control probes.
Panels A-L show images of i*n situ* hybridization with sense probes for *PLA2G6* to sections at CS19 (A, J), CS23 (B, D-I) and 9PCW (C, K, L). **A)-C)** Developing neocortex. **D)** Low magnification image showing developing neocortex, ganglionic eminences and thalamus. The boxed areas are shown at higher magnification in panels **E** and **F**. **G)** Low magnification image showing developing midbrain, isthmus, cerebellum and pons. The boxed areas are shown at higher magnification in panels **H** and **I**. **J)** Developing midbrain. **K)** Developing cerebellum and medulla. Boxed area is seen at higher magnification in **L**. A- alar plate C- cerebellum, CP- cortical plate; GE- ganglionic eminences, IO- inferior olive, I- isthmus, LV- lateral ventricle, M- medulla, MB- midbrain, NC- neocortex, P= pons, SVZ- subventricular zone, T- thalamus, VZ- ventricular zone. Scale bars are: 100μm in A,C,J,L; 200μm in B,E,F,H,I; 1000μm in D,G,K. *(Supplemental Figure 1 in submitted manuscript)*

to the spinal cord and is the source of all neurons and neuroglia of the developing nervous system (Bayer, 2006). By CS23, *PLA2G6* expression is detected in both the VZ and SVZ of the pallium, while by 9PCW strong signal is also detected in the differentiating neurons of the cortical plate (Figure 4.1B and C respectively). Strong expression is also seen in proliferative zones in other regions of the developing forebrain such as the ganglionic eminences (Figure 4.1B, D, E) and thalamus (Figure 4.1B, E).

In the midbrain, *PLA2G6* expression is detectable in the VZ of the alar plate at CS19 and persists through to 9PCW (Figure 4.1J, H and data not shown). In contrast, expression in the hindbrain is barely detectable at CS19. Yet at CS23 and 9PCW, *PLA2G6* is expressed in the VZ in the isthmus, cerebellum, pons and medulla oblongata (Figure 4.1H, I, K and L) and clearly present in differentiating neurons of developing nuclei in the medulla (Figure 4.1K and L). *PLA2G6* expression is also seen in the telencephalic choroid plexus, a glycogen-rich epithelial tissue formed by proliferative stem cells that may play a part in anaerobic metabolism during early development (Bayer, 2006) (data not shown).

3.2 PLA2G6 expression in the eye and spinal cord

PLA2G6 expression was found in the lens and developing neurosensory retina at CS19, CS23 and PCW9 (Figure 4.3). Expression in the retina was sparse initially but became stronger and more widespread throughout the developing retina by 9PCW. Interestingly, in one CS23 sample, we also observed strong staining in the optic nerve (Figure 4.3B). The optic nerve comprises axons from retinal ganglion cells and glial precursors: astrocyte precursors arising from the optic stalk and oligodendrocyte precursors from the preoptic area (Ono et al., 1997; Small et al., 1987). However, the

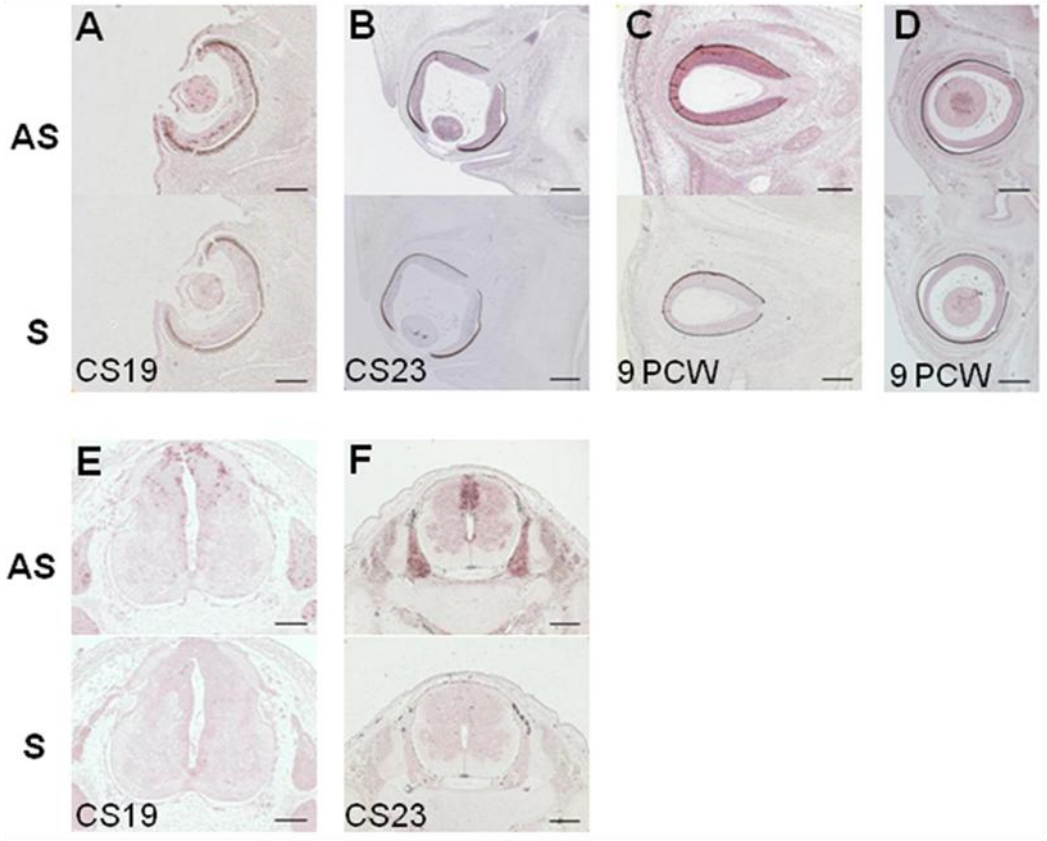

Figure 4.3 *PLA2G6* expression in human eye and spinal cord at CS19 (A,E) CS23 (B, F) and 9PCW (C,D).

Each panel has 2 images, the top one showing *in situ* hybridization using antisense (AS) probes and the lower one using sense (S) probes for *PLA2G6.* No signal was detected using sense control probes **A)** *PLA2G6* staining in retina and lens at CS19. **B)** *PLA2G6* staining in lens, retina and optic nerve at CS23. **C-D)** *PLA2G6* staining in retina at PCW9. **E)** *PLA2G6* staining in dorsal root ganglia at CS19. **F)** *PLA2G6* staining in dorsal root ganglia at 9PCW A- alar plate, AS- antisense, DRG- dorsal root ganglia, L- lens, ON- optic nerve, R-retina, S-sense, Scale bars are: 100μm in A,E; 200μm in B,C,D,F

optic nerve only begins to be myelinated at five months of gestation (Edward and Kaufman, 2003). *PLA2G6* expression was detected in the spinal cord, principally in the alar plate, as well as in the dorsal root ganglia at CS19 and CS23. Spinal cord expression was not analyzed at 9PCW; however, we did observe it throughout the spinal cord and in dorsal root ganglia at 13PCW (data not shown).

3.3 PLA2G6 in non-neuronal tissues

Results from RT-PCR experiments in a battery of RNAs from different tissues at 9PCW suggested that *PLA2G6* was expressed widely in non-neuronal tissues (data not shown). This was confirmed by tissue *in situ* hybridisation as shown in Figure 4.4. *PLA2G6* expression was detected in lung (Figure 4.4A), kidney (both metanephros and mesonephros Figure 4.4B and C respectively), gonad (Figure 4.4C), muscles in the tongue and surrounding the eye (Figure 4.4 D and H), nasal epithelium (Figure 4.4E), surrounding the developing bones (Figure 4.4F) and in the intestine (Figure 4.4G).

4. DISCUSSION

The present study was carried out to characterize *PLA2G6* expression in the developing human embryonic and fetal nervous system. We found that *PLA2G6* has a dynamic expression pattern both in terms of the location of expression and the differentiation state of expressing cells. *PLA2G6* is expressed in forebrain and midbrain before it is detectable in hindbrain. Throughout the developing brain, *PLA2G6* is expressed in proliferative zones: VZ in all regions, as well as the SVZ in the developing telencephalon including the ganglionic eminences. In the diencephalon there is strong expression in the thalamus and hypothalamus. This expression pattern is in contrast to the only available comparative data derived from studies in developing mouse: in murine

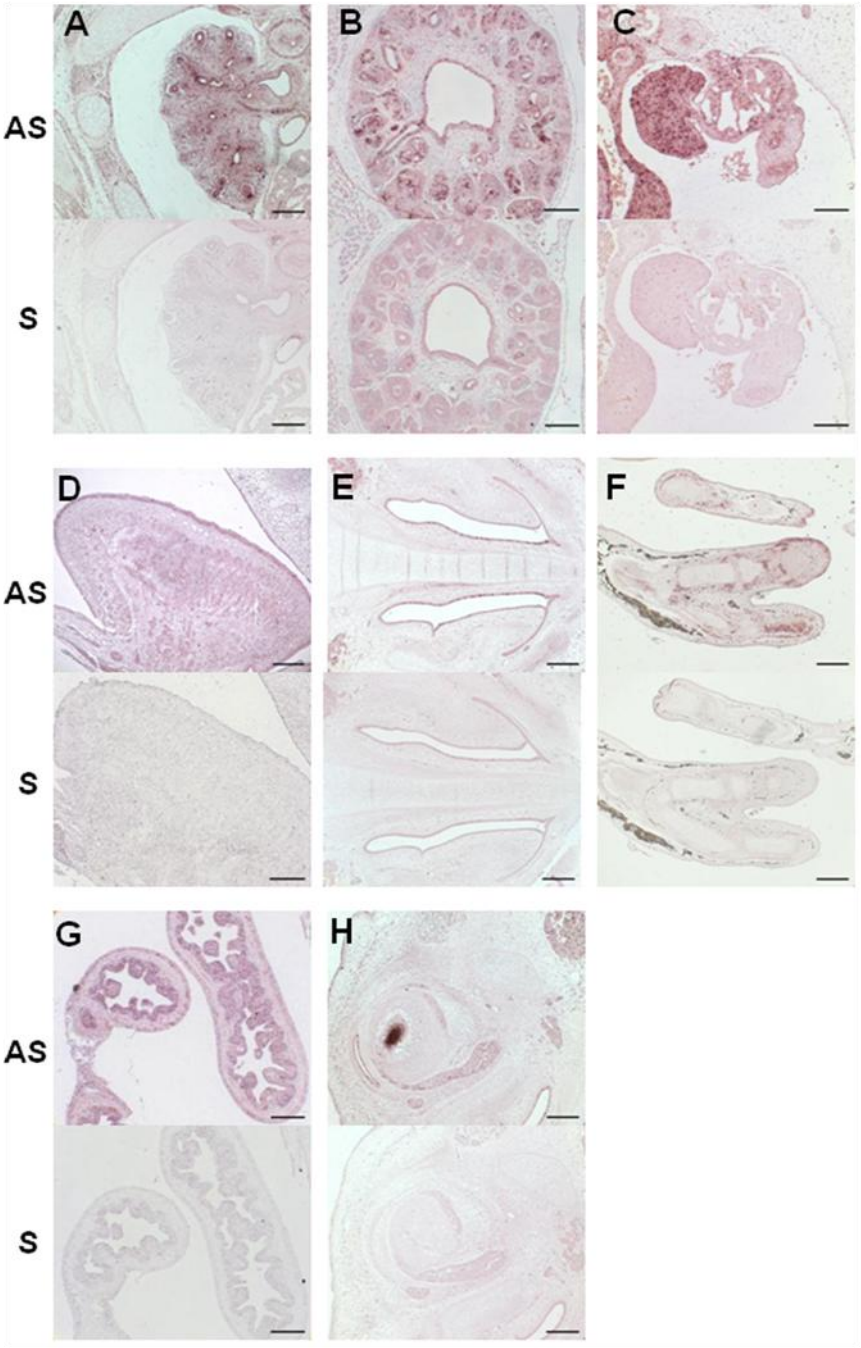

Figure 4.4 Expression of *PLA2G6* in non-neuronal tissues.

Each panel has 2 images, the top one showing *in situ* hybridization using AS probes and the lower one using S probes for *PLA2G6.* No signal was detected using sense control probes. Panels A, B and D-H are of sections at 9PCW. Panel C is of a section from a CS23 embryo. **A)** Lung **B)** Metanephros **C)** Gonad and mesonephros **D)** Tongue **E)** Nasal area **F)** Upper limb **G)** Intestine **H)** Eye muscle. NE- nasal epithelium, OM=- ocular muscles. Scale bars are: 100μm in B,C,D,G; 200μm in A,E,F,H.

studies expression in the alar plate VZ of the midbrain and hindbrain has been described, but none is seen in the VZ of the forebrain (diencephalon or telencephalon) and there is only weak expression in the outer cortical plate/mantle layer in the developing neocortex (EMAGE entry ID 18166). However, this mouse data is only from a single stage and does not capture the dynamic changes in expression pattern seen in human as described above. In our studies of the human forebrain, *PLA2G6* was also detected in the differentiated neurons of the cortical plate in the developing cerebral neocortex. Similarly, expression is seen in differentiated neurons in the hindbrain; for example, in the inferior olives of the medulla. At the stages examined, there is no *PLA2G6* expression in differentiated neurons of the midbrain.

Broad expression of $iPLA_2$ in the brain has also been reported in adult mammals. In adult monkey brain, high $iPLA_2$ expression was detected in the cerebral neocortex, hippocampus, cerebellum and brain stem, with lower expression in the thalamus and hypothalamus (Ong et al., 2005b). Within the basal ganglia, the caudate nucleus, putamen and nucleus accumbens were densely labeled while the globus pallidus, subthalamic nucleus and substantia niagra pars compacta were lightly labelled (Ong et al., 2005b). Within these tissues, $iPLA_2$ expression was predominately localized to the nuclear envelope of neurons, dendritic spines or axon terminals, while expression was sparse or absent in myelinated axons, large diameter dendrites, glial cells and endothelial cells (Ong et al., 2005b). $iPLA_2$ expression has also been reported in rat cerebellum, with strong expression in the nuclei of Purkinje cells and granule and stellate cells (Shirai and Ito, 2004). These findings are consistent with an ongoing role for $iPLA_2$ in signal transduction and lipid metabolism in a variety of CNS cell types.

In the adult eye, iPLA$_2$-VIA expression has previously been reported as very strong in the retinal pigment epithelium, strong in the optic nerve axons and cornea, and moderate in the iris, ciliary body and lens (Kolko et al., 2007). Interestingly, iPLA$_2$-VIA is proposed to regulate RPE proliferation and migration, and may play a role in proliferative vitreoretinopathy (Kolko et al., 2009). Our data indicates that *PLA2G6* is expressed in retina and lens as early as CS19 (approx 7 PCW). In addition, we observed expression in the sheath of the optic nerve in one sample. Although retinopathy is not common in *PLA2G6*-associated disease, optic atrophy is typical (Gregory et al., 2008). Indeed, Kurian et al observed reduced volume in the optic chiasm and optic nerves on radiographical imaging in eight out of ten *PLA2G6* mutation-positive patients (Kurian et al., 2008), consistent with an important postnatal role for *PLA2G6* in maintaining optic nerve integrity.

A survey of non-neuronal embryonic tissues revealed broad *PLA2G6* expression. Previously, *PLA2G6* was detected in all 23 adult human tissues examined by Northern blot (Larsson Forsell et al., 1999). In our study, strong expression was detected surrounding the developing bones of the arm and in the lung, kidney, gut and muscles of the tongue and surrounding the eye. At the stages examined, we did not detect strong expression in the developing bones of the face and skull. Again, this result is in contrast with the available data in developing mouse. However, the latter data are limited and differences between the species may be temporal rather than spatial. In other studies, iPLA$_2$-VIA is shown to be expressed in numerous cell lines including macrophages (Ackermann et al., 1994), pancreatic cells (Ramanadham et al., 2004), astrocytes (Peterson et al., 2007) and renal cells (Cummings et al., 2004). Broad *PLA2G6*

expression is consistent with its role in membrane phospholipid maintenance and divergent signaling pathways (Balsinde and Balboa, 2005).

Several disorders with predominantly neurodevelopmental defects are caused by genes with a widespread expression pattern during human development (Miyake et al., 2008; Tischfield et al.). In addition, degenerative neurological disorders can be caused by mutations in a widely expressed gene, exemplified by Rett syndrome and pantothenate kinase-associated neurodegeneration (Shahbazian et al., 2002; Zhou et al., 2001). Similarly, in several trinucleotide repeat disorders, expanded polyglutamine proteins are ubiquitously expressed but cause selective neurodegeneration in specific brain regions (Orr and Zoghbi, 2007).

Our results suggest that *PLA2G6* is positioned to play a role in early neuronal development. Disruption of this process may contribute to the widespread neurological problems observed in INAD. In fact, embryonic and fetal *PLA2G6* expression suggests that INAD pathogenesis could initiate *in utero*. Several INAD mouse models are available to further investigate the effect of *PLA2G6* mutations on embryonic development (Bouley et al., 2006; Malik et al., 2008; Shinzawa et al., 2008; Wada et al., 2009). Certainly, *in utero PLA2G6* function should be considered when treatment strategies for INAD are in development.

Acknowledgements

This work was supported by National Institute of Child Health and Human Development (RO1 HD050832 to S.H.), the Neurodegeneration with Brain Iron Accumulation (NBIA)

Disorders Association (to S.H), the Association Internationale De Dystrophie Neuro Axonale Infantile (AIDNAI) (to S.H.) and the Huebner Family Pediatric Neurobiology of Disease Fellowship (to B.P.). The human embryonic and fetal material was provided by the Joint MRC-Wellcome Trust Human Developmental Biology Resource (http://www.hdbr.org) at the IHG, Newcastle-upon-Tyne, UK.

Chapter 4.2

Additional Studies on *PANK2* and *PLA2G6* expression in human fetal development

Unpublished Results

4.2.1 Pilot study on *PANK2* expression in human fetal development

Experimental Rationale

The effects of *PANK2* mutation in mouse and human suggest that the gene is important in early stages of development. In patients with classic PKAN, disease onset is within the first six years of life (Gregory et al., 2009) and parents with several affected children report a peculiar cry in their affected newborns before overt neurological signs are present. These patients have the eye-of-the-tiger sign on MRI, which indicates iron accumulation and necrosis within the globus pallidus (McNeill et al., 2008). In comparison, *Pank2* knockout mice lack a neurodegenerative phenotype, but male mice are infertile due to azoospermia (Kuo et al., 2005). Our laboratory has observed disorganization and increased apoptosis in the testis as early as 3 weeks after birth and we predict that the underlying pathogenesis begins *in utero*. Due to these early onset phenotypes, we hypothesize that *PANK2* has critical function before birth and PKAN pathogenesis may initiate in the uterus. In this study, we attempted to examine *PANK2* expression in early human development.

Materials and Methods

I designed two *PANK2* probes for *in situ* hybridization. "PANK2 probe 5" corresponds to 400bp of unique sequence in exon 1 of *PANK2* transcript variant 1 (nucleotides 235-634 in NM_153638) and "PANK2 probe 3" corresponds to 535bp of unique sequence in the *PANK2* 3'UTR, beginning with the *PANK2* stop codon (nucleotides 1717-2251 in NM_153638). The sequences were amplified from human genomic DNA and cloned into pBluescriptIISK (+) (Strategene). The construct sequences

were verified by sequencing, prepared using HiSpeed Plasmid Midi kit (Qiagen) and sent to MRC-Wellcome Trust Human Developmental Biology Resource (HDBR). At the HDBR, sense and antisense probes were created and samples handled as described in Chapter 4 Materials and Methods.

Results and Discussion

The preliminary results from *PANK2 in situ* hybridization studies suggest strong expression in neuronal tissue. Results generated with *PANK2* probe 3 are shown in Figure 4.5a. On a saggital section of a CS19 (7 post conception weeks) embryo, *PANK2* expression is evident throughout the brain from lateral ventricles to the cerebellum, as well as in the hand and mantle layer of the lower back. Transverse section of a second CS19 embryo reveals expression in the eye and optic groove. Finally, a CS23 (8 post conception weeks) embryo demonstrated expression in the retina, lens, olfactory epithelium, hypothalamus and lateral cerebellum. Similar results were obtained with the *PANK2* probe 5, as shown in Figure 4.5b. I've include the results from two saggital CS19 sections that demonstrate *PANK2* staining in the fourth ventricle, ganglia in the neck, digits of the hand and eye.

Unfortunately, the *PANK2* sense control probes demonstrated staining patterns similar to the antisense probe in all samples (Figure 4.5). The HDBR tested the probe sets on several CS19 and CS23 embryos, with a variety of hybridization conditions, and repeatedly found problematic sense staining. As part of their troubleshooting protocols, the HDBR tried reducing the amount of probe used for hybridization. However, 70ng

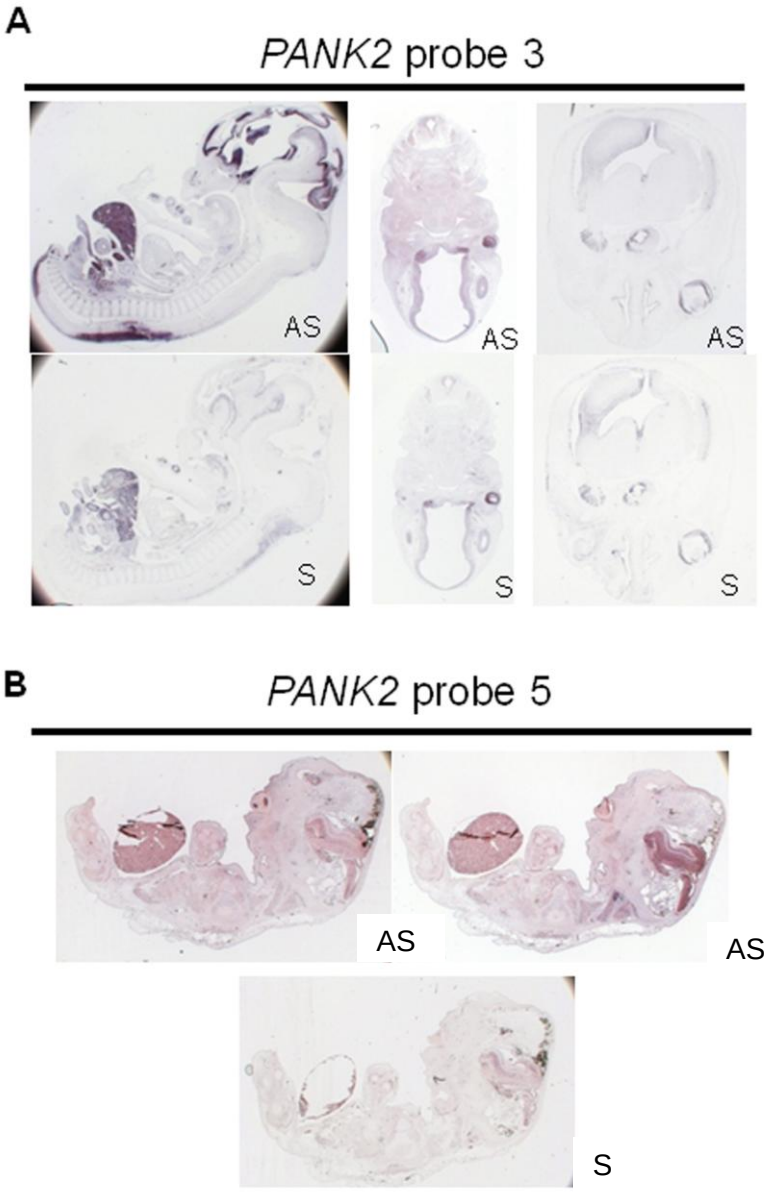

Figure 4.5: *PANK2* expression in CS19 and CS23 human fetal tissues

A) *In-situ* hybridization for *PANK2* expression using *PANK2* probe 3. The left and center images are CS19 samples and the image on the right is a CS23 sample.
B) *In-situ* hybridization for *PANK2* expression using *PANK2* probe 5. The samples are CS19.

and 140ng of sense and antisense probes still gave background signal (Figure 4.6a). Possible reasons for the sense probe background include hybridizing to another gene or hybridizing to a common regulatory element, although I did not predict such complications by *in silico* analysis of the probe sequence.

In light of these complications, the HDBR also conducted a competition experiment to verify *PANK2* probe 3 specificity. They labeled antisense PANK2 probe 3 with a non-DIG label and used it with the DIG labeled probe in ratios of 0:1, 1:1, 10:1 and 100:1 (Figure 4.6b). They found that 100X of non-DIG labeled probe competes out most of the expression, indicating that the signal detected with the antisense probe is specific.

These preliminary results suggest that *PANK2* is expressed in human neuronal tissues at CS19 and CS23; however, this project did not advance beyond the pilot study stage due to problematic staining by *PANK2* sense probes.

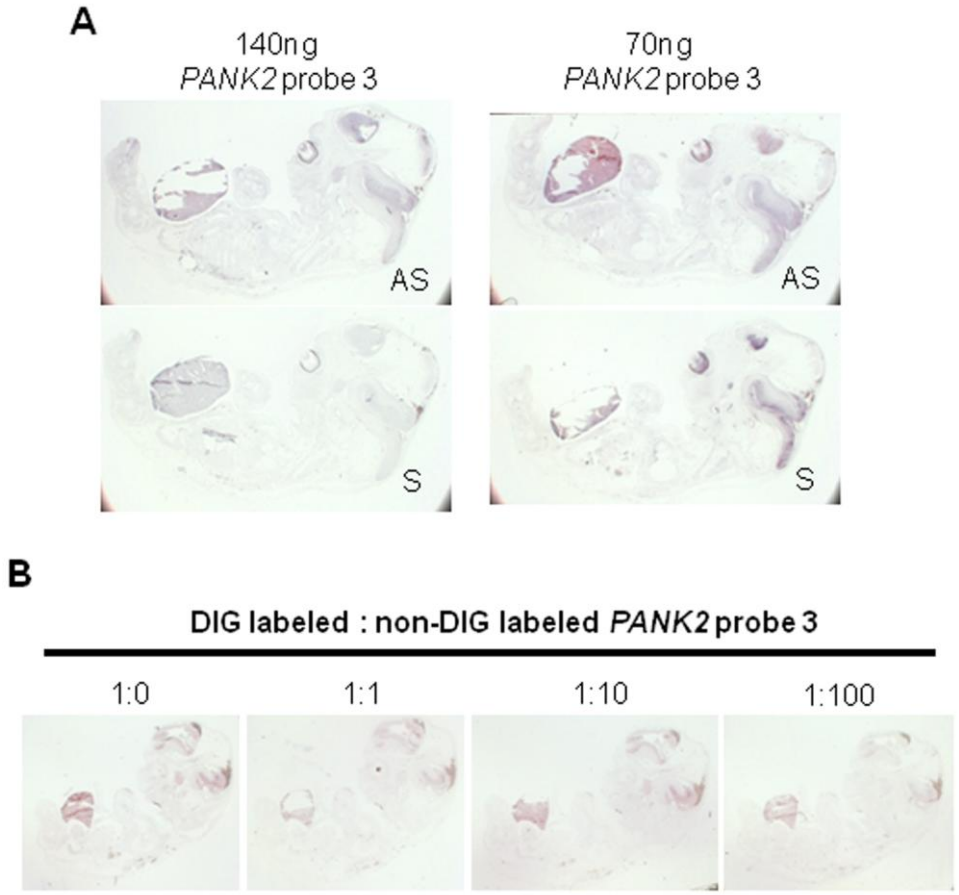

Figure 4.6: Optimization and specificity of *PANK2* probe 3

A) *In-situ* hybridization for *PANK2* expression in CS19 saggital sections using 140ng and 70ng of *PANK2* probe 3. Sense staining is observed at both concentrations. B) Competition experiment in CS19 saggital sections to demonstrate *PANK2* probe 3 specificity. 70ng of DIG-labeled *PANK2* probe 3 was competed with unlabeled probe, as indicated.

4.2.2 Relative expression of *PANK2* and *PLA2G6* in human fetal tissues

Experimental Rationale

As a compliment to *in situ* hybridization studies, I measured the relative expression of *PANK2* and *PLA2G6* mRNA in human fetal brain, spinal cord, kidney, liver, eye and lung. I also measured relative gene expression in various regions of the brain, including basal ganglia, lateral ventricle, midbrain and thalamus. The purpose of these experiments was twofold. First, the results helped to guide *PLA2G6 in situ* hybridization experiments on non-neuronal tissues. Second, we aimed to compare the relative levels of *PANK2* and *PLA2G6* expression in fetal tissues. Since mutations in these genes lead to similar disease, we are interested to evaluate whether the genes have similar patterns of expression. Previously, ubiquitous *PANK2* (Zhou et al., 2001) and *PLA2G6* (Larsson Forsell et al., 1999) expression has been demonstrated by northern blot on adult human tissues. However, expression of these genes has not been studied in early human development.

Materials and Methods

The HDBR harvested total RNA from human fetal tissues. Lung, kidney, spinal cord, liver and total brain RNA were from the F2 stage sample, N868. Basal ganglia, lateral ventricle, midbrain and thalamus RNA were from the F2 stage sample, N1046. The spinal cord RNA was from an F1 stage sample, N1084. I measured the RNA integrity of each sample using an Agilent 2100 Bioanalyzer, and confined my analysis to samples with an RNA integrity number (RIN) of 5 of higher. 2μg of RNA was DNase treated and reverse transcribed using High-capacity cDNA Reverse Transcription kit

(Applied Biosystems). Relative expression of *PANK2* and *PLA2G6* mRNA was quantified using TaqMan Gene Expression Assays (Applied Biosystems). *TBP*, *HMBS* and *RPLP0* were used to normalize *PLA2G6* and *PANK2* expression across tissues. All data was analyzed using the comparative Ct method in the qBasePlus software. Unfortunately, due to the scarcity of human fetal RNA samples, I was unable to examine gene expression in biological replicates. The data shown in Figure 4.7 is representative of a single fetal sample for each tissue, although the PCR reactions were preformed in triplicate.

Results and Discussion

PANK2 and *PLA2G6* expression were detected in fetal brain, eye, spinal cord, kidney, liver and lung (Figure 4.7). *PANK2* showed very similar expression levels across all the tissues, while *PLA2G6* had enriched expression in the eye and lower expression in spinal cord and liver. Analysis of specific regions of the brain revealed that *PANK2* and *PLA2G6* have similar relative expression in the basal ganglia, lateral ventricle, midbrain and thalamus. These results are in agreement with our *in situ* hybridization results.

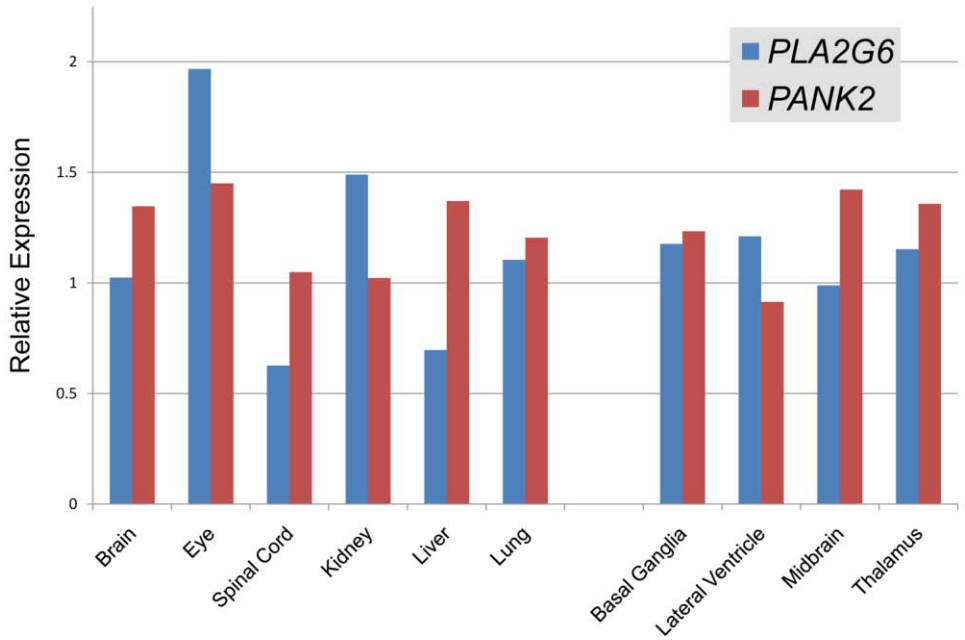

Figure 4.7: Relative expression of *PANK2* and *PLA2G6* in human fetal tissues

Each bar represents gene expression in a single biological sample. Brain, eye, kidney, liver, lung, basal ganglia, lateral ventricle, midbrain and thalamus samples are from a F2 stage human fetus. The spinal cord sample is from an F1 stage human fetus. *PLA2G6* and *PANK2* expression levels were normalized to *TBP*, *HMBS* and *RPLP0*.

Chapter 5

Summary and Future Directions

Neurodegeneration with brain iron accumulation (NBIA) describes a spectrum of neurological disease in children and adults with high amounts of iron in the basal ganglia. Within this spectrum, mutations in *PANK2* and *PLA2G6* are the genetic basis for classic and atypical PKAN and infantile and atypical neuroaxonal dystrophy, respectively. *PANK2* and *PLA2G6* play important roles in lipid metabolism; *PANK2* encodes a mitochondrial pantothenate kinase, which is the rate limiting enzyme in the biosynthesis of coenzyme A, and *PLA2G6* encodes a calcium independent phospholipase, which plays roles in membrane homeostasis and other processes. In my thesis research, I investigated the transcriptional regulation of *PANK2* and expression of *PLA2G6* in human fetal development. In addition, I examined the expression and function of miR-103/7, a family of microRNAs conserved within pantothenate kinase genes.

Transcriptional regulation of *PANK2*

As presented in Chapter 2.1, I have identified a *PANK2* promoter and potential transcriptional regulators of the short isoform of PANK2 (sPANK2). Luciferase reporter assays established the presence of a minimal promoter located -327/-76 nucleotides upstream of the sPANK2 translational start site, and 5'RACE confirmed at least three transcriptional start sites in the region (-78, -87, -122). The -327/-76 promoter region has 62.9% identity to mouse, which is typical for core promoter elements conserved in human and mouse orthologs (Jin et al., 2006). In addition, by mutational analysis, electrophoresis mobility shift assays and proteomic analysis of the promoter, I identified potential regulators of *PANK2* expression, including NF-Y, FOXN4 and the human heterogeneous nuclear ribonucleoprotein A/B family.

A significant finding in this work is that sPANK2 and pPANK2 are transcribed from different promoters. This differential expression may mediate specialized function of the short and long isoforms. Therefore, an intriguing future direction from these studies is to identify the pPANK2 promoter and examine whether pPANK2 and sPANK2 are differentially expressed in human tissues.

Additionally, further study is necessary to confirm *PANK2* transcriptional regulation by specific transcription factors. As described in Chapter 2.2, I have preliminary evidence that hnRNPA2 and hnRNPA3 may inhibit *PANK2* transcription. Interestingly, hnRNPA2 has recently been identified as a coactivator in the nuclear transcription response to mitochondrial respiratory stress (Guha et al., 2009). Therefore, confirmation of *PANK2* regulation by hnRNPA2 may provide a mechanism by which *PANK2* transcription is mediated by cellular stress.

As presented in Chapter 2.2, my preliminary investigations did not reveal *PANK2* regulation by hydrogen peroxoide-induced oxidative stress. However, due to the mitochondrial localization of PANK2, it would be interesting to determine whether specifically compromising mitochondrial function has an effect on *PANK2* expression. There are several methods for compromising mitochondria in cell culture, such as treatment with NaN_3, an inhibitor of cytochrome c oxidase, or rotenone, an inhibitor of mitochondrial complex I (Ding et al., 2008; Sherer et al., 2002).

Likewise, as presented in Chapter 2.2, my preliminary investigations did not reveal *PANK2* regulation by metabolic signaling through PPAR. However, I hypothesize that *PANK2* could be transcriptionally regulated through other metabolic signaling pathways. Interestingly, *PLA2G6* is transcriptionally regulated by sterol regulatory

element binding protein (SREPB). I could investigate *PANK2* regulation through this pathway by depleting sterol in cell culture media, which activates SREPBs.

Expression and function of miR-103/7

In the third chapter my thesis research, I presented evidence that the miR-103/7 family is not co-expressed with pantothenate kinase genes. In Chapter 3.1, I demonstrated by qRT-PCR that mir-103 and miR-107 expression does not correlate with the expression of their host pantothenate kinase genes in mouse tissues. In Chapter 3.2, I demonstrated by Northern blot that miR-103-2 and miR-103 expression patterns also did not correlate in mouse tissues. Therefore, post-transcriptional processing of miR-103-2 may modify miR-103 expression. Continuation of these studies by comparing miR-103-1, pre-miR-107 and mature miR-107 expression in tissues may clarify whether the regulation of post-transcriptional processing is unique to miR-103-2.

Also, as presented in Chapter 3.2, I was unable to validate a miR-103 target by luciferase reporter assay and over expression experiments. However, my results indicate that PRPF4b may be regulated by miR-103. If this is the case, it has interesting implications for miR-103 function. PRPF4b is involved in pre-mRNA splicing and signal transduction. It is not associated with disease; however, mutations in three other pre-mRNA-processing factor gene homologs (PRPF31, PRPF8 and HPRP3) are associated with familial retinitis pigmentosa (Chakarova et al., 2002; McKie et al., 2001; Vithana et al., 2001), a common feature of PKAN. Therefore, miR-103 mediated-regulation of PRPF4b may tie into PKAN pathogenesis.

Interestingly, several recent reports support the hypothesis that miR-103/7 plays a role in neurodegeneration. For example, miR-103/7 is expressed in brain regions that are often impacted by neurodegeneration (Nelson et al., 2010), and there is a correlation of decreased miR-103/7 expression and increased neurotic plaques and neurofibrillary tangles in Alzheimer's disease (AD) brains (Nelson and Wang, 2010; Wang et al., 2008). In addition, validated miR-103/7 targets include BACE1 (Wang et al., 2008), HIF1β (Yamakuchi et al., 2010) and granulin (GRN) (Wang et al., 2010): three proteins with proposed roles in neurodegeneration. These results strengthen the likelihood that miR-103/7 may play a role in NBIA pathogenesis.

To investigate the role of miR-103/7 in PKAN, I propose the following experiments. First, miR-103/7 expression could be compared in normal and PKAN human brain to determine whether there is a correlation with neuropathy, similar to AD. Second, I propose that the pantothenate kinase Drosophila mutant, *fumble* (Afshar et al., 2001), could be exploited to determine whether miR-103/7 function complements pantothenate kinase function, and if it can rescue neurodegeneration. In Drosophila, there is only one pantothenate kinase gene and miR-103 and miR-107 are not found. Therefore, I propose to transiently express miR-103 in Drosophila and determine whether it has an effect on the defects typically observed in *fumble*, such as movement defects and decreased life expectancy (Bosveld et al., 2008; Wu et al., 2009). I hypothesize that if miR-103 and pantothenate kinase have complementary functions, transient expression of miR-103 will increase life expectancy and improve the movement abnormalieies observerd in *fumble* mutants.

Expression of NBIA genes in human fetal development

In the fourth chapter of my thesis research, I analyzed the expression of *PLA2G6* and *PANK2* in human fetal development. As described in Chapter 4.1, *PLA2G6* has a dynamic expression pattern both in terms of the location of expression and the differentiation state of expressing cells. Throughout the developing brain, *PLA2G6* is expressed in proliferative zones, as well as in the differentiated neurons in the developing cerebral neocortex and hindbrain. As described in Chapter 4.2, the *PANK2* results were limited to a preliminary study due to technical difficulties, but expression was noted in the brain and eye. Also, *PANK2* and *PLA2G6* expression were observed in basal ganglia, lateral ventricle, midbrain and thalamus of the fetal brain, as well as in spinal cord, kidney, liver, eye and lung. These results suggest that *PLA2G6* and *PANK2* are positioned to play a role in early neuronal development. Disruption of this process may contribute to the widespread neurological problems observed in NBIA.

An important application of these results lies in the development of therapy to treat NBIA. Notably, fetal *PLA2G6* and *PANK2* expression suggests that NBIA pathogenesis could initiate *in utero*. Indeed, our laboratory observes disorganization and increased apoptosis in the *Pank2* knockout mice as young as 3 weeks old. Therefore, an obstacle to delivering neuroprotective therapy may be timing of treatment in both mouse models and human patients. A study of the temporal and spatial expression of *PANK2* and *PLA2G6* in mouse neurodevelopment will inform future studies to develop of effective treatments.

Final Conclusions

All together, this diverse group of experiments makes a significant contribution to our understanding of the transcriptional regulation and expression of NBIA genes. My results bring to light new questions and considerations for continued research in NBIA pathogenesis. In particular, are pPANK2 and sPANK2 regulated by distinct mechanisms and do they serve specialized functions within the cell? What is the role of miR-103/7 in PKAN pathogenesis? How does the early expression pattern of *PLA2G6* and *PANK2* contribute to NBIA pathogenesis and how can we leverage this information to develop effective treatments? The answers to these questions will continue to bring us closer to the ultimate goal: developing effective treatment for NBIA.

References

Ackermann, E. J., Kempner, E. S. and Dennis, E. A. (1994). Ca(2+)-independent cytosolic phospholipase A2 from macrophage-like P388D1 cells. Isolation and characterization. *J Biol Chem* **269**, 9227-33.
Afshar, K., Gonczy, P., DiNardo, S. and Wasserman, S. A. (2001). fumble Encodes a pantothenate kinase homolog required for proper mitosis and meiosis in Drosophila melanogaster. *Genetics* **157**, 1267-76.
Andrews, D. L., Beames, B., Summers, M. D. and Park, W. D. (1988). Characterization of the lipid acyl hydrolase activity of the major potato (Solanum tuberosum) tuber protein, patatin, by cloning and abundant expression in a baculovirus vector. *Biochem J* **252**, 199-206.
Atsumi, G., Murakami, M., Kojima, K., Hadano, A., Tajima, M. and Kudo, I. (2000). Distinct roles of two intracellular phospholipase A2s in fatty acid release in the cell death pathway. Proteolytic fragment of type IVA cytosolic phospholipase A2alpha inhibits stimulus-induced arachidonate release, whereas that of type VI Ca2+-independent phospholipase A2 augments spontaneous fatty acid release. *J Biol Chem* **275**, 18248-58.
Auboeuf, D., Rieusset, J., Fajas, L., Vallier, P., Frering, V., Riou, J. P., Staels, B., Auwerx, J., Laville, M. and Vidal, H. (1997). Tissue distribution and quantification of the expression of mRNAs of peroxisome proliferator-activated receptors and liver X receptor-alpha in humans: no alteration in adipose tissue of obese and NIDDM patients. *Diabetes* **46**, 1319-27.
Babak, T., Zhang, W., Morris, Q., Blencowe, B. J. and Hughes, T. R. (2004). Probing microRNAs with microarrays: tissue specificity and functional inference. *RNA* **10**, 1813-9.
Balboa, M. A. and Balsinde, J. (2002). Involvement of calcium-independent phospholipase A2 in hydrogen peroxide-induced accumulation of free fatty acids in human U937 cells. *J Biol Chem* **277**, 40384-9.
Balboa, M. A., Saez, Y. and Balsinde, J. (2003). Calcium-independent phospholipase A2 is required for lysozyme secretion in U937 promonocytes. *J Immunol* **170**, 5276-80.
Balsinde, J. and Balboa, M. A. (2005). Cellular regulation and proposed biological functions of group VIA calcium-independent phospholipase A2 in activated cells. *Cell Signal* **17**, 1052-62.
Balsinde, J., Balboa, M. A. and Dennis, E. A. (1997). Antisense inhibition of group VI Ca2+-independent phospholipase A2 blocks phospholipid fatty acid remodeling in murine P388D1 macrophages. *J Biol Chem* **272**, 29317-21.
Balsinde, J., Bianco, I. D., Ackermann, E. J., Conde-Frieboes, K. and Dennis, E. A. (1995). Inhibition of calcium-independent phospholipase A2 prevents arachidonic acid incorporation and phospholipid remodeling in P388D1 macrophages. *Proc Natl Acad Sci U S A* **92**, 8527-31.
Balsinde, J. and Dennis, E. A. (1996). Bromoenol lactone inhibits magnesium-dependent phosphatidate phosphohydrolase and blocks triacylglycerol biosynthesis in mouse P388D1 macrophages. *J Biol Chem* **271**, 31937-41.
Balsinde, J., Perez, R. and Balboa, M. A. (2006). Calcium-independent phospholipase A2 and apoptosis. *Biochim Biophys Acta* **1761**, 1344-50.
Bao, S., Miller, D. J., Ma, Z., Wohltmann, M., Eng, G., Ramanadham, S., Moley, K. and Turk, J. (2004). Male mice that do not express group VIA phospholipase A2 produce spermatozoa with impaired motility and have greatly reduced fertility. *J Biol Chem* **279**, 38194-200.
Bartel, D. P. (2004). MicroRNAs: genomics, biogenesis, mechanism, and function. *Cell* **116**, 281-97.
Baskerville, S. and Bartel, D. P. (2005). Microarray profiling of microRNAs reveals frequent coexpression with neighboring miRNAs and host genes. *RNA* **11**, 241-7.
Bateman, A. and Bennett, H. P. (2009). The granulin gene family: from cancer to dementia. *Bioessays* **31**, 1245-54.
Bayer, S. A. (2006). The Human Brain during the Late First Trimester: Taylor & Francis.

Bohnsack, M. T., Czaplinski, K. and Gorlich, D. (2004). Exportin 5 is a RanGTP-dependent dsRNA-binding protein that mediates nuclear export of pre-miRNAs. *RNA* **10**, 185-91.
Borchert, G. M., Lanier, W. and Davidson, B. L. (2006). RNA polymerase III transcribes human microRNAs. *Nat Struct Mol Biol* **13**, 1097-101.
Bosveld, F., Rana, A., van der Wouden, P. E., Lemstra, W., Ritsema, M., Kampinga, H. H. and Sibon, O. C. (2008). De novo CoA biosynthesis is required to maintain DNA integrity during development of the Drosophila nervous system. *Hum Mol Genet* **17**, 2058-69.
Bouley, D. M., McIntire, J. J., Harris, B. T., Tolwani, R. J., Otto, G. M., DeKruyff, R. H. and Hayflick, S. J. (2006). Spontaneous murine neuroaxonal dystrophy: a model of infantile neuroaxonal dystrophy. *J Comp Pathol* **134**, 161-70.
Bragt, M. C. and Popeijus, H. E. (2008). Peroxisome proliferator-activated receptors and the metabolic syndrome. *Physiol Behav* **94**, 187-97.
Bucher, P. (1990). Weight matrix descriptions of four eukaryotic RNA polymerase II promoter elements derived from 502 unrelated promoter sequences. *J Mol Biol* **212**, 563-78.
Bullen, P. and Wilson, D. (1997). The Carnegie staging of human embryos: a practical guide. In *Molecular genetics of early human development*, (ed. T. Strachan S. Lindsay and D. Wilson), pp. 27-50: Oxford: BIOS Scientific Publishers.
Burke, J. E. and Dennis, E. A. (2009). Phospholipase A2 biochemistry. *Cardiovasc Drugs Ther* **23**, 49-59.
Cai, X., Hagedorn, C. H. and Cullen, B. R. (2004). Human microRNAs are processed from capped, polyadenylated transcripts that can also function as mRNAs. *RNA* **10**, 1957-66.
Calabrese, V., Cornelius, C., Mancuso, C., Lentile, R., Stella, A. M. and Butterfield, D. A. (2010). Redox homeostasis and cellular stress response in aging and neurodegeneration. *Methods Mol Biol* **610**, 285-308.
Campillos, M., Lamas, J. R., Garcia, M. A., Bullido, M. J., Valdivieso, F. and Vazquez, J. (2003). Specific interaction of heterogeneous nuclear ribonucleoprotein A1 with the -219T allelic form modulates APOE promoter activity. *Nucleic Acids Res* **31**, 3063-70.
Carnevale, K. A. and Cathcart, M. K. (2001). Calcium-independent phospholipase A(2) is required for human monocyte chemotaxis to monocyte chemoattractant protein 1. *J Immunol* **167**, 3414-21.
Cartharius, K., Frech, K., Grote, K., Klocke, B., Haltmeier, M., Klingenhoff, A., Frisch, M., Bayerlein, M. and Werner, T. (2005). MatInspector and beyond: promoter analysis based on transcription factor binding sites. *Bioinformatics* **21**, 2933-42.
Casey, J. L., Hentze, M. W., Koeller, D. M., Caughman, S. W., Rouault, T. A., Klausner, R. D. and Harford, J. B. (1988). Iron-responsive elements: regulatory RNA sequences that control mRNA levels and translation. *Science* **240**, 924-8.
Chakarova, C. F., Hims, M. M., Bolz, H., Abu-Safieh, L., Patel, R. J., Papaioannou, M. G., Inglehearn, C. F., Keen, T. J., Willis, C., Moore, A. T. et al. (2002). Mutations in HPRP3, a third member of pre-mRNA splicing factor genes, implicated in autosomal dominant retinitis pigmentosa. *Hum Mol Genet* **11**, 87-92.
Chang, Y. Z., Qian, Z. M., Du, J. R., Zhu, L., Xu, Y., Li, L. Z., Wang, C. Y., Wang, Q., Ge, X. H., Ho, K. P. et al. (2007). Ceruloplasmin expression and its role in iron transport in C6 cells. *Neurochem Int* **50**, 726-33.
Chen, H., Hewison, M., Hu, B. and Adams, J. S. (2003). Heterogeneous nuclear ribonucleoprotein (hnRNP) binding to hormone response elements: a cause of vitamin D resistance. *Proc Natl Acad Sci U S A* **100**, 6109-14.

Chendrimada, T. P., Gregory, R. I., Kumaraswamy, E., Norman, J., Cooch, N., Nishikura, K. and Shiekhattar, R. (2005). TRBP recruits the Dicer complex to Ago2 for microRNA processing and gene silencing. *Nature* **436**, 740-4.
Ching, K. H., Westaway, S. K., Gitschier, J., Higgins, J. J. and Hayflick, S. J. (2002). HARP syndrome is allelic with pantothenate kinase-associated neurodegeneration. *Neurology* **58**, 1673-4.
Cicatiello, L., Mutarelli, M., Grober, O. M., Paris, O., Ferraro, L., Ravo, M., Tarallo, R., Luo, S., Schroth, G. P., Seifert, M. et al. (2010). Estrogen receptor alpha controls a gene network in luminal-like breast cancer cells comprising multiple transcription factors and microRNAs. *Am J Pathol* **176**, 2113-30.
Corcoran, D. L., Pandit, K. V., Gordon, B., Bhattacharjee, A., Kaminski, N. and Benos, P. V. (2009). Features of mammalian microRNA promoters emerge from polymerase II chromatin immunoprecipitation data. *PLoS One* **4**, e5279.
Correia, S. C. and Moreira, P. I. (2010). Hypoxia-inducible factor 1: a new hope to counteract neurodegeneration? *J Neurochem* **112**, 1-12.
Cummings, B. S., Gelasco, A. K., Kinsey, G. R., McHowat, J. and Schnellmann, R. G. (2004). Inactivation of endoplasmic reticulum bound Ca2+-independent phospholipase A2 in renal cells during oxidative stress. *J Am Soc Nephrol* **15**, 1441-51.
Curtis, A. R., Fey, C., Morris, C. M., Bindoff, L. A., Ince, P. G., Chinnery, P. F., Coulthard, A., Jackson, M. J., Jackson, A. P., McHale, D. P. et al. (2001). Mutation in the gene encoding ferritin light polypeptide causes dominant adult-onset basal ganglia disease. *Nat Genet* **28**, 350-4.
De Sarno, P., Shestopal, S. A., King, T. D., Zmijewska, A., Song, L. and Jope, R. S. (2003). Muscarinic receptor activation protects cells from apoptotic effects of DNA damage, oxidative stress, and mitochondrial inhibition. *J Biol Chem* **278**, 11086-93.
Denli, A. M., Tops, B. B., Plasterk, R. H., Ketting, R. F. and Hannon, G. J. (2004). Processing of primary microRNAs by the Microprocessor complex. *Nature* **432**, 231-5.
Dennis, E. A. (1994). Diversity of group types, regulation, and function of phospholipase A2. *J Biol Chem* **269**, 13057-60.
Ding, H., Gao, J., Zhu, Z., Xiong, Y. and Liu, J. (2008). Mitochondrial dysfunction enhances susceptibility to oxidative stress by down-regulation of thioredoxin in human neuroblastoma cells. *Neurochem Res* **33**, 43-50.
Edward, D. P. and Kaufman, L. M. (2003). Anatomy, development, and physiology of the visual system. *Pediatr Clin North Am* **50**, 1-23.
Egan, R. A., Weleber, R. G., Hogarth, P., Gregory, A., Coryell, J., Westaway, S. K., Gitschier, J., Das, S. and Hayflick, S. J. (2005). Neuro-ophthalmologic and electroretinographic findings in pantothenate kinase-associated neurodegeneration (formerly Hallervorden-Spatz syndrome). *Am J Ophthalmol* **140**, 267-74.
Eisenstein, R. S. (2000). Iron regulatory proteins and the molecular control of mammalian iron metabolism. *Annu Rev Nutr* **20**, 627-62.
Fernaeus, S. and Land, T. (2005). Increased iron-induced oxidative stress and toxicity in scrapie-infected neuroblastoma cells. *Neurosci Lett* **382**, 217-20.
Filipowicz, W., Bhattacharyya, S. N. and Sonenberg, N. (2008). Mechanisms of post-transcriptional regulation by microRNAs: are the answers in sight? *Nat Rev Genet* **9**, 102-14.
Gao, J., Sun, H. Y., Zhu, Z. R., Ding, Z. and Zhu, L. (2005). Antioxidant effects of dehydroepiandrosterone are related to up-regulation of thioredoxin in SH-SY5Y cells. *Acta Biochim Biophys Sin (Shanghai)* **37**, 119-25.

Ghavami, S., Hashemi, M., Ande, S. R., Yeganeh, B., Xiao, W., Eshraghi, M., Bus, C. J., Kadkhoda, K., Wiechec, E., Halayko, A. J. et al. (2009). Apoptosis and cancer: mutations within caspase genes. *J Med Genet* **46**, 497-510.
Gouge, A., Holt, J., Hardy, A. P., Sowden, J. C. and Smith, H. K. (2001). Foxn4--a new member of the forkhead gene family is expressed in the retina. *Mech Dev* **107**, 203-6.
Gregory, A., Polster, B. J. and Hayflick, S. J. (2009). Clinical and genetic delineation of neurodegeneration with brain iron accumulation. *J Med Genet* **46**.
Gregory, A., Westaway, S. K., Holm, I. E., Kotzbauer, P. T., Hogarth, P., Sonek, S., Coryell, J. C., Nguyen, T. M., Nardocci, N., Zorzi, G. et al. (2008). Neurodegeneration associated with genetic defects in phospholipase A(2). *Neurology* **71**, 1402-9.
Griffiths-Jones, S., Grocock, R. J., van Dongen, S., Bateman, A. and Enright, A. J. (2006). miRBase: microRNA sequences, targets and gene nomenclature. *Nucleic Acids Res* **34**, D140-4.
Guha, M., Pan, H., Fang, J. K. and Avadhani, N. G. (2009). Heterogeneous nuclear ribonucleoprotein A2 is a common transcriptional coactivator in the nuclear transcription response to mitochondrial respiratory stress. *Mol Biol Cell* **20**, 4107-19.
Guo, T. and Hobbs, D. W. (2006). Development of BACE1 inhibitors for Alzheimer's disease. *Curr Med Chem* **13**, 1811-29.
Hallervorden, J. and Spatz, H. (1922). Eigenartige Erkrankung im extrapyramidalen System mit besonderer Beteiligung des Globus pallidus und der Substantia nigra. *Z. Gesamte Neurol. Psychiatr.* **79**, 254-302.
Halliday, W. (1995). The nosology of Hallervorden-spatz disease. *J Neurol Sci* **134 Suppl**, 84-91.
Haniu, M., Denis, P., Young, Y., Mendiaz, E. A., Fuller, J., Hui, J. O., Bennett, B. D., Kahn, S., Ross, S., Burgess, T. et al. (2000). Characterization of Alzheimer's beta -secretase protein BACE. A pepsin family member with unusual properties. *J Biol Chem* **275**, 21099-106.
Hayflick, S. J., Westaway, S. K., Levinson, B., Zhou, B., Johnson, M. A., Ching, K. H. and Gitschier, J. (2003). Genetic, clinical, and radiographic delineation of Hallervorden-Spatz syndrome. *N Engl J Med* **348**, 33-40.
He, Y. and Smith, R. (2009). Nuclear functions of heterogeneous nuclear ribonucleoproteins A/B. *Cell Mol Life Sci* **66**, 1239-56.
Heinaniemi, M., Uski, J. O., Degenhardt, T. and Carlberg, C. (2007). Meta-analysis of primary target genes of peroxisome proliferator-activated receptors. *Genome Biol* **8**, R147.
Heneka, M. T. and Landreth, G. E. (2007). PPARs in the brain. *Biochim Biophys Acta* **1771**, 1031-45.
Heo, S. R., Han, A. M., Kwon, Y. K. and Joung, I. (2009). p62 protects SH-SY5Y neuroblastoma cells against H2O2-induced injury through the PDK1/Akt pathway. *Neurosci Lett* **450**, 45-50.
Hern, W. M. (1984). Correlation of fetal age and measurements between 10 and 26 weeks of gestation. *Obstet Gynecol* **63**, 26-32.
Herrera, B. M., Lockstone, H. E., Taylor, J. M., Ria, M., Barrett, A., Collins, S., Kaisaki, P., Argoud, K., Fernandez, C., Travers, M. E. et al. (2010). Global microRNA expression profiles in insulin target tissues in a spontaneous rat model of type 2 diabetes. *Diabetologia* **53**, 1099-109.
Hong, B. S., Senisterra, G., Rabeh, W. M., Vedadi, M., Leonardi, R., Zhang, Y. M., Rock, C. O., Jackowski, S. and Park, H. W. (2007). Crystal structures of human pantothenate kinases: Insights into allosteric regulation and mutations linked to neurodegeneration disorder. *J Biol Chem*.
Hong, B. S., Yun, M. K., Zhang, Y. M., Chohnan, S., Rock, C. O., White, S. W., Jackowski, S., Park, H. W. and Leonardi, R. (2006). Prokaryotic type II and type III pantothenate kinases: The same monomer fold creates dimers with distinct catalytic properties. *Structure* **14**, 1251-61.

Hortnagel, K., Prokisch, H. and Meitinger, T. (2003). An isoform of hPANK2, deficient in pantothenate kinase-associated neurodegeneration, localizes to mitochondria. *Hum Mol Genet* **12**, 321-7.
Hutvagner, G., Simard, M. J., Mello, C. C. and Zamore, P. D. (2004). Sequence-specific inhibition of small RNA function. *PLoS Biol* **2**, E98.
Jenkins, C. M., Han, X., Mancuso, D. J. and Gross, R. W. (2002). Identification of calcium-independent phospholipase A2 (iPLA2) beta, and not iPLA2gamma, as the mediator of arginine vasopressin-induced arachidonic acid release in A-10 smooth muscle cells. Enantioselective mechanism-based discrimination of mammalian iPLA2s. *J Biol Chem* **277**, 32807-14.
Jenkins, C. M., Wolf, M. J., Mancuso, D. J. and Gross, R. W. (2001). Identification of the calmodulin-binding domain of recombinant calcium-independent phospholipase A2beta. implications for structure and function. *J Biol Chem* **276**, 7129-35.
Jiang, H. and Xiang, M. (2009). Subtype specification of GABAergic amacrine cells by the orphan nuclear receptor Nr4a2/Nurr1. *J Neurosci* **29**, 10449-59.
Jin, V. X., Singer, G. A., Agosto-Perez, F. J., Liyanarachchi, S. and Davuluri, R. V. (2006). Genome-wide analysis of core promoter elements from conserved human and mouse orthologous pairs. *BMC Bioinformatics* **7**, 114.
John, B., Enright, A. J., Aravin, A., Tuschl, T., Sander, C. and Marks, D. S. (2004). Human MicroRNA targets. *PLoS Biol* **2**, e363.
Johnson, M. A., Kuo, Y. M., Westaway, S. K., Parker, S. M., Ching, K. H., Gitschier, J. and Hayflick, S. J. (2004). Mitochondrial localization of human PANK2 and hypotheses of secondary iron accumulation in pantothenate kinase-associated neurodegeneration. *Ann N Y Acad Sci* **1012**, 282-98.
Jung, M., Schaefer, A., Steiner, I., Kempkensteffen, C., Stephan, C., Erbersdobler, A. and Jung, K. (2010). Robust microRNA stability in degraded RNA preparations from human tissue and cell samples. *Clin Chem* **56**, 998-1006.
Katoh, M. (2004). Human FOX gene family (Review). *Int J Oncol* **25**, 1495-500.
Kent, W. J., Sugnet, C. W., Furey, T. S., Roskin, K. M., Pringle, T. H., Zahler, A. M. and Haussler, D. (2002). The human genome browser at UCSC. *Genome Res* **12**, 996-1006.
Kersten, S., Desvergne, B. and Wahli, W. (2000). Roles of PPARs in health and disease. *Nature* **405**, 421-4.
Kimura, K., Wakamatsu, A., Suzuki, Y., Ota, T., Nishikawa, T., Yamashita, R., Yamamoto, J., Sekine, M., Tsuritani, K., Wakaguri, H. et al. (2006). Diversification of transcriptional modulation: large-scale identification and characterization of putative alternative promoters of human genes. *Genome Res* **16**, 55-65.
Kiriakidou, M., Nelson, P. T., Kouranov, A., Fitziev, P., Bouyioukos, C., Mourelatos, Z. and Hatzigeorgiou, A. (2004). A combined computational-experimental approach predicts human microRNA targets. *Genes Dev* **18**, 1165-78.
Kolko, M., Kiilgaard, J. F., Wang, J., Poulsen, K. A., Andreasen, J. R., la Cour, M., Nissen, M. H., Heegaard, S., Bazan, N. G. and Prause, J. U. (2009). Calcium-independent phospholipase A2 regulates retinal pigment epithelium proliferation and may be important in the pathogenesis of retinal diseases. *Exp Eye Res* **89**, 383-91.
Kolko, M., Wang, J., Zhan, C., Poulsen, K. A., Prause, J. U., Nissen, M. H., Heegaard, S. and Bazan, N. G. (2007). Identification of intracellular phospholipases A2 in the human eye: involvement in phagocytosis of photoreceptor outer segments. *Invest Ophthalmol Vis Sci* **48**, 1401-9.
Kotzbauer, P. T., Truax, A. C., Trojanowski, J. Q. and Lee, V. M. (2005). Altered neuronal mitochondrial coenzyme A synthesis in neurodegeneration with brain iron accumulation caused

by abnormal processing, stability, and catalytic activity of mutant pantothenate kinase 2. *J Neurosci* **25**, 689-98.
Kozak, M. (1989). The scanning model for translation: an update. *J Cell Biol* **108**, 229-41.
Kozak, M. (1990). Downstream secondary structure facilitates recognition of initiator codons by eukaryotic ribosomes. *Proc Natl Acad Sci U S A* **87**, 8301-5.
Krichevsky, A. M., King, K. S., Donahue, C. P., Khrapko, K. and Kosik, K. S. (2003). A microRNA array reveals extensive regulation of microRNAs during brain development. *RNA* **9**, 1274-81.
Kruer, M. C., Paisán-Ruiz, C., Boddaert, N., Yoon, M. Y., Hama, H., Gregory, A., Malandrini, A., Woltjer, R. L., Munnich, A., Polster, B. J. et al. (2010). Defective FA2H leads to a novel form of neurodegeneration with brain iron accumulation (NBIA). *Ann Neurol*.
Kumar, A., Williams, K. R. and Szer, W. (1986). Purification and domain structure of core hnRNP proteins A1 and A2 and their relationship to single-stranded DNA-binding proteins. *J Biol Chem* **261**, 11266-73.
Kuo, Y. M., Duncan, J. L., Westaway, S. K., Yang, H., Nune, G., Xu, E. Y., Hayflick, S. J. and Gitschier, J. (2005). Deficiency of pantothenate kinase 2 (Pank2) in mice leads to retinal degeneration and azoospermia. *Hum Mol Genet* **14**, 49-57.
Kurian, M. A., Morgan, N. V., MacPherson, L., Foster, K., Peake, D., Gupta, R., Philip, S. G., Hendriksz, C., Morton, J. E. V., Kingston, H. M. et al. (2008). Phenotypic spectrum of neurodegeneration associated with mutations in the PLA2G6 gene (PLAN). *Neurology* **70**, 1623-1629.
Larkin, M. A., Blackshields, G., Brown, N. P., Chenna, R., McGettigan, P. A., McWilliam, H., Valentin, F., Wallace, I. M., Wilm, A., Lopez, R. et al. (2007). Clustal W and Clustal X version 2.0. *Bioinformatics* **23**, 2947-8.
Larsson Forsell, P. K., Kennedy, B. P. and Claesson, H. E. (1999). The human calcium-independent phospholipase A2 gene multiple enzymes with distinct properties from a single gene. *Eur J Biochem* **262**, 575-85.
Larsson, P. K., Claesson, H. E. and Kennedy, B. P. (1998). Multiple splice variants of the human calcium-independent phospholipase A2 and their effect on enzyme activity. *J Biol Chem* **273**, 207-14.
Lau, J. S., Baumeister, P., Kim, E., Roy, B., Hsieh, T. Y., Lai, M. and Lee, A. S. (2000). Heterogeneous nuclear ribonucleoproteins as regulators of gene expression through interactions with the human thymidine kinase promoter. *J Cell Biochem* **79**, 395-406.
Lauber, K., Bohn, E., Krober, S. M., Xiao, Y. J., Blumenthal, S. G., Lindemann, R. K., Marini, P., Wiedig, C., Zobywalski, A., Baksh, S. et al. (2003). Apoptotic cells induce migration of phagocytes via caspase-3-mediated release of a lipid attraction signal. *Cell* **113**, 717-30.
Lee, E. J., Baek, M., Gusev, Y., Brackett, D. J., Nuovo, G. J. and Schmittgen, T. D. (2008). Systematic evaluation of microRNA processing patterns in tissues, cell lines, and tumors. *RNA* **14**, 35-42.
Lee, K. H., Lotterman, C., Karikari, C., Omura, N., Feldmann, G., Habbe, N., Goggins, M. G., Mendell, J. T. and Maitra, A. (2009). Epigenetic silencing of MicroRNA miR-107 regulates cyclin-dependent kinase 6 expression in pancreatic cancer. *Pancreatology* **9**, 293-301.
Lee, Y., Kim, M., Han, J., Yeom, K. H., Lee, S., Baek, S. H. and Kim, V. N. (2004). MicroRNA genes are transcribed by RNA polymerase II. *EMBO J* **23**, 4051-60.
Lehmann, J. M., Moore, L. B., Smith-Oliver, T. A., Wilkison, W. O., Willson, T. M. and Kliewer, S. A. (1995). An antidiabetic thiazolidinedione is a high affinity ligand for peroxisome proliferator-activated receptor gamma (PPAR gamma). *J Biol Chem* **270**, 12953-6.
Leonardi, R., Rock, C. O., Jackowski, S. and Zhang, Y. M. (2007a). Activation of human mitochondrial pantothenate kinase 2 by palmitoylcarnitine. *Proc Natl Acad Sci U S A*.

Leonardi, R., Zhang, Y. M., Lykidis, A., Rock, C. O. and Jackowski, S. (2007b). Localization and regulation of mouse pantothenate kinase 2. *FEBS Lett* **581**, 4639-44.
Leonardi, R., Zhang, Y. M., Rock, C. O. and Jackowski, S. (2005). Coenzyme A: back in action. *Prog Lipid Res* **44**, 125-53.
Lewis, B. P., Shih, I. H., Jones-Rhoades, M. W., Bartel, D. P. and Burge, C. B. (2003). Prediction of mammalian microRNA targets. *Cell* **115**, 787-98.
Li, S., Misra, K., Matise, M. P. and Xiang, M. (2005). Foxn4 acts synergistically with Mash1 to specify subtype identity of V2 interneurons in the spinal cord. *Proc Natl Acad Sci U S A* **102**, 10688-93.
Liang, Y., Ridzon, D., Wong, L. and Chen, C. (2007). Characterization of microRNA expression profiles in normal human tissues. *BMC Genomics* **8**, 166.
Ma, Q. (2010). Transcriptional responses to oxidative stress: pathological and toxicological implications. *Pharmacol Ther* **125**, 376-93.
Ma, Z., Ramanadham, S., Kempe, K., Chi, X. S., Ladenson, J. and Turk, J. (1997). Pancreatic islets express a Ca2+-independent phospholipase A2 enzyme that contains a repeated structural motif homologous to the integral membrane protein binding domain of ankyrin. *J Biol Chem* **272**, 11118-27.
Ma, Z. and Turk, J. (2001). The molecular biology of the group VIA Ca2+-independent phospholipase A2. *Prog Nucleic Acid Res Mol Biol* **67**, 1-33.
Ma, Z., Wang, X., Nowatzke, W., Ramanadham, S. and Turk, J. (1999). Human pancreatic islets express mRNA species encoding two distinct catalytically active isoforms of group VI phospholipase A2 (iPLA2) that arise from an exon-skipping mechanism of alternative splicing of the transcript from the iPLA2 gene on chromosome 22q13.1. *J Biol Chem* **274**, 9607-16.
Makeyev, A. V., Kim, C. B., Ruddle, F. H., Enkhmandakh, B., Erdenechimeg, L. and Bayarsaihan, D. (2005). HnRNP A3 genes and pseudogenes in the vertebrate genomes. *J Exp Zool A Comp Exp Biol* **303**, 259-71.
Malik, I., Turk, J., Mancuso, D. J., Montier, L., Wohltmann, M., Wozniak, D. F., Schmidt, R. E., Gross, R. W. and Kotzbauer, P. T. (2008). Disrupted membrane homeostasis and accumulation of ubiquitinated proteins in a mouse model of infantile neuroaxonal dystrophy caused by PLA2G6 mutations. *Am J Pathol* **172**, 406-16.
Mancuso, D. J., Jenkins, C. M. and Gross, R. W. (2000). The genomic organization, complete mRNA sequence, cloning, and expression of a novel human intracellular membrane-associated calcium-independent phospholipase A(2). *J Biol Chem* **275**, 9937-45.
Mancuso, D. J., Jenkins, C. M., Sims, H. F., Cohen, J. M., Yang, J. and Gross, R. W. (2004). Complex transcriptional and translational regulation of iPLAgamma resulting in multiple gene products containing dual competing sites for mitochondrial or peroxisomal localization. *Eur J Biochem* **271**, 4709-24.
Mantovani, R. (1998). A survey of 178 NF-Y binding CCAAT boxes. *Nucleic Acids Res* **26**, 1135-43.
Mantovani, R. (1999). The molecular biology of the CCAAT-binding factor NF-Y. *Gene* **239**, 15-27.
Maragkakis, M., Reczko, M., Simossis, V. A., Alexiou, P., Papadopoulos, G. L., Dalamagas, T., Giannopoulos, G., Goumas, G., Koukis, E., Kourtis, K. et al. (2009). DIANA-microT web server: elucidating microRNA functions through target prediction. *Nucleic Acids Res* **37**, W273-6.
Marsit, C. J., Eddy, K. and Kelsey, K. T. (2006). MicroRNA responses to cellular stress. *Cancer Res* **66**, 10843-8.
Martin, G., Schoonjans, K., Lefebvre, A. M., Staels, B. and Auwerx, J. (1997). Coordinate regulation of the expression of the fatty acid transport protein and acyl-CoA synthetase genes by PPARalpha and PPARgamma activators. *J Biol Chem* **272**, 28210-7.

McKie, A. B., McHale, J. C., Keen, T. J., Tarttelin, E. E., Goliath, R., van Lith-Verhoeven, J. J., Greenberg, J., Ramesar, R. S., Hoyng, C. B., Cremers, F. P. et al. (2001). Mutations in the pre-mRNA splicing factor gene PRPC8 in autosomal dominant retinitis pigmentosa (RP13). *Hum Mol Genet* **10**, 1555-62.
McNeill, A., Birchall, D., Hayflick, S. J., Gregory, A., Schenk, J. F., Zimmerman, E. A., Shang, H., Miyajima, H. and Chinnery, P. F. (2008). T2* and FSE MRI distinguishes four subtypes of neurodegeneration with brain iron accumulation. *Neurology* **70**, 1614-9.
Meister, G., Landthaler, M., Dorsett, Y. and Tuschl, T. (2004). Sequence-specific inhibition of microRNA- and siRNA-induced RNA silencing. *RNA* **10**, 544-50.
Mellios, N., Huang, H. S., Grigorenko, A., Rogaev, E. and Akbarian, S. (2008). A set of differentially expressed miRNAs, including miR-30a-5p, act as post-transcriptional inhibitors of BDNF in prefrontal cortex. *Hum Mol Genet* **17**, 3030-42.
Michael, M. Z., SM, O. C., van Holst Pellekaan, N. G., Young, G. P. and James, R. J. (2003). Reduced accumulation of specific microRNAs in colorectal neoplasia. *Mol Cancer Res* **1**, 882-91.
Miska, E. A., Alvarez-Saavedra, E., Townsend, M., Yoshii, A., Sestan, N., Rakic, P., Constantine-Paton, M. and Horvitz, H. R. (2004). Microarray analysis of microRNA expression in the developing mammalian brain. *Genome Biol* **5**, R68.
Miyake, N., Chilton, J., Psatha, M., Cheng, L., Andrews, C., Chan, W. M., Law, K., Crosier, M., Lindsay, S., Cheung, M. et al. (2008). Human CHN1 mutations hyperactivate alpha2-chimaerin and cause Duane's retraction syndrome. *Science* **321**, 839-43.
Monteys, A. M., Spengler, R. M., Wan, J., Tecedor, L., Lennox, K. A., Xing, Y. and Davidson, B. L. (2010). Structure and activity of putative intronic miRNAs promoters. *RNA*.
Moorman, A. F., Houweling, A. C., de Boer, P. A. and Christoffels, V. M. (2001). Sensitive nonradioactive detection of mRNA in tissue sections: novel application of the whole-mount in situ hybridization protocol. *J Histochem Cytochem* **49**, 1-8.
Morgan, N. V., Westaway, S. K., Morton, J. E., Gregory, A., Gissen, P., Sonek, S., Cangul, H., Coryell, J., Canham, N., Nardocci, N. et al. (2006). PLA2G6, encoding a phospholipase A2, is mutated in neurodegenerative disorders with high brain iron. *Nat Genet* **38**, 752-4.
Morlando, M., Ballarino, M., Gromak, N., Pagano, F., Bozzoni, I. and Proudfoot, N. J. (2008). Primary microRNA transcripts are processed co-transcriptionally. *Nat Struct Mol Biol* **15**, 902-9.
Mourelatos, Z., Dostie, J., Paushkin, S., Sharma, A., Charroux, B., Abel, L., Rappsilber, J., Mann, M. and Dreyfuss, G. (2002). miRNPs: a novel class of ribonucleoproteins containing numerous microRNAs. *Genes Dev* **16**, 720-8.
Nardocci, N., Zorzi, G., Farina, L., Binelli, S., Scaioli, W., Ciano, C., Verga, L., Angelini, L., Savoiardo, M. and Bugiani, O. (1999). Infantile neuroaxonal dystrophy: clinical spectrum and diagnostic criteria. *Neurology* **52**, 1472-8.
Nelson, P. T., Dimayuga, J. and Wilfred, B. R. (2010). MicroRNA in Situ Hybridization in the Human Entorhinal and Transentorhinal Cortex. *Front Hum Neurosci* **4**, 7.
Nelson, P. T. and Wang, W. X. (2010). MiR-107 is Reduced in Alzheimer's Disease Brain Neocortex: Validation Study. *J Alzheimers Dis*.
O'Rahilly, R., Müller, F. and Streeter, G. L. (1987). Developmental stages in human embryos : including a revision of Streeter's "Horizons" and a survey of the Carnegie collection. [Washington, D.C.]: Carnegie Institution of Washington.
Obernosterer, G., Leuschner, P. J., Alenius, M. and Martinez, J. (2006). Post-transcriptional regulation of microRNA expression. *RNA* **12**, 1161-7.
Ong, W. Y., Ling, S. F., Yeo, J. F., Chiueh, C. C. and Farooqui, A. A. (2005a). Injury and recovery of pyramidal neurons in the rat hippocampus after a single episode of oxidative stress induced by intracerebroventricular injection of ferrous ammonium citrate. *Reprod Nutr Dev* **45**, 647-62.

Ong, W. Y., Yeo, J. F., Ling, S. F. and Farooqui, A. A. (2005b). Distribution of calcium-independent phospholipase A2 (iPLA 2) in monkey brain. *J Neurocytol* **34**, 447-58.
Ono, K., Yasui, Y., Rutishauser, U. and Miller, R. H. (1997). Focal ventricular origin and migration of oligodendrocyte precursors into the chick optic nerve. *Neuron* **19**, 283-92.
Orr, H. T. and Zoghbi, H. Y. (2007). Trinucleotide repeat disorders. *Annu Rev Neurosci* **30**, 575-621.
Ovcharenko, I., Loots, G. G., Giardine, B. M., Hou, M., Ma, J., Hardison, R. C., Stubbs, L. and Miller, W. (2005). Mulan: multiple-sequence local alignment and visualization for studying function and evolution. *Genome Res* **15**, 184-94.
Ovcharenko, I., Nobrega, M. A., Loots, G. G. and Stubbs, L. (2004). ECR Browser: a tool for visualizing and accessing data from comparisons of multiple vertebrate genomes. *Nucleic Acids Res* **32**, W280-6.
Ozsolak, F., Poling, L. L., Wang, Z., Liu, H., Liu, X. S., Roeder, R. G., Zhang, X., Song, J. S. and Fisher, D. E. (2008). Chromatin structure analyses identify miRNA promoters. *Genes Dev* **22**, 3172-83.
Paisan-Ruiz, C., Bhatia, K. P., Li, A., Hernandez, D., Davis, M., Wood, N. W., Hardy, J., Houlden, H., Singleton, A. and Schneider, S. A. (2009). Characterization of PLA2G6 as a locus for dystonia-parkinsonism. *Ann Neurol* **65**, 19-23.
Peltier, H. J. and Latham, G. J. (2008). Normalization of microRNA expression levels in quantitative RT-PCR assays: identification of suitable reference RNA targets in normal and cancerous human solid tissues. *RNA* **14**, 844-52.
Perry, T. L., Norman, M. G., Yong, V. W., Whiting, S., Crichton, J. U., Hansen, S. and Kish, S. J. (1985). Hallervorden-Spatz disease: cysteine accumulation and cysteine dioxygenase deficiency in the globus pallidus. *Annals of Neurology* **18**, 482-9.
Peterson, B., Knotts, T. and Cummings, B. S. (2007). Involvement of Ca2+-independent phospholipase A2 isoforms in oxidant-induced neural cell death. *Neurotoxicology* **28**, 150-60.
Polster, B. J., Yoon, M. Y. and Hayflick, S. J. (2010). Characterization of the human PANK2 promoter. *Gene*.
Pugh, C. W. and Ratcliffe, P. J. (2003). Regulation of angiogenesis by hypoxia: role of the HIF system. *Nat Med* **9**, 677-84.
Qian, Z. M. and Wang, Q. (1998). Expression of iron transport proteins and excessive iron accumulation in the brain in neurodegenerative disorders. *Brain Res Brain Res Rev* **27**, 257-67.
Ramanadham, S., Hsu, F. F., Zhang, S., Jin, C., Bohrer, A., Song, H., Bao, S., Ma, Z. and Turk, J. (2004). Apoptosis of insulin-secreting cells induced by endoplasmic reticulum stress is amplified by overexpression of group VIA calcium-independent phospholipase A2 (iPLA2 beta) and suppressed by inhibition of iPLA2 beta. *Biochemistry* **43**, 918-30.
Ramaswamy, G., Karim, M. A., Murti, K. G. and Jackowski, S. (2004). PPARalpha controls the intracellular coenzyme A concentration via regulation of PANK1alpha gene expression. *J Lipid Res* **45**, 17-31.
Redell, J. B., Liu, Y. and Dash, P. K. (2009). Traumatic brain injury alters expression of hippocampal microRNAs: potential regulators of multiple pathophysiological processes. *J Neurosci Res* **87**, 1435-48.
Rhead, B., Karolchik, D., Kuhn, R. M., Hinrichs, A. S., Zweig, A. S., Fujita, P. A., Diekhans, M., Smith, K. E., Rosenbloom, K. R., Raney, B. J. et al. (2010). The UCSC Genome Browser database: update 2010. *Nucleic Acids Res* **38**, D613-9.
Robishaw, J. D. and Neely, J. R. (1985). Coenzyme A metabolism. *Am J Physiol* **248**, E1-9.
Rock, C. O., Calder, R. B., Karim, M. A. and Jackowski, S. (2000). Pantothenate kinase regulation of the intracellular concentration of coenzyme A. *J Biol Chem* **275**, 1377-83.

Rock, C. O., Karim, M. A., Zhang, Y. M. and Jackowski, S. (2002). The murine pantothenate kinase (Pank1) gene encodes two differentially regulated pantothenate kinase isozymes. *Gene* **291**, 35-43.
Rodriguez, A., Griffiths-Jones, S., Ashurst, J. L. and Bradley, A. (2004). Identification of mammalian microRNA host genes and transcription units. *Genome Res* **14**, 1902-10.
Roldo, C., Missiaglia, E., Hagan, J. P., Falconi, M., Capelli, P., Bersani, S., Calin, G. A., Volinia, S., Liu, C. G., Scarpa, A. et al. (2006). MicroRNA expression abnormalities in pancreatic endocrine and acinar tumors are associated with distinctive pathologic features and clinical behavior. *J Clin Oncol* **24**, 4677-84.
Ruby, J. G., Jan, C. H. and Bartel, D. P. (2007). Intronic microRNA precursors that bypass Drosha processing. *Nature* **448**, 83-6.
Schaloske, R. H. and Dennis, E. A. (2006). The phospholipase A2 superfamily and its group numbering system. *Biochim Biophys Acta* **1761**, 1246-59.
Schlake, T., Schorpp, M., Nehls, M. and Boehm, T. (1997). The nude gene encodes a sequence-specific DNA binding protein with homologs in organisms that lack an anticipatory immune system. *Proc Natl Acad Sci U S A* **94**, 3842-7.
Schneider, S. A., Paisan-Ruiz, C., Quinn, N. P., Lees, A. J., Houlden, H., Hardy, J. and Bhatia, K. P. (2010). ATP13A2 mutations (PARK9) cause neurodegeneration with brain iron accumulation. *Mov Disord*.
Schoonjans, K., Peinado-Onsurbe, J., Lefebvre, A. M., Heyman, R. A., Briggs, M., Deeb, S., Staels, B. and Auwerx, J. (1996). PPARalpha and PPARgamma activators direct a distinct tissue-specific transcriptional response via a PPRE in the lipoprotein lipase gene. *EMBO J* **15**, 5336-48.
Schwarz, D. S., Hutvagner, G., Du, T., Xu, Z., Aronin, N. and Zamore, P. D. (2003). Asymmetry in the assembly of the RNAi enzyme complex. *Cell* **115**, 199-208.
Seitelberger, F. and Gross, H. (1957). [Late infantile form of Hallervorden-Spatz disease. II. Histochemical findings; discussion on nosology.]. *Dtsch Z Nervenheilkd* **176**, 104-25.
Shahbazian, M. D., Antalffy, B., Armstrong, D. L. and Zoghbi, H. Y. (2002). Insight into Rett syndrome: MeCP2 levels display tissue- and cell-specific differences and correlate with neuronal maturation. *Hum Mol Genet* **11**, 115-24.
Sherer, T. B., Betarbet, R., Stout, A. K., Lund, S., Baptista, M., Panov, A. V., Cookson, M. R. and Greenamyre, J. T. (2002). An in vitro model of Parkinson's disease: linking mitochondrial impairment to altered alpha-synuclein metabolism and oxidative damage. *J Neurosci* **22**, 7006-15.
Shevell, M. (2003). Hallervorden and history. *N Engl J Med* **348**, 3-4.
Shinzawa, K., Sumi, H., Ikawa, M., Matsuoka, Y., Okabe, M., Sakoda, S. and Tsujimoto, Y. (2008). Neuroaxonal dystrophy caused by group VIA phospholipase A2 deficiency in mice: a model of human neurodegenerative disease. *J Neurosci* **28**, 2212-20.
Shirai, Y. and Ito, M. (2004). Specific differential expression of phospholipase A2 subtypes in rat cerebellum. *J Neurocytol* **33**, 297-307.
Sinha, S., Maity, S. N., Lu, J. and de Crombrugghe, B. (1995). Recombinant rat CBF-C, the third subunit of CBF/NFY, allows formation of a protein-DNA complex with CBF-A and CBF-B and with yeast HAP2 and HAP3. *Proc Natl Acad Sci U S A* **92**, 1624-8.
Six, D. A. and Dennis, E. A. (2000). The expanding superfamily of phospholipase A(2) enzymes: classification and characterization. *Biochim Biophys Acta* **1488**, 1-19.
Small, R. K., Riddle, P. and Noble, M. (1987). Evidence for migration of oligodendrocyte--type-2 astrocyte progenitor cells into the developing rat optic nerve. *Nature* **328**, 155-7.

Smani, T., Zakharov, S. I., Leno, E., Csutora, P., Trepakova, E. S. and Bolotina, V. M. (2003). Ca2+-independent phospholipase A2 is a novel determinant of store-operated Ca2+ entry. *J Biol Chem* **278**, 11909-15.
Snowden, J. S., Pickering-Brown, S. M., Mackenzie, I. R., Richardson, A. M., Varma, A., Neary, D. and Mann, D. M. (2006). Progranulin gene mutations associated with frontotemporal dementia and progressive non-fluent aphasia. *Brain* **129**, 3091-102.
Steiner, G., Skriner, K., Hassfeld, W. and Smolen, J. S. (1996). Clinical and immunological aspects of autoantibodies to RA33/hnRNP-A/B proteins--a link between RA, SLE and MCTD. *Mol Biol Rep* **23**, 167-71.
Sun, G. Y., Shelat, P. B., Jensen, M. B., He, Y., Sun, A. Y. and Simonyi, A. (2009). Phospholipases A2 and Inflammatory Responses in the Central Nervous System. *Neuromolecular Med*.
Takahashi, Y., Forrest, A. R., Maeno, E., Hashimoto, T., Daub, C. O. and Yasuda, J. (2009). MiR-107 and MiR-185 can induce cell cycle arrest in human non small cell lung cancer cell lines. *PLoS One* **4**, e6677.
Takai, D. and Jones, P. A. (2003). The CpG island searcher: a new WWW resource. *In Silico Biol* **3**, 235-40.
Takimoto, M., Tomonaga, T., Matunis, M., Avigan, M., Krutzsch, H., Dreyfuss, G. and Levens, D. (1993). Specific binding of heterogeneous ribonucleoprotein particle protein K to the human c-myc promoter, in vitro. *J Biol Chem* **268**, 18249-58.
Tang, J., Kriz, R. W., Wolfman, N., Shaffer, M., Seehra, J. and Jones, S. S. (1997). A novel cytosolic calcium-independent phospholipase A2 contains eight ankyrin motifs. *J Biol Chem* **272**, 8567-75.
Tang, X., Muniappan, L., Tang, G. and Ozcan, S. (2009). Identification of glucose-regulated miRNAs from pancreatic {beta} cells reveals a role for miR-30d in insulin transcription. *RNA* **15**, 287-93.
Tenenbaum, A., Motro, M. and Fisman, E. Z. (2005). Dual and pan-peroxisome proliferator-activated receptors (PPAR) co-agonism: the bezafibrate lessons. *Cardiovasc Diabetol* **4**, 14.
Thakur, S., Nakamura, T., Calin, G., Russo, A., Tamburrino, J. F., Shimizu, M., Baldassarre, G., Battista, S., Fusco, A., Wassell, R. P. et al. (2003). Regulation of BRCA1 transcription by specific single-stranded DNA binding factors. *Mol Cell Biol* **23**, 3774-87.
Tischfield, M. A., Baris, H. N., Wu, C., Rudolph, G., Van Maldergem, L., He, W., Chan, W. M., Andrews, C., Demer, J. L., Robertson, R. L. et al. Human TUBB3 mutations perturb microtubule dynamics, kinesin interactions, and axon guidance. *Cell* **140**, 74-87.
Valentiner, U., Carlsson, M., Erttmann, R., Hildebrandt, H. and Schumacher, U. (2005). Ligands for the peroxisome proliferator-activated receptor-gamma have inhibitory effects on growth of human neuroblastoma cells in vitro. *Toxicology* **213**, 157-68.
Vallari, D. S., Jackowski, S. and Rock, C. O. (1987). Regulation of pantothenate kinase by coenzyme A and its thioesters. *J Biol Chem* **262**, 2468-71.
Vella, M. C., Choi, E. Y., Lin, S. Y., Reinert, K. and Slack, F. J. (2004). The C. elegans microRNA let-7 binds to imperfect let-7 complementary sites from the lin-41 3'UTR. *Genes Dev* **18**, 132-7.
Visel, A., Thaller, C. and Eichele, G. (2004). GenePaint.org: an atlas of gene expression patterns in the mouse embryo. *Nucleic Acids Res* **32**, D552-6.
Vithana, E. N., Abu-Safieh, L., Allen, M. J., Carey, A., Papaioannou, M., Chakarova, C., Al-Maghtheh, M., Ebenezer, N. D., Willis, C., Moore, A. T. et al. (2001). A human homolog of yeast pre-mRNA splicing gene, PRP31, underlies autosomal dominant retinitis pigmentosa on chromosome 19q13.4 (RP11). *Mol Cell* **8**, 375-81.

Volinia, S., Calin, G. A., Liu, C. G., Ambs, S., Cimmino, A., Petrocca, F., Visone, R., Iorio, M., Roldo, C., Ferracin, M. et al. (2006). A microRNA expression signature of human solid tumors defines cancer gene targets. *Proc Natl Acad Sci U S A* **103**, 2257-61.
Wada, H., Yasuda, T., Miura, I., Watabe, K., Sawa, C., Kamijuku, H., Kojo, S., Taniguchi, M., Nishino, I., Wakana, S. et al. (2009). Establishment of an improved mouse model for infantile neuroaxonal dystrophy that shows early disease onset and bears a point mutation in Pla2g6. *Am J Pathol* **175**, 2257-63.
Wang, D., Lu, M., Miao, J., Li, T., Wang, E. and Cui, Q. (2009). Cepred: predicting the co-expression patterns of the human intronic microRNAs with their host genes. *PLoS One* **4**, e4421.
Wang, W. X., Rajeev, B. W., Stromberg, A. J., Ren, N., Tang, G., Huang, Q., Rigoutsos, I. and Nelson, P. T. (2008). The expression of microRNA miR-107 decreases early in Alzheimer's disease and may accelerate disease progression through regulation of beta-site amyloid precursor protein-cleaving enzyme 1. *J Neurosci* **28**, 1213-23.
Wang, W. X., Wilfred, B. R., Madathil, S. K., Tang, G., Hu, Y., Dimayuga, J., Stromberg, A. J., Huang, Q., Saatman, K. E. and Nelson, P. T. (2010). MiR-107 Regulates Granulin/Progranulin with Implications for Traumatic Brain Injury and Neurodegenerative Disease. *Am J Pathol*.
Wang, X. (2006). Systematic identification of microRNA functions by combining target prediction and expression profiling. *Nucleic Acids Res* **34**, 1646-52.
Wang, Y. P. and Li, K. B. (2009). Correlation of expression profiles between microRNAs and mRNA targets using NCI-60 data. *BMC Genomics* **10**, 218.
Whittemore, E. R., Loo, D. T., Watt, J. A. and Cotman, C. W. (1995). A detailed analysis of hydrogen peroxide-induced cell death in primary neuronal culture. *Neuroscience* **67**, 921-32.
Wilfred, B. R., Wang, W. X. and Nelson, P. T. (2007). Energizing miRNA research: a review of the role of miRNAs in lipid metabolism, with a prediction that miR-103/107 regulates human metabolic pathways. *Mol Genet Metab* **91**, 209-17.
Wu, Z., Li, C., Lv, S. and Zhou, B. (2009). Pantothenate kinase-associated neurodegeneration: insights from a Drosophila model. *Hum Mol Genet* **18**, 3659-72.
Xia, H. (2005). Regulation of gamma-fibrinogen chain expression by heterogeneous nuclear ribonucleoprotein A1. *J Biol Chem* **280**, 13171-8.
Xie, H., Lim, B. and Lodish, H. F. (2009). MicroRNAs induced during adipogenesis that accelerate fat cell development are downregulated in obesity. *Diabetes* **58**, 1050-7.
Yamakuchi, M., Lotterman, C. D., Bao, C., Hruban, R. H., Karim, B., Mendell, J. T., Huso, D. and Lowenstein, C. J. (2010). P53-induced microRNA-107 inhibits HIF-1 and tumor angiogenesis. *Proc Natl Acad Sci U S A* **107**, 6334-9.
Yoshida, K., Furihata, K., Takeda, S., Nakamura, A., Yamamoto, K., Morita, H., Hiyamuta, S., Ikeda, S., Shimizu, N. and Yanagisawa, N. (1995). A mutation in the ceruloplasmin gene is associated with systemic hemosiderosis in humans. *Nat Genet* **9**, 267-72.
Yue, D., Liu, H. and Huang, Y. (2009). Survey of Computational Algorithms for MicroRNA Target Prediction. *Curr Genomics* **10**, 478-92.
Zhang, M. Q. (2005). Using CorePromoter to find human core promoters. *Curr Protoc Bioinformatics* **Chapter 2**, Unit 2 9.
Zhang, Y. M., Chohnan, S., Virga, K. G., Stevens, R. D., Ilkayeva, O. R., Wenner, B. R., Bain, J. R., Newgard, C. B., Lee, R. E., Rock, C. O. et al. (2007). Chemical knockout of pantothenate kinase reveals the metabolic and genetic program responsible for hepatic coenzyme A homeostasis. *Chem Biol* **14**, 291-302.
Zhang, Y. M., Rock, C. O. and Jackowski, S. (2005). Feedback regulation of murine pantothenate kinase 3 by coenzyme A and coenzyme A thioesters. *J Biol Chem* **280**, 32594-601.

Zhang, Y. M., Rock, C. O. and Jackowski, S. (2006). Biochemical properties of human pantothenate kinase 2 isoforms and mutations linked to pantothenate kinase-associated neurodegeneration. *J Biol Chem* **281**, 107-14.
Zhang, Z., Chang, H., Li, Y., Zhang, T., Zou, J., Zheng, X. and Wu, J. (2010). MicroRNAs: Potential regulators involved in human anencephaly. *Int J Biochem Cell Biol* **42**, 367-374.
Zhao, S., Korzan, W. J., Chen, C. C. and Fernald, R. D. (2008). Heterogeneous nuclear ribonucleoprotein A/B and G inhibits the transcription of gonadotropin-releasing-hormone 1. *Mol Cell Neurosci* **37**, 69-84.
Zhou, B., Westaway, S. K., Levinson, B., Johnson, M. A., Gitschier, J. and Hayflick, S. J. (2001). A novel pantothenate kinase gene (*PANK2*) is defective in Hallervorden- Spatz syndrome. *Nat Genet* **28**, 345-9.
Zhu, Q. S., Qian, B. and Levy, D. (2004). CCAAT/enhancer-binding protein alpha (C/EBPalpha) activates transcription of the human microsomal epoxide hydrolase gene (EPHX1) through the interaction with DNA-bound NF-Y. *J Biol Chem* **279**, 29902-10.

Appendix A

Additional *PLA2G6 in situ* hybridization histochemistry images received from the MRC-Wellcome Trust Human Developmental Biology Resource (HDBR)

*image descriptions are the verbatim commentaries provided by HDBR

A.1: Initial test of *PLA2G6* probe 1b and probe 3b on CS19 saggital sections

A.2: Additional images of *PLA2G6* expression in CS19 samples

A.3: Additional images of *PLA2G6* expression in 9PCW samples (N268)

A.4: Additional images of *PLA2G6* expression in 9PCW samples (N477)

A.5: Additional images of *PLA2G6* expression in spinal cord

Appendix A.1:

Initial test of *PLA2G6* probe 1b and probe 3b on CS19 saggital sections

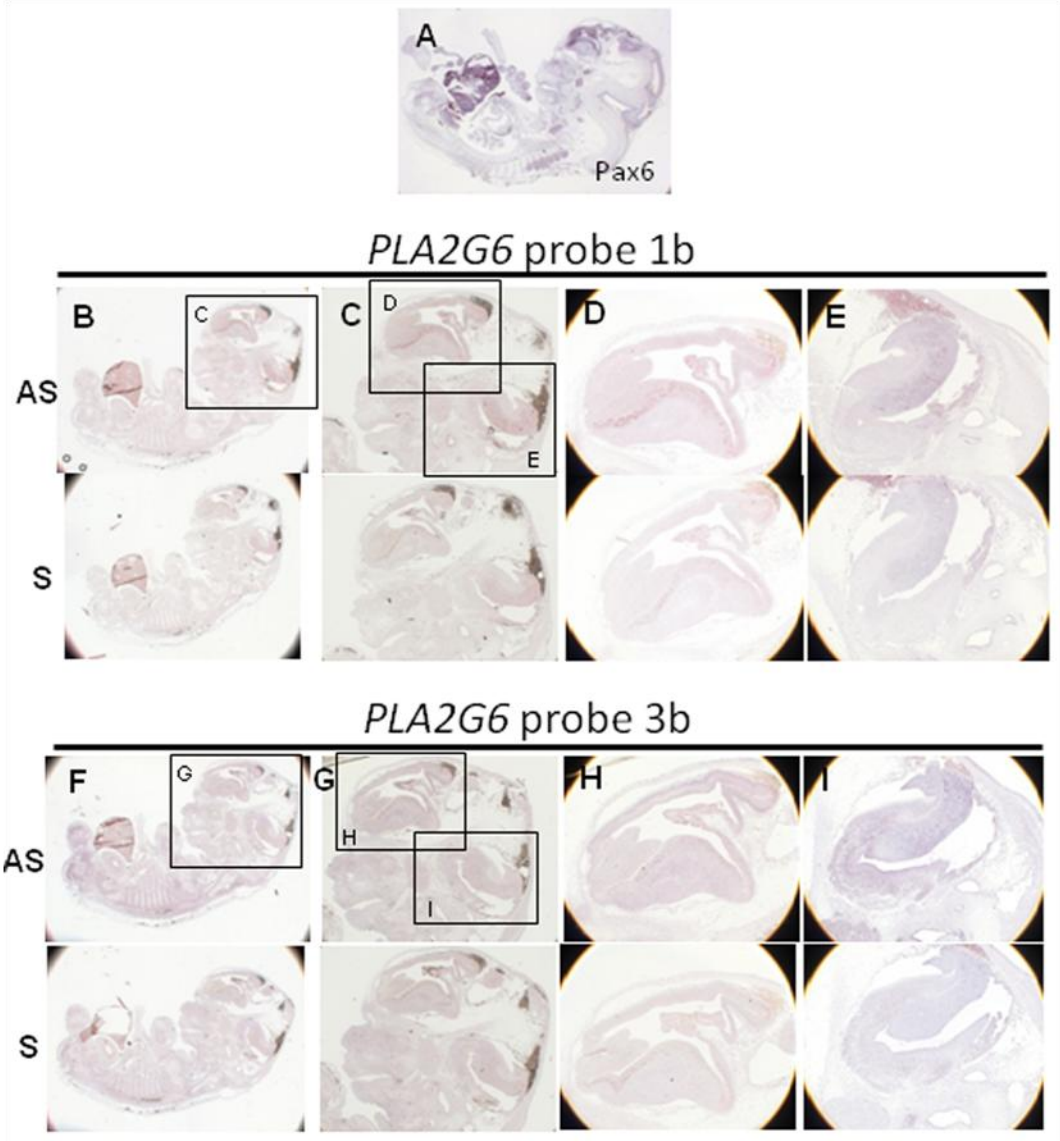

Appendix A.1: Initial test of *PLA2G6* probes 1b and probe 3b on CS19 saggital sections

A) **Positive control: *PAX6*; Sample N457, CS19, x1.25**
   AS: Expression seen in lateral ventricle and roof of midbrain. Expression in dorsal root ganglia and digits of hand.
   S: Palisade of cells in ganglionic eminence remains and there seems to be some staining in the choroid plexus

B) ***PLA2G6* probe 1b; sample N457, CS19, x1.25**
   AS: Expression seen in a palisade of cells lining the ganglionic eminence and the resulting choroid plexus. Mild expression is also seen in the 4th ventricle
   S: no comment

C) ***PLA2G6* probe 1b; sample N457, CS19, x2.5**
   AS: Expression seen in a palisade of cells lining the ganglionic eminence and the resulting choroid plexus. Mild expression is also seen around the 4th ventricle
   S: no comment

D) ***PLA2G6* probe 1b; sample N457, CS19, x5**
   AS: Expression seen in a palisade of cells lining the ganglionic eminence and the resulting choroid plexus.
   S: no comment

E) ***PLA2G6* probe 1b; sample N457, CS19, x5**
   AS: Very pale expresssion around the 4th ventricle
   S: 4th ventricle

F) ***PLA2G6* probe 3b; sample N457, CS19, x1.25**
   AS: Expression of this probe looks different to probe 1B. Expression is seen in the inner ventricular layer and outer layer of the preplate of the lateral ventricle. Mild expression also seen around the 4th ventricle and in the limbs which appears stronger in the lowers.
   S: Some staining is observed in the ganglionic eminence

G) ***PLA2G6* probe 3b; sample N457, CS19, x2.5**
   AS: Expression of this probe looks different to probe 1B. Expression is seen in the inner ventricular layer and outer layer of the preplate of the lateral ventricle. Mild expression is also seen around the 4th ventricle
   S: no comment

H) ***PLA2G6* probe 3b; sample N457, CS19, x5**
   AS: Expression of this probe looks different to probe 1B. Expression is seen in the inner ventricular layer and outer layer of the preplate of the lateral ventricle.
   S: no comment

I) ***PLA2G6* probe 3b; sample N457, CS19, x5**
   AS: Pale expression in 4th ventricle
   S: 4th ventricle

Appendix A.2:

Additional images of *PLA2G6* expression in CS19 samples

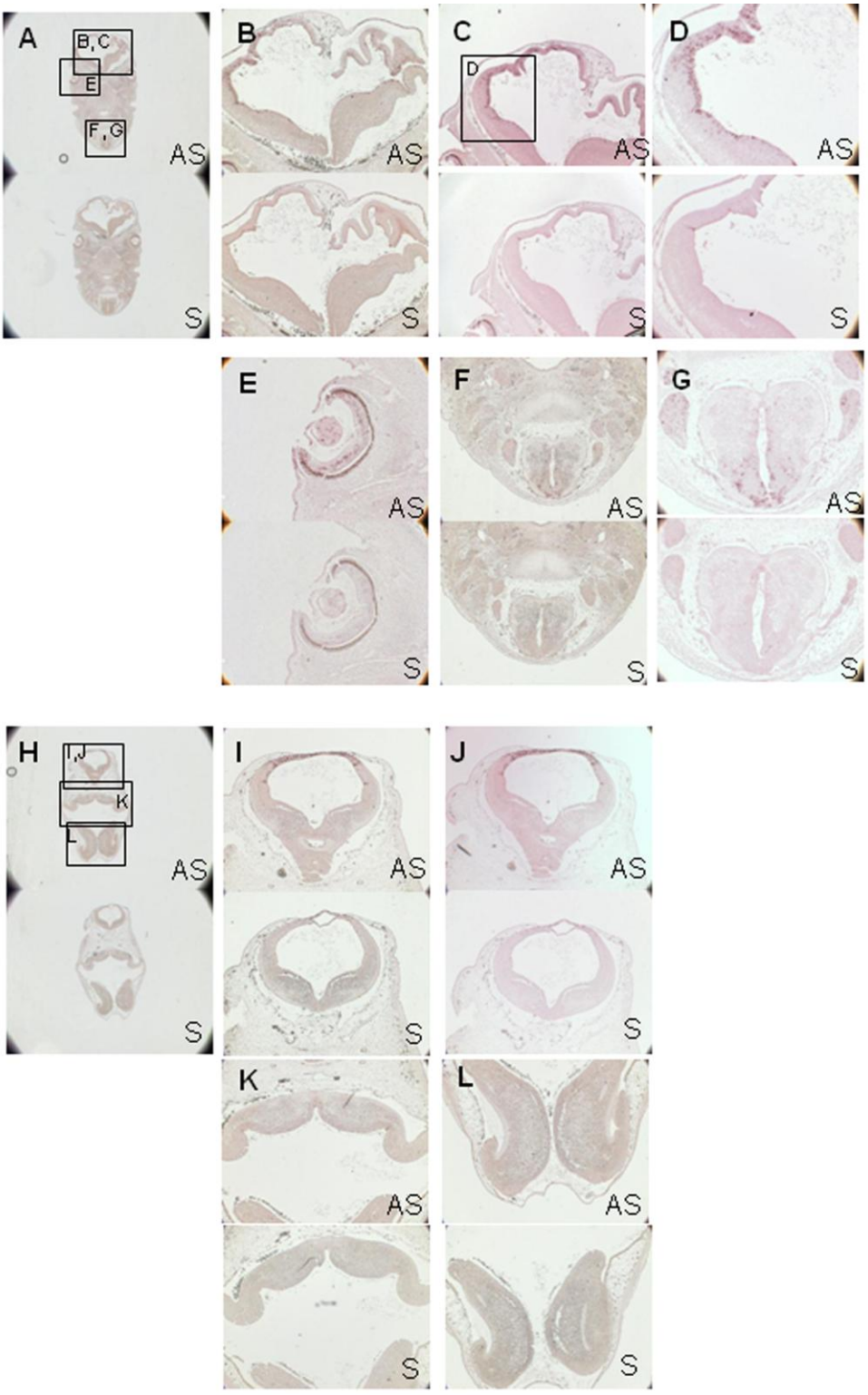

Appendix A.2: Additional images of *PLA2G6* expression in CS19 samples

A) PLA2G6 probe 3b; sample N206, CS19, x1.25
AS: no comment
S: no comment

B) *PLA2G6* probe 3b; sample N206, CS19, x5
AS: venticle
S: ventricle

C) Repeat image of ***PLA2G6* probe 3b; sample N206, CS19, x5**
AS: venticle
S: ventricle

D) *PLA2G6* probe 3b; sample N206, CS19, x10
AS: ventricle
S: ventricle

E) *PLA2G6* probe 3b; sample N206, CS19, x5
AS: eye
S: eye

F) *PLA2G6* probe 3b; sample N206, CS19, x5
AS: neural tube
S: neural tube

G) Repeat image of ***PLA2G6* probe 3b; sample N206, CS19, x5**
AS:spinal cord
S: spinal cord

H) *PLA2G6* probe 3b; sample N206, CS19, x1.25
AS: midbrain and hindbrain
S: midbrain and hindbrain

I) *PLA2G6* probe 3b; sample N206, CS19, x5
AS: midbrain
S: midbrain

J) Repeat image of ***PLA2G6* probe 3b; sample N206, CS19, x5**
AS: midbrain
S: midbrain

K) *PLA2G6* probe 3b; sample N206, CS19, x5
AS: hindbrain
S: hindbrain

L) *PLA2G6* probe 3b; sample N206, CS19, x5
AS: hindbrain
S: hindbrain

Appendix A.3:

Additional images of *PLA2G6* expression in 9PCW samples (N268)

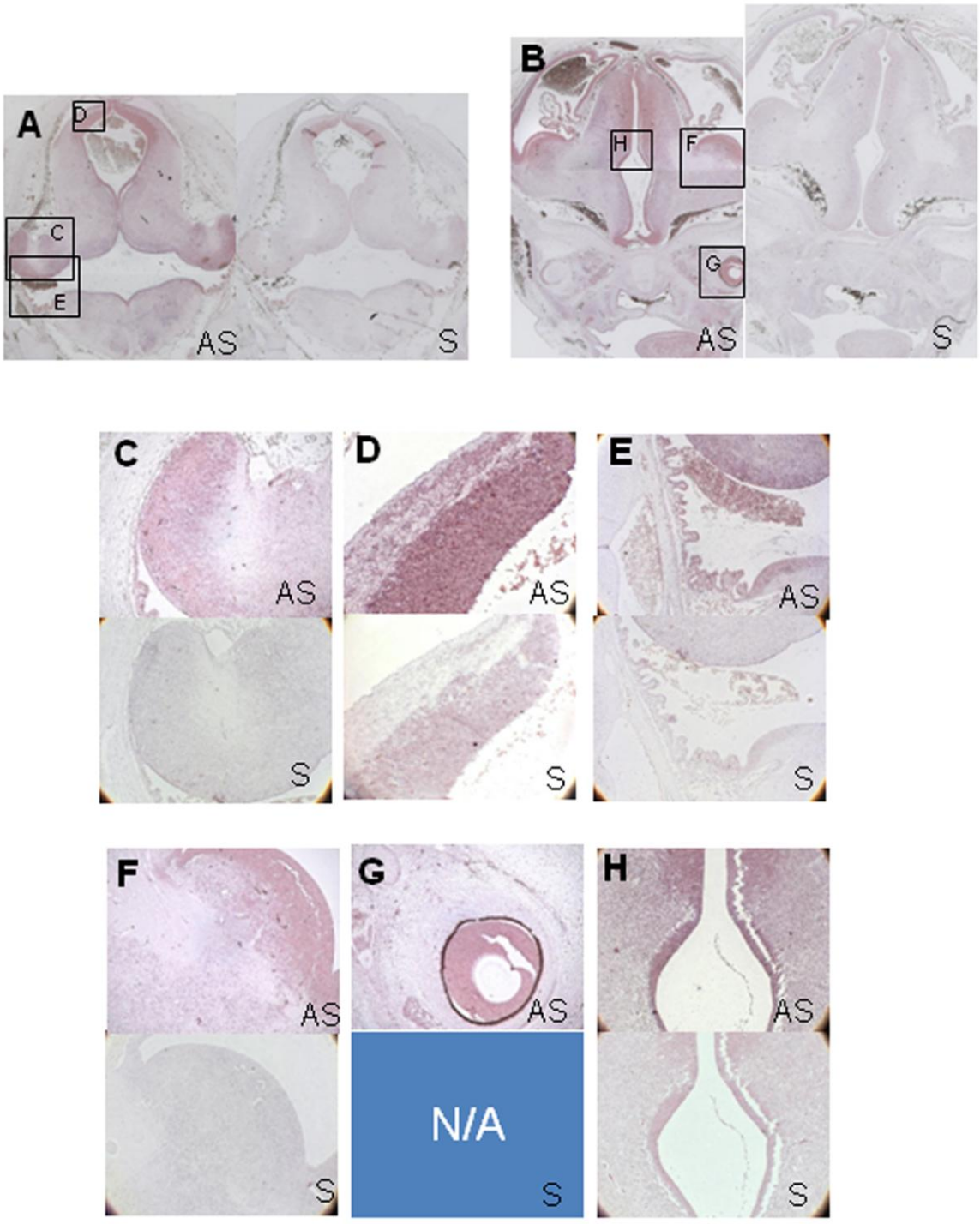

Appendix A.3: Additional images of *PLA2G6* expression in 9PCW samples (N268)

A) *PLA2G6* probe 3b; sample N268, F1, x1.25

AS: Expression seen at the roof and neuroepithelium of the midbrain and in the cerebellum and expression in the cerebellum and in the neuroepithelium of the pons and attached choroid plexus

S: no comment

B) *PLA2G6* probe 3b; sample N268, F1, x1.25

AS:expression seen in the layers of the ventricles, the thalamus, choroid plexus and the ganglionic eminences and expression seen in the hypothalamus neuroepithelium, the eye and the tongue

S: no comment

C) *PLA2G6* probe 3b; sample N268, F1, x5

AS: Expression seen in the cerebellum

S: no comment

D) *PLA2G6* probe 3b; sample N268, F1, x20

AS: 9wk midbrain

S: no comment

E) *PLA2G6* probe 3b; sample N268, F1, x10

AS: 9wk rombencephalic choroid plexus

S: 9wk rombencephalic choroid plexus

F) *PLA2G6* probe 3b; sample N268, F1, x5

AS: Expression seen in ganglionic neuroepithelium,weaker expression in differentated neurones

S: no comment

G) *PLA2G6* probe 3b; sample N268, F1, x5

AS: Expression seen in the neural retina..The optic nerve is at the top of the photo but is at rather an oblique angle

S: N/A

H) *PLA2G6* probe 3b; sample N268, F1, x10

AS: 9wk thalamus/hypothalamus

S: 9wk thalamus/hypothalamus

Appendix A.4:

Additional images of *PLA2G6* expression in 9PCW samples (N477)

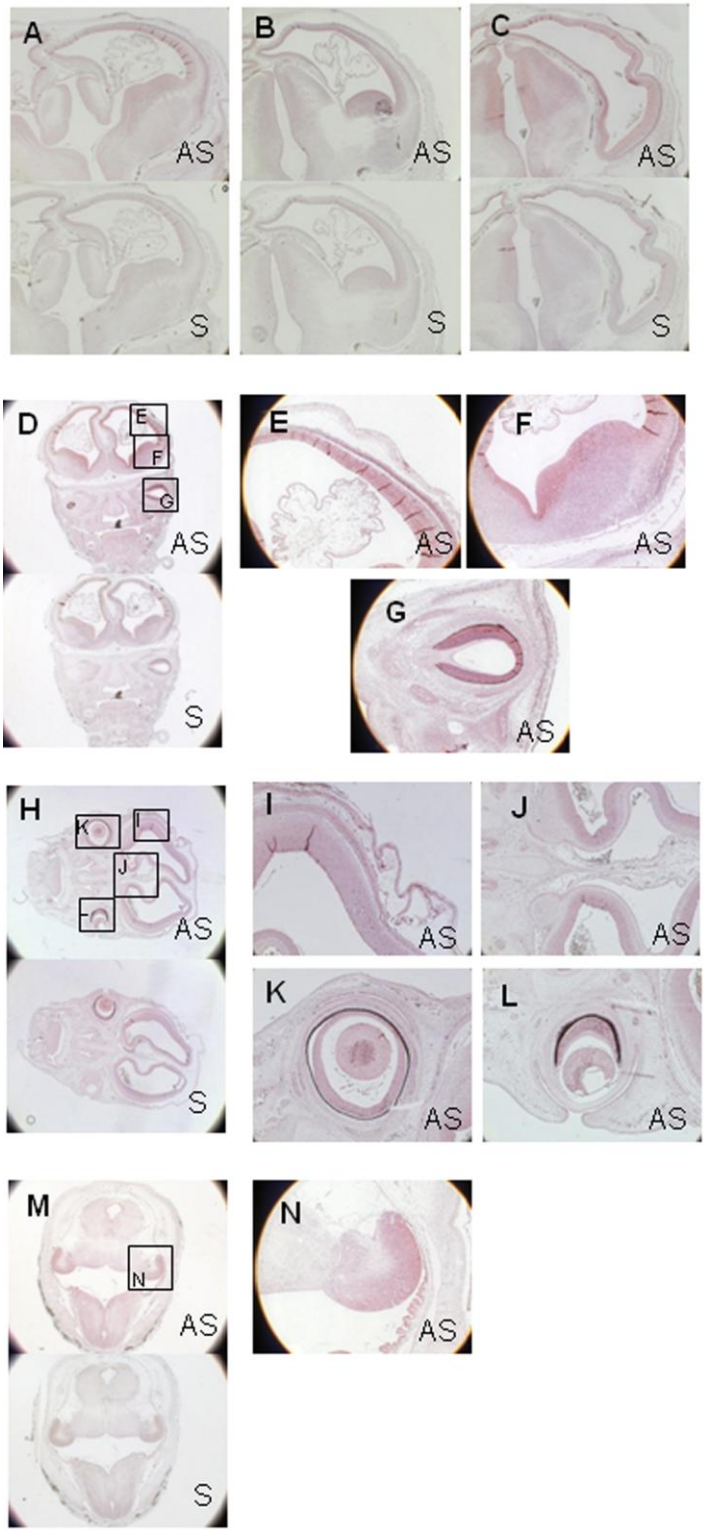

Appendix A.4: Additional images of *PLA2G6* expression in 9PCW samples (N477)

A) *PLA2G6* probe 3b; sample N477, F1, x2.5

AS: Expression is seen in cortical plate but not as it approaches medial wall. Area of basal ganglia appears weak. Expression seen in ventricular layer of dorsal pallium and in the ganglionic eminences.
S: no comment

B) *PLA2G6* probe 3b; sample N477, F1, x2.5

AS: Expression seen in the cortical plate, hippocampus, ventricular layer of dorsal pallium and ganglionic eminences.
S: no comment

C) *PLA2G6* probe 3b; sample N477, F1, x2.5

AS: There is distinct expression in the medial wall and an area in the cortical plate. There is also expression restricted to the anterior diencephalon
S: no comment

D) *PLA2G6* probe 3b; sample N477, F1, x1.25

AS: Expression seen in the ventriclar layers, ganglionic neuroepithelium and the eye. The tongue is very pale compared to the previous embryo.
S: no comment

E) *PLA2G6* probe 3b; sample N477, F1, x5

AS: Expression seen in the subcortical plate and the ventricular and subventricular layers further down the ventricle

F) *PLA2G6* probe 3b; sample N477, F1, x5

AS: Expression seen in the ganglionic neuroepithelium

G) *PLA2G6* probe 3b; sample N477, F1, x5

AS: Expression seen in the eye, optic nerve remains clear

H) *PLA2G6* probe 3b; sample N477, F1, x1.25

AS: no comment, S: no comment

I) *PLA2G6* probe 3b; sample N477, F1, x5

AS: Ventricle and skin

J) *PLA2G6* probe 3b; sample N477, F1, x5

AS: no comment

K) *PLA2G6* probe 3b; sample N477, F1, x5

AS:eye

L) *PLA2G6* probe 3b; sample N477, F1, x5

AS: eye

M) *PLA2G6* probe 3b; sample N477, F1, x1.25

AS: Expression in cerebellum and neuroepithelium of pons and choroid plexus
S: no comment

N) *PLA2G6* probe 3b; sample N477, F1, x5

AS: Cerebellum and choroid plexus

Appendix A.5:

Additional images of *PLA2G6* expression in spinal cord

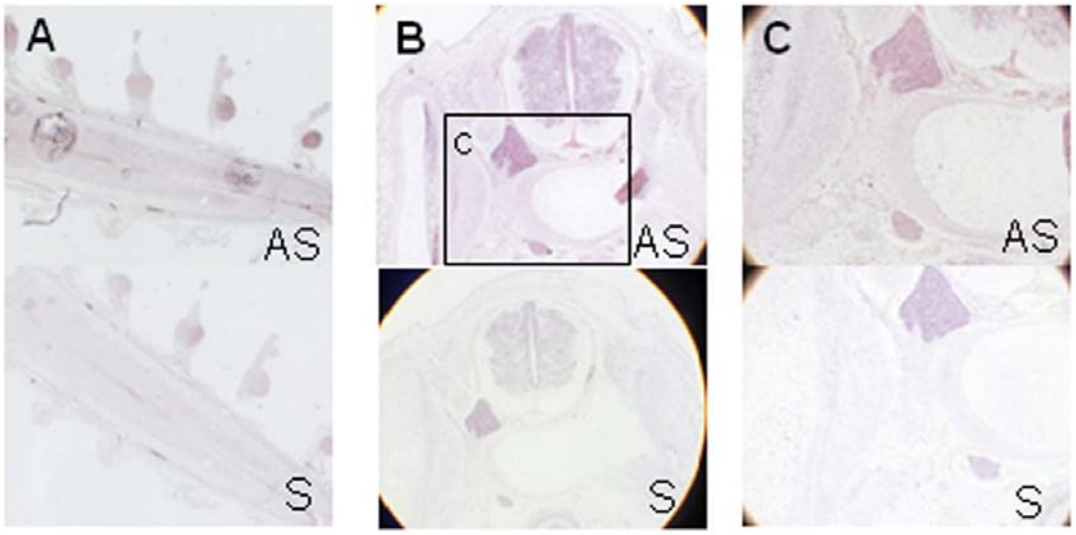

Appendix A.5: Additional images of *PLA2G6* expression in spinal cord

A) *PLA2G6* probe 3b; sample H53, F3, x1.25
AS: Stage F3 dissected spinal cord, saggital
Expression seen in dorsal root ganglia and in the body of the spinal cord
S: F3 dissected spinal cord saggital

B) *PLA2G6* probe 3b; sample N923, F1, x5
AS**:** Expression seen in spinal cord
S: no comment

C) *PLA2G6* probe 3b; sample N477, F1, x10
AS: Expression in spinal ganglion connected to femoral nerve
S: no comment